7-12-2014

BIOSENSING OF MATRIX METALLOPROTEINASE ACTIVITY WITH CD-FREE QUANTUM DOTS

John Plumley

John Bryan Plumley
Candidate

Nanoscience and Microsystems
Department

This dissertation is approved, and it is acceptable in quality and form for publication:

Approved by the Dissertation Committee:

Marek Osinski , Chairperson

Ganesh Balakrishnan

Erin Milligan

Mani Hossein-Zadeh

BIOSENSING OF MATRIX METALLOPROTEINASE ACTIVITY WITH CD-FREE QUANTUM DOTS

by

JOHN BRYAN PLUMLEY

B.S. CHEMICAL ENGINEERING, UNIVERSITY OF NEW MEXICO, 2008
M.S. NANOSCIENCE AND MICROSYSTEMS, UNIVERSITY OF NEW MEXICO, 2012

Dissertation

Submitted in Partial Fulfillment of the
Requirements for the Degree of

Doctor of Philosophy
Nanoscience and Microsystems

The University of New Mexico
Albuquerque, New Mexico

May, 2014

ACKNOWLEDGEMENTS

I would like to give my heartfelt thanks to my committee chair and advisor Dr. Marek Osinski, whose guidance and encouragement made this dissertation possible.

I would also like to thank Dr. Ganesh Balakrishnan, Dr. Erin Milligan, and Dr. Mani Hossein-Zadeh for accepting the position of committee members for my dissertation defense. Extra special thanks goes to Dr. Erin Milligan for her continued support over the years and for allowing me the use of her facilities, which were crucial to this research.

Additional gratitude and appreciation goes to all my co-workers at CHTM and high school interns as well as the CHTM staff for endless support.

Finally, I would like to thank my family and friends for their support during my time in college.

BIOSENSING OF MATRIX METALLOPROTEINASE ACTIVITY WITH CD-FREE QUANTUM DOTS

by

John Bryan Plumley

B.S. Chemical Engineering, University of New Mexico, 2008
M.S. Nanoscience and Microsystems, University of New Mexico, 2012
Ph.D. Nanoscience and Microsystems, University of New Mexico, 2014

ABSTRACT

Quantum dots (QDs) have become attractive in the biomedical field on account of their superior optical properties and stability, in comparison to traditional fluorophores. QDs also have properties which make them ideal for complex *in vivo* conditions. However, toxicity has been a chief concern in the eventual implementation of QDs for *in vivo* applications such as biosensing and tumor imaging. Commercially available QDs contain a notoriously noxious Cd component and therefore continuous research has gone into developing QDs without toxic heavy metals, generally Cd, that would still yield comparable performance in terms of their optical properties. Nonetheless, even in the case of Cd-free QDs, toxicity should be evaluated on a case by case basis, as other properties such as size, coating, stability, and charge can affect toxicity of nanomaterials as well, making it a very complex issue.

With the high promise of QDs in the field of biomedical development as a motivation, this work strives to develop the efficient and repeatable synthesis of Cd-free QDs with high stability and luminescence, with proven low toxicity, and the ability to detect active

matrix metalloproteinase (MMP) in a biosensing system, designed to identify direct biomarkers for pathological conditions, which in turn would enable early disease diagnosis and better treatment development.

In this work, highly luminescent ZnSe:Mn/ZnS QDs have been synthesized, characterized, and modified with peptides with a bioconjugation procedure that utilized thiol-metal affinity. Experiments aiming at MMP detection were conducted using the peptide/QD conjugates. In addition, the ApoTox-Glo^{TM} Triplex assay was utilized to evaluate cytotoxicity, and a safe concentration below 0.125 μM was identified for peptide-coated ZnSe:Mn/ZnS QDs in water. Finally, in contribution to developing an *in vivo* fiberoptic system for sensing MMP activity, the QDs were successfully tethered to silica and MMP detection was demonstrated with the peptide/QD conjugates.

Table of Contents Pages

List of Figures Pages

List of Tables Page

List of Publications

1. K. Sankar, J. B. Plumley, B. A. Akins, T. A. Memon, N. J. Withers, G. A. Smolyakov, and M. Osiński, "*Synthesis and characterization of scintillating cerium-doped lanthanum fluoride nanocrystals*", Colloidal Quantum Dots for Biomedical Applications IV (M. Osiński, T. M. Jovin, and K. Yamamoto, Eds.), SPIE International Symposium on Biomedical Optics BiOS 2009, San Jose, California, 24-26 January 2009, Proceedings of SPIE, Vol. 7189, Paper 718909 (12 pp.).

2. N. J. Withers, J. B. Plumley, N. D. Triño, K. Sankar, B. A. Akins, A. C. Rivera, G. A. Smolyakov, G. S. Timmins, and M. Osiński, "*Scintillating-nanoparticle-induced enhancement of absorbed radiation dose*", Colloidal Quantum Dots for Biomedical Applications IV (M. Osiński, T. M. Jovin, and K. Yamamoto, Eds.), SPIE International Symposium on Biomedical Optics BiOS 2009, San Jose, California, 24-26 January 2009, Proceedings of SPIE, Vol. 7189, Paper 718917 (8 pp.).

3. N. J. Withers, B. A. Akins, A. C. Rivera, J. B. Plumley, G. A. Smolyakov, and M. Osiński, "*Lead-iodide based nanoscintillators for detection of ionizing radiation*", Chemical, Biological, Radiological, Nuclear, and Explosives (CBRNE) Sensing X (A. W. Fountain, III and P. J. Gardner, Eds.), SPIE Defense, Security, and Sensing Symposium, Orlando, Florida, 14-16 April 2009, Proceedings of SPIE, Vol. 7304, Paper 73041N (12 pp.).

4. M. Osiński, K. Sankar, N. J. Withers, J. B. Plumley, A. C. Rivera, B. A. Akins, and G. A. Smolyakov, "*Lanthanide-halide-based nanoscintillators for portable radiological detectors (Invited Paper)*", Optics and Photonics in Global Homeland Security V and Biometric Technology for Human Identification VI (C. S. Halvorson, Š. O. Southern, B. V. K. V. Kumar, S. Prabhakar, and A. A. Ross, Eds.), SPIE Defense, Security, and Sensing Symposium, Orlando, Florida, 13-16 April 2009, Proceedings of SPIE, Vol. 7306, Paper 730617 (16 pp.).

5. N. J. Withers, K. Sankar, J. B. Plumley, B. A. Akins, T. A. Memon, A. C. Rivera, G. A. Smolyakov, and M. Osiński, "*Optimization of Ce content in $Ce_xLa_{1-x}F_3$ colloidal nanocrystals for gamma radiation detection*", Nuclear Radiation Detection Materials – 2009 (D. L. Perry, A. Burger, L. Franks, K. Yasuda, and M. Fiederle, Eds.), 2009 MRS Spring Meeting, San Francisco, California, 13-17 April 2009, MRS Symposium Proceedings, Vol. 1164, Paper L07-02 (6 pp.).

6. N. J. Withers, J. B. Plumley, B. A. Akins, G. Medina, G. Timmins, G. A. Smolyakov, and M. Osiński, "*Radiation sensitivity enhancement in cells using high-Z nanoparticles*", accepted for Colloidal Quantum Dots for Biomedical Applications V (M. Osiński, W. J. Parak, T. M. Jovin, and K. Yamamoto, Eds.), SPIE International Symposium on Biomedical Optics BiOS 2010, San Francisco, California, 23-25 January 2010, Proceedings of SPIE, Vol. 7575, Paper 7575-33.

7. M. Osiński, J. B. Plumley, N. J. Withers, B. A. Akins, G. Medina, A. C. Rivera, and G. A. Smolyakov, "*Synthesis and characterization of lanthanide halide scintillating nanocrystals for gamma radiation detection*", Symposium 2. Nanomaterials, 2010 International Conference on Nanoscience and Nanotechnology ICONN 2010, Sydney, Australia, 22-26 February 2010 (4 pp.)

8. J. B. Plumley, N. J. Withers, A. C. Rivera, B. A. Akins, J. M. Vargas, K. Carpenter, G. A. Smolyakov, R. D. Busch, and M. Osiński, "*Thermal neutron detectors based on gadolinium-containing lanthanide-halide nanoscintillators*", Chemical, Biological, Radiological, Nuclear, and Explosives (CBRNE) Sensing XI (A. W. Fountain, III and P. J. Gardner, Eds.), SPIE Defense, Security, and Sensing Symposium, Orlando, Florida, 6-8 April 2010, Proceedings of SPIE, Vol. 7665, Paper 76651F (13 pp.).

9. N. J. Withers, N. N. Glazener, J. B. Plumley, B. A. Akins, A. C. Rivera, N. C. Cook, G. A. Smolyakov, G. S. Timmins, and M. Osiński, "*Locally increased mortality of gamma-irradiated cells in presence of lanthanide-halide nanoparticles*", Colloidal Quantum Dots/Nanocrystals for Biomedical Applications VI (W. J. Parak, K. Yamamoto, and M. Osiński, Eds.), SPIE International Symposium on Biomedical Optics BiOS 2011, San Francisco, California, 22-24 January 2011, Proceedings of SPIE, Vol. 7909, Paper 7909-0L (12 pp.).

10. M. Osiński, Y. Brandt, J. M. Vargas, J. B. Plumley, S. R. Maestas, A. C. Rivera, N. C. Cook, N. J. Withers, G. A. Smolyakov, N. L. Adolphi, S. L. McGill, I. El-Sherbiny, and H. D. C. Smyth, "*Multifunctional nanoparticles for lung delivery of drugs (Invited Paper)*", Fifth International Conference on Advanced Materials and Nanotechnology AMN-5, Wellington, New Zealand, 7-11 February 2011.

11. J. M. Vargas, A. A. McBride, J. B. Plumley, Y. Fichou, T. A. Memon, V. Shah, N. Cook, B. A. Akins, A. C. Rivera, G. A. Smolyakov, J. R. O'Brien, N. L. Adolphi, H. D. C. Smyth, and M. Osiński, "*Synthesis and characterization of core/shell Fe_3O_4/ZnSe fluorescent magnetic nanoparticles*", Journal of Applied Physics **109** (#7), Art. 07B536 (3 pp.), April 2011.

12. A. C. Rivera, N. N. Glazener, N. C. Cook, B. A. Akins, J. B. Plumley, N. J. Withers, K. Carpenter, G. A. Smolyakov, R. D. Busch, and M. Osiński, "*Detection of thermal neutrons using gadolinium-oxide-based nanocrystals*", Chemical, Biological, Radiological, Nuclear, and Explosives (CBRNE) Sensing XII (A. W. Fountain, III and P. J. Gardner, Eds.), SPIE Defense, Security, and Sensing Symposium, Orlando, Florida, 25-29 April 2011, Proceedings of SPIE, Vol. 8018, Paper 80180F (12 pp.).

13. A. C. Rivera, N. C. Cook, N. N. Glazener, N. J. Withers, J. B. Plumley, B. A. Akins, G. A. Smolyakov, R. D. Busch, and M. Osiński, "*Dysprosium-containing nanocrystals for thermal neutron detection*", Symposium U, Nuclear Radiation Detection Materials (A. Burger, M. Fiederle, L. Franks, K. Lynn, D. L. Perry, and

K. Yasuda, Eds.), 2011 MRS Spring Meeting, San Francisco, CA, 26-28 April 2011, MRS Proceedings, Vol. 1341, Paper U9.2 (6 pp.)

14. M. Osiński, B. A. Akins, J. B. Plumley, A. C. Rivera, N. C. Cook, A. Agarwal, and G. A. Smolyakov, "*High-temperature nanophosphors for white-light-emitting diodes (Invited Paper)*", Proceedings of the 16th Opto-Electronics and Communications Conference OECC 2011, Kaohsiung, Taiwan, 4-8 July 2011 (4 pp.).

15. M. Osiński, L. M. Armijo, Y. Brandt, S. R. Maestas, A. C. Rivera, N. C. Cook, J. B. Plumley, B. A. Akins, G. A. Smolyakov, N. L. Adolphi, D. L. Huber, S. L. McGill, L. Gong, and H. D. C. Smyth, "*Multifunctional nanoparticles for drug delivery in cystic fibrosis (Invited Paper)*", Zing Nanomaterials Conference, Xcaret, Quintana Roo, Mexico, 28 November – 2 December 2011.

16. A. C. Rivera, N. N. Glazener, N. C. Cook, L. M. Armijo, J. B. Plumley, B. A. Akins, K. Carpenter, G. A. Smolyakov, R. D. Busch, and M. Osiński, "*Dysprosium-containing nanocrystals for use as a neutron detector in a solvent suspension*", Zing Nanomaterials Conference, Xcaret, Quintana Roo, Mexico, 28 November – 2 December 2011.

17. L. M. Armijo, Y. Brandt, D. L. Huber, N. J. Withers, J. B. Plumley, N. C. Cook, A. C. Rivera, G. A. Smolyakov, S. Yadav, H. D. C. Smyth, and M. Osiński, "*Multifunctional superparamagnetic nanocrystals for imaging and targeted drug delivery to the lung*", accepted for Colloidal Quantum Dots/Nanocrystals for Biomedical Applications VII (W. J. Parak, M. Osiński, and K. Yamamoto, Eds.), SPIE International Symposium on Biomedical Optics BiOS 2012, San Francisco, California, 21-23 January 2012, Proceedings of SPIE, Vol. 8232, Paper 22.

18. M. Osiński, L. M. Armijo, Y. Brandt, S. R. Maestas, A. C. Rivera, N. C. Cook, J. B. Plumley, B. A. Akins, G. A. Smolyakov, N. L. Adolphi, L. Gong, and H. D. C. Smyth, , "*Multifunctional superparamagnetic nanoparticles for drug delivery in cystic fibrosis (Invited Paper)*", International Conference and Workshop on Nanostructured Ceramics and Nanomaterials ICWNCN-12, New Delhi, India, 13-16 March 2012.

19. A. C. Rivera, N. N. Glazener, N. C. Cook, S. Maestas, B. A. Akins, L. M. Armijo, J. B. Plumley, N. J. Withers, K. Carpenter, G. A. Smolyakov, R. D. Busch, and M. Osiński, "*Thermal neutron detection with PMMA nanocomposites containing dysprosium fluoride nanocrystals*", accepted for Chemical, Biological, Radiological, Nuclear, and Explosives (CBRNE) Sensing XIII, SPIE Defense, Security, and Sensing Symposium, Baltimore, Maryland, 23-27 April 2012, Paper 8358-66.

20. B. A. Akins, A. C. Rivera, J. B. Plumley, N. C. Cook, S. A. Ivanov, G. A. Smolyakov, and M. Osiński, "*Cadmium-free ZnSe:Mn/ZnS high temperature*

nanophosphors with record high quantum efficiency for white LED applications", Technical Digest, 7th International Conference on Quantum Dots, Santa Fe, New Mexico, 13-18 May 2012, Paper Th-72.

21. N. C. Cook, A. C. Rivera, N. N. Glazener, B. A. Akins, L. M. Armijo, J. B. Plumley, N. J. Withers, K. Carpenter, G. A. Smolyakov, R. D. Busch, and M. Osiński, "*Polyvinyl toluene/Gd_2O_3:10%Ce scintillating nanocomposites for thermal neutron detection*", Technical Digest, 7th International Conference on Quantum Dots, Santa Fe, New Mexico, 13-18 May 2012, Paper Th-73.

22. A. C. Rivera, N. N. Glazener, N. C. Cook, S. R. Maestas, B. A. Akins, L. M. Armijo, J. B. Plumley, N. J. Withers, K. Carpenter, G. A. Smolyakov, R. D. Busch, and M. Osiński, "*Thermal neutron detection with Gd_2O_3:10%Ce nanocrystals loaded into a polyvinyl toluene matrix*", IEEE Symposium on Radiation Measurements and Applications SORMA WEST 2012, Oakland, California, 14-17 May 2012.

23. L. M. Armijo, B. A. Akins, J. B. Plumley, A. C. Rivera, N. J. Withers, N. C. Cook, G. A. Smolyakov, D. L. Huber, H. D. C. Smyth, and M. Osiński, "*Highly efficient multifunctional MnSe/ZnSeS quantum dots for biomedical applications*", Colloidal Nanoparticles for Biomedical Applications VIII (W. J. Parak, M. Osiński, and K. Yamamoto, Eds.), SPIE International Symposium on Biomedical Optics BiOS 2013, San Francisco, California, 2-4 February 2013, Proceedings of SPIE, Vol. 8595, Paper 859517 (7 pp.).

24. N. J. Withers, N. N. Glazener, A. C. Rivera, B. A. Akins, L. M. Armijo, J. B. Plumley, N. C. Cook, J. M. Sugar, R. Chan, Y. I. Brandt, G. A. Smolyakov, P. H. Heintz, and M. Osiński, "*Effects of $La_{0.2}Ce_{0.6}Eu_{0.2}F_3$ nanocrystals capped with polyethylene glycol on human pancreatic cancer cells in vitro*", Colloidal Nanoparticles for Biomedical Applications VIII (W. J. Parak, M. Osiński, and K. Yamamoto, Eds.), SPIE International Symposium on Biomedical Optics BiOS 2013, San Francisco, California, 2-4 February 2013, Proceedings of SPIE, Vol. 8595, Paper 85951O (9 pp.).

25. M. Osiński, J. B. Plumley, B. A. Akins, N. J. Withers, Y. I. Brandt, and E. D. Milligan, "*Quantum-dot-based biosensor of matrix metalloproteinase activity (Invited Paper)*", Proceedings of 2nd International Conference and Exhibition on Biosensors and Bioelectronics, Chicago, Illinois, 17-19 June 2013, Journal of Biosensors and Bioelectronics, vol. 4, no. 3, p. 41, June 2013.

26. B. A. Akins, S. A. Ivanov, J. B. Plumley, S. M. Stephens, N. C. Cook, G. A. Smolyakov, and M. Osiński, "*High-temperature ZnSe:Mn/ZnS nanophosphors with very high quantum efficiency for white LEDs*", Technical Digest, Tenth Conference on Lasers and Electro-Optics Pacific Rim CLEO-PR 2013, Kyoto, Japan, 30 June – 4 July 2013, Paper ThI3-7 (2 pp.).

27. L. M. Armijo, M. Kopciuch, B. A. Akins, J. B. Plumley, N. J. Withers, A. C. Rivera, N. C. Cook, Y. I. Brandt, J. M. Baca, S. J. Wawrzyniec, G. A. Smolyakov, D. L. Huber, and M. Osiński, "*Low-toxicity magnetic nanomaterials for biomedical applications*", accepted for 21st Annual International Conference on Composites / Nano Engineering ICCE-21, Tenerife, Spain, July 21-27, 2013.

28. N. N. Glazener, A. C. Rivera, N. C. Cook, S. R. Maestas, B. A. Akins, L. M. Armijo, J. B. Plumley, N. J. Withers, K. Carpenter, G. A. Smolyakov, R. D. Busch, and M. Osiński, "*Thermal neutron detection with Gd_2O_3:10%Ce nanocrystals loaded into a polyvinyl toluene matrix*", submitted to Beilstein Journal of Nanotechnology.

29. J. B. Plumley, B. A. Akins, G. J. Alas, M. E. Fetrow, J. Nguyen, P. Jain, S. Yang, Y. I. Brandt, G. A. Smolyakov, W. Ornatowski, E. D. Milligan, and M. Osiński, "*Noncytotoxic Mn-doped ZnSe/ZnS quantum dots for biomedical applications"*, accepted for Colloidal Nanocrystals for Biomedical Applications IX (W. J. Parak, M. Osiński, and K. Yamamoto, Eds.), SPIE International Symposium on Biomedical Optics BiOS 2014, San Francisco, California, 01 February 2014, Proceedings of SPIE, Vol. 8955.

30. L. M. Armijo, M. Kopciuch, Z Olszówka, S. J. Wawrzyniec, A.C. Rivera, J. B. Plumley, N. C. Cook, Y. I. Brandt, D. L. Huber, G. A. Smolyakov, N. L. Adolphi, H. D. C. Smyth, and M. Osiński, "*Delivery of tobramycin coupled to iron oxide nanoparticles across the biofilm of mucoidal Pseudonomas aeruginosa and investigation of its efficacy*", accepted for Colloidal Quantum Dots/Nanocrystals for Biomedical Applications IX (W. J. Parak, M. Osiński, and K. Yamamoto, Eds.), SPIE International Symposium on Biomedical Optics BiOS 2014, San Francisco, California, 01 February 2014, Proceedings of SPIE, Vol. 8955.

31. A.C. Rivera, N. N. Glazener, N. C. Cook, B. A. Akins, L. M. Armijo, J. B. Plumley, N. J. Withers, K. Carpenter, G. A. Smolyakov, R. D. Busch, and M. Osiński, "*Characterisation of potassium bromide loaded with dysprosium fluoride nanocrystals for neutron detection*", International Journal of Nanotechnology **11** (#5), 529-538, April 21, 2014.

32. J. B. Plumley, B. Akins, G. J. Alas, M. E. Fetrow, J. Nguyen, P. Jain, S. Yang, Y. Brandt, G. Smolyakov, W. Ornatowski, E. D. Milligan, M. Osiński' "*In vitro Cytotoxicity of peptide coated Mn-doped ZnSe/ZnS quantum dots on macrophage cells*", Journal of Bionanotechnology, pending submission.

Patent applications

1. M. Osiński, J. B. Plumley, G. A. Smolyakov, N. J. Withers, A. C. Rivera, B. A. Akins, and J. M. Vargas, "*Thermal neutron detectors based on gadolinium-containing nanoscintillators*", United States Provisional Patent Application 61/473,071 filed on 7 April 2011.

2. J. B. Plumley, A. D. Milligan, and M. Osiński, "*Amyotrophic lateral sclerosis detection devices, methods, and biomarkers*", United States Provisional Patent Application filed on 5 December 2011.

Chapter 1

Introduction to matrix metalloproteinase, quantum dots, and quantum dot-based biosensing

1.1 Matrix metalloproteinase (MMPs) and their potential as biomarkers

MMPs are enzymes which consist of a vast family of zinc-dependent endopeptidases that can bind to non-terminal amino acids in peptides and catalyze hydrolysis, splitting the peptide substrate into two separate molecules (cleaving). MMP types are differentiated based on their size and the specific substrates they interact with. So far, at least 26 different types of human MMPs have been identified[1]. They are responsible for tissue repair and break down of the extracellular matrix. Abnormal MMP activity can be indicative of many different pathological disorders. On one hand, MMPs partake in a large number of physiological processes such as tissue repair, immune system activation, inflammation, apoptosis, etc. On the other hand, their abnormal activity is associated with many different pathological conditions, such as cancer, arthritis, central nervous system (CNS) disorders, and so on.

MMPs are initially synthesized as inactive, but become active due to injury, inflammation, or the presence of other proteinases, foreign bodies, and pathogens. **Figure 1.1** is a diagram depicting MMP activation in the presence of reactive oxygen species or the presences of other MMPs or proteinases[2]. In specific, MMPS are made active by the removal of a peptide blocking the active region due to a bond between the Zn ion and the thiol group in the cysteine amino acid residue.

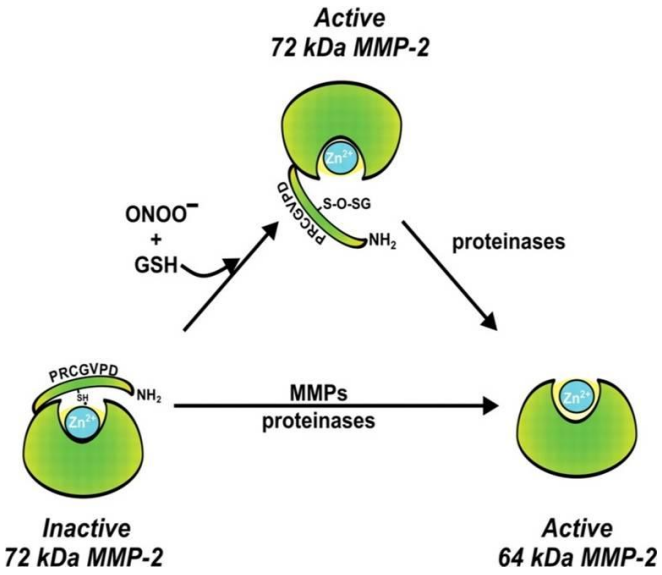

Figure 1.1: *Diagram depicting the activation of a MMP-2 enzyme by being converted from its pro-inactive form to its pro-active form through reactive oxygen species and its active form from additional proteinase activity*[2].

The ubiquitous presence of MMPs in a large number of pathological conditions offers an attractive new way of early detection of these conditions through biosensing of MMP activity at specific sites. For example, biosensors placed at pain signaling sites could be used for detection of neuropathic pain. However, at present no sensors exist capable of real-time in vivo reporting of MMP activity. (Table 1.1) illustrates numerous processes, pathological and physiological, that MMPs play a role in.

Physiological processes	Pathological processes	
Angiogenesis	Arthritis	Multiple sclerosis
Apoptosis	Alzheimer's disease	Nephritis
Blastocyst implantation	Atherosclerosis	Neurological disease
Bone remodeling	Breakdown of blood–brain barrier	Osteoarthritis (OA)
Cervical dilation	Cancer	Periodontal disease
Embryonic development	Cardiovascular disease	Rheumatoid
Endometrial cycling	Central nervous system disorders	Skin ulceration
Hair follicle cycling	Corneal ulceration	Sorby's fundus disease
Immune response	Emphysema	Vascular disease
Inflammation	Fibrotic lung disease	
Nerve growth	Gastric ulcer	
Organ morphogenesis	Guillian-Barre disease	
Ovulation	Liver cirrhosis	
Postpartum uterine involution	Liver fibrosis	
Wound healing	Metastasis	

Table 1.1: *List of several pathological and physiological processes MMPs play a role in*[1].

Currently, there are no biomarkers for neuropathic pain, and yet it is important to objectively identify patients in need of treatment. Targeting non-neuronal signaling mechanisms could lead to a novel biomarker for identifying neuropathic pain. Spinal cord glia contribute to chronic pathological pain by responding to and releasing proinflammatory cytokines and MMPs[3]. Identifying MMP-based biomarkers for neuropathic pain has the potential to yield a better understanding of the mechanisms behind pain processing and a way of objectively characterizing pain, therefore contributing to treatment development. Existing pain treatments that target neurons are not very effective, because pain is only reduced by 25-40% in less than half of the 15 million patients in the US that suffer from chronic neuropathic pain[4]. The present lack of effective therapeutic agents is largely due to a poor understanding of the mechanisms that

underlie neuropathic pain[3]. It can be expected that with the identification of pathophysiological mechanisms that contribute to pain, new and improved neuropathic pain treatments can be developed[5].

Consequently, there has been an increasing interest in studying MMP enzyme expression in neuropathic pain. Several studies on MMP activity in traumatic nerve injury generally indicate modulations in MMP expression in the CNS. In particular, MMP-9 is rapidly upregulated and induces pain initially upon nerve injury, while the response of MMP-2 is delayed and induces pain at a later time[6]. Also, in the case of lumbar disc herniation that leads to chronic pain, MMP-1 and MMP-3 expression is correlated to the age of patients as well as the degree of disc herniation[7]. Most of these studies were done using multistep endpoint assay processes, such as gel electrophoresis (gelatin zymography), enzyme-linked immunosorbent assay (ELISA), or immunohistochemical (IHC) staining. A simple and highly effective sensing method for indicating these findings at pain-processing sites could have a tremendous impact on how we study the mechanisms underlying neuropathic pain, such as being able to monitor and quantify MMP modulations in real time in the direct vicinity of nerve lesions.

Additionally, MMP-based biomarkers have the potential for early diagnosis of CNS disorders, in particular amyotrophic lateral sclerosis (ALS). ALS is a progressive neurodegenerative disease in which motor neurons degrade and can no longer transmit signals to muscles and is ultimately fatal. Symptoms of the disease include progressive weakening of muscles, muscle spasms, and muscle atrophy. 100,000 people suffer from the disease worldwide[8], with patients dying from respiratory failure usually 3-5 years after being diagnosed[9]. 10% of ALS cases are due to genetic defects while the other 90%

are sporadic with unknown causes. Currently there is no cure for ALS and as it stands there is no definitive diagnostic test for ALS. The current way to diagnose ALS involves a series of physical examination tests as well as additional tests to rule out other diseases with ALS like symptoms, such as HIV and Lyme disease[9]. In order to diagnose someone with ALS, a physician will have to evaluate a patient suffering from ALS like symptoms at regular intervals in order to determine if these symptoms are getting progressively worse. The symptom evaluation is supplemented with a series of test such as MRI, blood, and urine test in order to rule out other diseases or causes for ALS like symptoms in a patient. Because of the lengthy diagnostic testing, it is reasonable to believe that patients are not diagnosed with ALS in the early stages of the disease.

A reliable ALS biomarker will enable earlier diagnosis which will contribute to treatment development for ALS. Earlier diagnosis will aid treatment development because future treatments will more likely be efficacious in the early stages of disease development[10].

There has been an increasing interest in MMP activity as a biomarker for other CNS disorders and diseases, as well. There have been several studies on MMP activity in patients with neurological diseases with the results generally indicating abnormal MMP activity in the serum and CSF. In specific, patients with ALS statistically show 3 times lower MMP-9 activity in the CSF and 2 time higher MMP-9 activity in the serum in comparison to healthy controls by using gel zymography testing[11]. Furthermore, it was statistically shown that patients with HIV[12] and multiple sclerosis[13] have increased MMP-9 activity while patients with Alzheimer's show no abnormal MMP-9 activity at all[14].

MMPs also play a necessary role in wound healing, in that they regulate tissue reformation and are highly expressed at the site of a wound. With at least 10 different types of MMPs being upregulated during the skin healing process in mammals[15], being able to quantitatively probe the involvement of MMPs in situ would be attractive. This is mainly because in order to optimally care for and treat a chronic wound an understanding of the role that the ECM plays in healing is required[16].

1.2 Colloidal quantum dots and their merits

Luminescent semiconductor nanocrystals, also known as quantum dots (QDs), have been on the frontier of scientific research for the past few decades. Colloidal QDs are traditionally composed of a CdSe core and a ZnS shell, which acts as a passivation layer that enhances optical properties. CdSe/ZnS QDs are synthesized colloidally at high temperatures, and their size and shape can be controlled from synthesis conditions such as temperature, solvent, and surfactant. The fluorescence of CdSe/ZnS QDs is tunable based on their size, resulting in the unique characteristic that different batches of CdSe/ZnS QDs can appear to have different emission colours. When the semiconductor material becomes smaller than its exciton Bohr radius, which is typically less than 10 nm, quantum confinement is achieved, and band gap energies become a function of QD size. These band gap energies scale inversely with QD size, meaning band gap energies increase as the size of QDs become smaller. The effect is that as QDs get smaller their emission color shifts from red to blue (**Figure 1.2a**). Also, QDs have broad spectroscopic absorption bands and narrow emission lines (**Figure 1.2b**) with the primary benefit being

that with a single excitation wavelength multiple QD emissions can be excited with good resolution at the same time.

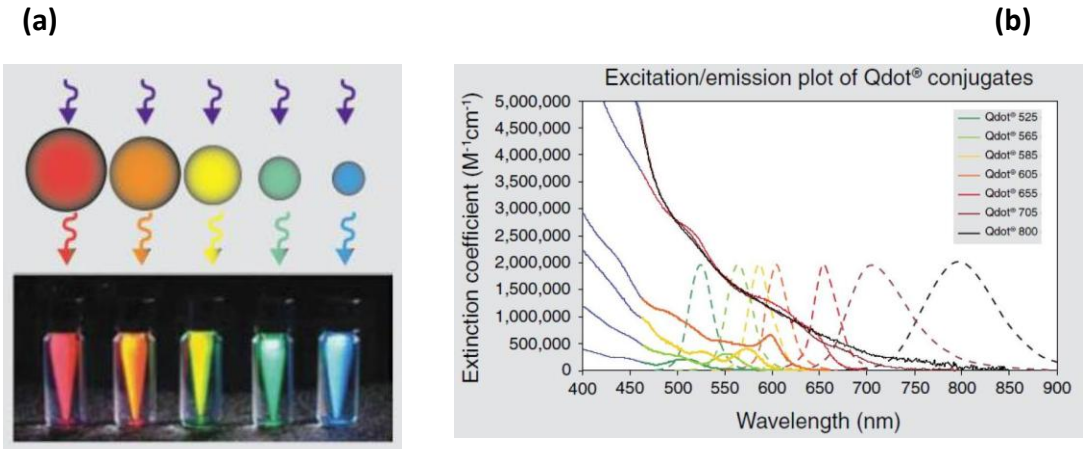

Figure 1.2: (a) *Size tunable fluorescence emission from multiple colloidal solutions of CdSe/ZnS QDs and* ***(b)*** *excitation/emission spectra illustrating the narrow emission and broad absorption*[19]*. Under the same excitation wavelength, the fluorescence shifts along the visible spectrum from red to blue as the size of the QDs decreases. The CdSe/ZnS nanocomposite material undergoes an increase in bandgap energy as its size decreases.*

The number of inherent advantages of QDs over traditional fluorophores, which includes high photoluminescence intensity, high quantum efficiency, high stability, high surface to volume ratio, and narrow emission spectra with broad absorption spectra, contribute to their beneficial use as optical detectors that are compatible with biological processes in the human body[17, 18]. Further advantages include resistance to photobleaching, broad absorption spectra (with 10-50 times larger molar extinction

coefficients), and high efficiency for applications involving Forster resonance energy transfer (FRET), due to multiple binding sites of energy acceptors[19].

Due to their bright and stable fluorescence properties, colloidal quantum dots (QDs) may be suitable for complex *in vivo* conditions[20]. QDs have 10-20 times larger absorption coefficients than conventional dyes which results in more efficient probe excitation under *in vivo* conditions where light scatter is greatly reduced[21]. In addition, the large Stokes shift of QDs helps to eliminate self-absorption and allows the target fluorescence signal to be more clearly separated from the excitation light.

Also, traditional fluorophores have limitations in multicolor detection applications, due to their broad and overlapping emission lines and relatively narrow excitation bands[22]. In contrast, QD fluorophores can have narrow emission and broad absorption lines, resulting in the ability to efficiently excite multiple emission colors with a single excitation source. Commercial CdSe/ZnS QDs are not, however, acceptable for any in vivo applications due to high toxicity of Cd. Replacing the Cd component with Zn as in the case of Mn-doped ZnSe QDs is speculated to be a less toxic alternative to CdSe and is a primary topic explored in this dissertation.

1.3 QD-based MMP biosensing

Biosensors utilize biorecognition strategies as a way of detecting, in real time, the presence or activity of specific biomolecules of interest. A biosensor consists of a biorecognition element such as antibodies, DNA, peptides, and enzymes, which recognizes and interacts/binds with an analyte. A biosensor also consists of a transducer

element, which is responsible for transforming an optical or electrical signal into a quantifiable measurement upon detection of the analyte. Biosensors have numerous applications in the field of biomarkers and diagnostics.

MMP biosensors are commercially available and consist of an ensemble of peptide sensing elements encoded to have a motif specific for a particular MMP of interest, in buffer solution. The peptide, generally less than 10 nm long, will have a FRET acceptor on one side and a FRET donor on another side. The absorption wavelength range of the acceptor overlaps the emission wavelength range of the donor, and therefore the acceptor will quench the fluorescent emission from the donor. However, when an MMP cleaves the peptide sensing element, the donor and acceptor are no longer in the direct vicinity of one another and the fluorescence of the donor is restored, resulting in a quantifiable fluorescent signal that can be correlated to the concentration of active MMPs.

A QD can act as a FRET donor and multiple biomolecules that can act as FRET acceptors can be conjugated to the QD surface (Figure 1.3), resulting in an increase in FRET efficiency[19].

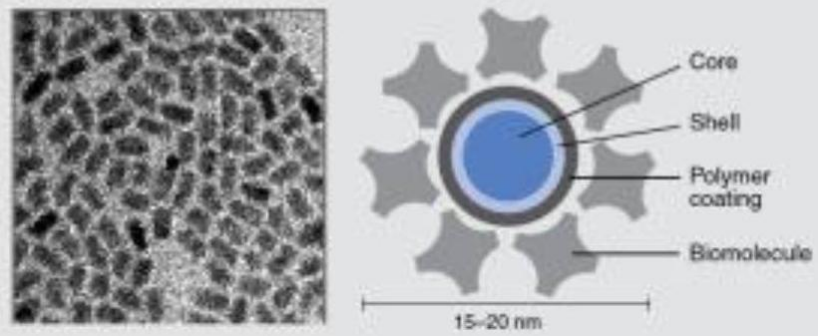

Figure 1.3: *Illustration of a single CdSe/ZnS QD bioconjugate containing an inorganic CdSe core, an inorganic ZnS shell, an organic polymer coating such as PEG, and an outer layer of biomolecules such as antibodies, peptides, streptavidin, DNA, etc*[19]*. For FRET based biosensing, the fluorescent inorganic core/shell works as a donor, and because of the high surface area to volume ratio, multiple acceptors can be conjugated around the surface increasing FRET efficiency.*

As a result of the considerable amount of multiplicity and substrate overlap with the different types of MMPs, there is a redundancy in the functioning of MMPs[23]. With the possibility to coat QDs with substrates for different MMP types, such as collagen, gelatin, or peptides, experiments with multiplexing capabilities are possible, which could better resolve the involvement of the different types of MMPs in pathological conditions.

The long term goal of this research is development of a novel functionalized Cd-free nanomaterial interface by means of self-assembly and bioconjugation strategies that ultimately would be capable of *in vivo* real-time fluorometric biosensing of matrix metalloproteinase (MMP) activity. The successful development of said biosensor is expected to have a great potential for novel applications that will benefit from determination of concentrations of various MMPs, such as characterizing aberrant pain processing at the spinal level during peripheral neuropathic conditions, monitoring and

control of wound healing process, detection of early signs of cancer, early diagnosis of CNS disorders such as ALS, etc.

This biosensing method would be capable of *in situ* studies for MMPs during wound healing. The current method used to study MMP activity at the site of a wound involves immunohistochemistry (IHC), in which fluorescently tagged antibodies can be used to visualize the MMP expression; however, IHC is primarily a qualitative analysis[24] and the inclusion of a biosensing method capable of quantitative analysis to supplement *in situ* IHC observations would be beneficial.

However, MMPs are thought to be implicated in the pathogenesis of other neurological diseases as well, and it is imperative that MMP activity be fully understood and characterized to the point that it can be a reliable biomarker. This may require a highly sensitive method that measures MMP activity directly at the site of motor neuron degradation in the CSF *in vivo*.

An essential feature of an *in vivo* QD-based biosensor is that it will utilize highly efficient Cd-free ZnSe/ZnS QDs that are not expected to display any cytotoxicity. Equally important is the fact that the QDs will be tethered to an optical fiber tip and at no point will be released into the body, thus avoiding the issue of how the QDs are metabolized, where they could end up accumulating, and what could be their long-term effects.

Real-time *in vivo* biosensing of MMP activity is at this stage completely unexplored. Enzyme activity is very temperature- and environment- dependent and so performing experiments under *in vitro* conditions, where lab environment is not the same

as the local environment of the enzymes inside the body, may be distorting the actual kinetics of MMP activity. Measuring the activity outside of the body, as in an *in vitro* procedure, would diminish the enzyme activity due to a decrease in temperature[25]. By utilizing the proposed *in vivo* biosensor, it will be possible to explore the actual kinetics of MMP activity beyond what can be achieved with multi-step assay processes or *in vitro* biosensing.

The bio-interface of the intended biosensor would be peptides bioconjugated to QDs tethered to the silica tip of an optical fiber. By tethering the QDs to the fiber, no QDs would be released into the biosensing site, i.e. into the body, while *in vivo* measurements are being made. The transducer component of the biosensor will be based on measurable perturbations in QD fluorescence that could result from MMP interaction with the bioconjugated peptides. In order to develop a calibration curve, MMP activity sensing measurements will first need to be made in different known concentrations of MMPs in solution.

The two MMPs that have been so far studied much more extensively than the remaining MMPs are MMP-2 and MMP-9. Therefore, for this biosensing research the target molecules will be the MMP-2 and MMP-9 enzymes. It should be emphasized, however, that the proposed concept is very general, and numerous MMPs can be targeted. Also, multiplexing for different proteinase enzymes on the same fiber tip is feasible. The biorecognition mechanism will be based on enzyme substrate selectivity with a peptide of an amino acid sequence that the target MMP selectively binds to. In the case of MMP-9, the substrate peptide includes the motif Val-Val-Pro-Leu-Ser—Leu-Arg-Ser[26], with the MMP-9 enzyme catalyzing hydrolysis of the bond between Ser and Leu amino acid

residues, which results in a cleaved peptide. Peptides of the MMP-9 substrate sequence will be bioconjugated to the surface of QDs, with the intention of using the modified QDs to measure MMP-9 activity from observable changes that can occur in the fluorescence of the QDs when the peptides are cleaved. From the magnitude of perturbation in the QD fluorescence that takes place, a quantitative analysis of MMP-9 activity can be made.

The QDs will be immobilized onto the silica surface, via the use of the silane coupling reagent, 3-mercaptopropyltrimethoxysilane (MPTMS), which contains a thiol functional group that covalently binds to metallic surfaces, due to a known affinity between thiol molecules and metal. Hydrolyzable regions of MPTMS react with hydroxyl groups on hydroxyl modified silica and form stable oxane bonds acting as a linker molecule for covalently bonding QDs to silica.

The optical setup for the biosensor will consist of a diode laser excitation source coupled to a fiber, a Y-fiber (fiber coupler) for dual entrance and exit of the excitation and emission light respectively, and a spectrometer with an array detector at the output end (Fig. 4.1).

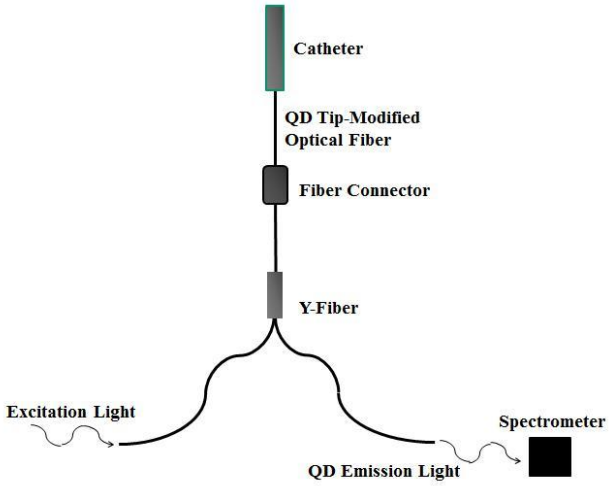

Figure 1.4: *Biosensor setup illustrating the approach to utilizing QD-modified optical fibers to quantify MMP activity by exciting the QDs with light through one input of the fiber coupler and subsequently measuring light emission at the output by a detector array at the output of a spectrometer.*

A number of different peptide motifs have been identified for different types of MMPs. The specific motif for MMP-9 is *Val-Val-Pro-Leu-Ser---Leu-Arg-Ser*, where the MMP-9 enzyme binds between serine and leucine and catalyzes hydrolysis, and the resulting effect is that of a protein cleaved in two, creating a new C and N-terminus. Interestingly enough, a recent finding shows that conjugating the MMP-9 peptide substrate to $Zn_{0.95}Mn_{0.05}Se/ZnS$ QDs results in the quantum efficiency of the sample dropping significantly between the QD and QD-conjugates. Most remarkable is that when the cleaved (enzyme digested) peptide that only contains four amino acids is conjugated to same $Zn_{0.95}Mn_{0.05}Se/ZnS$ QDs at the same QD to peptide ratio as the 9-amino acid polypeptide, the QE drops a lot less dramatically, twenty times less. The change in QE

between the substrate and remnant peptide/QD bioconjugates serves as the basis for the biosensing concept and is illustrated in Figure 1.5.

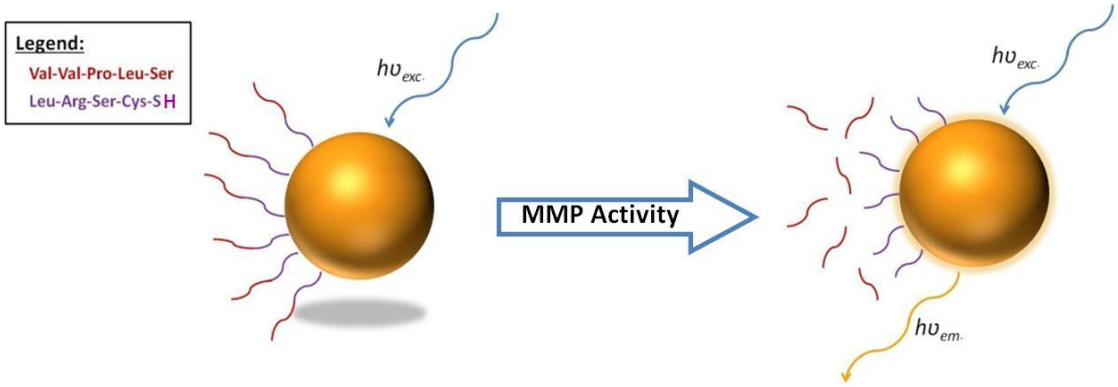

Figure 1.5: *Illustration of QD fluorescence* ***(a)*** *before and* ***(b)*** *after the surface peptide is cleaved.*

It is anticipated that when the MMP-9 enzymes cleave the polypeptide a de-quenching effect will take place of which the intensity can be used to quantify MMP-9 activity. Also, because different peptide motifs for different types of MMPs can be conjugated to QDs with different fluorescence emission wavelengths the biosensor is multiplexing capable, which provides the most powerful tool for diagnostic purposes due to the ability to map the activity of different MMP types at once.

1.4 Objective and scope of dissertation

The objective is to demonstrate MMP detection from CD-free QDs, synthesized under optimal conditions, characterized, and tested for minimal cytotoxicity. Initially different Cd-free QDs were synthesized and characterized, which include InP/ZnS,

InP:Cu/ZnSe, ZnSe:Cu/ZnSe, InP:Mn/ZnSe, ZnSe:Mn/ZnSe, ZnSe:Mn/ZnSeS, and ZnSe:Mn/ZnS QDs. Eventually, it was determined that ZnSe:Mn/ZnS QDs have the highest QE (>90%) and stability and became the QDs of choice for the biosensor development of this dissertation. Following successful development of the synthesis and characterization of ZnSe:Mn/ZnS QDs, thiol based bioconjugation strategies were developed for attaching peptides to the QDs. Because it is ultimately intended to use these Cd-free QD biosensors *in vivo*, a full cytotoxicity study was conducted on the ZnSe:Mn/ZnS QD material of interest. Following cytotoxicity studies different strategies for binding QDs to silica were developed. Finally, the sensitivity of the ZnSe:Mn/ZnS QD biosensors to MMPs was tested.

Chapter 1 introduces the concepts of MMPs, QDs, biosensors, and the rational for developing a Cd-free QD-based *in vivo* MMP biosensor. Chapter 2 details the synthesis and characterization of ZnSe:Mn/ZnS QDs in chloroform. Chapter 3 details the thiol-based bioconjugation strategy for attaching biomolecules to the ZnSe:Mn/ZnS QDs and their subsequent dispersion into cerebral spinal fluid (CSF). Chapter 4 contains the details and the results of the cytotoxicity studies of ZnSe:Mn/ZnS QDs with macrophage cells. Chapter 5 contains the strategies and results for attaching the ZnSe:Mn/ZnS QDs to silica. Chapter 6 contains the biosensing data from a commercially available assay and the developed ZnSe:Mn/ZnS QD biosensors to commercially available active mouse MMP-9 enzymes. Chapter 7 is the final chapter with concluding remarks and recommendations.

Chapter 2

Synthesis and characterization of ZnSe:Mn/ZnS colloidal quantum dots

2.1 Synthesis of highly luminescent Cd-free ZnSe:Mn/ZnS quantum dots

The synthesized ZnSe:Mn/ZnS QDs reached QE above 90%, which was drastically higher than QE values for any other colloidally synthesized QD materials: InP/ZnS, InP:Cu/ZnSe, ZnSe:Cu/ZnSe, InP:Mn/ZnSe, ZnSe:Mn/ZnSe, and ZnSe:Mn/ZnSeS. In addition, the ZnSe:Mn/ZnS QDs did not lose their fluorescence properties when undergoing any kind of processing. In specific, as a control the ZnSe:Mn/ZnSeS and ZnSe:Mn/ZnS QDs were subjected to the bioconjugation process (later described in chapter 3) without the peptide conjugate present (referred to here as raw processing for clarity) to evaluate how the fluorescence is affected by the steps of the process itself. Needless to say, ZnSe:Mn/ZnSeS QDs would lose fluorescence as a result of raw processing and ZnSe:Mn/ZnS QDs would not. Because of their superior fluorescent properties and resistance to raw processing, ZnSe:Mn/ZnS QDs became the QDs of choice for the development of the biosensor for this dissertation. In addition, like the previous doped QDs mentioned, the optical properties of ZnSe:Mn/ZnS QDs possess thermal stability in comparison to CdSe and ZnSe[27], meaning the fluorescence intensity drops very little in comparison to the fluorescence intensity of CdSe and ZnSe QDs with increases to temperature.

The colloidal synthesis of ZnSe:Mn/ZnS core/shell QDs is a one pot process; the synthesis is done all in one reaction vessel without any sub purification steps. The initial phase of the synthesis involves the formation of ZnSe seeds by reacting zinc stearate and selenourea. After formation of the ZnSe seeds the Mn precursor is added to the reaction

at a lower temperature, to allow adsorption of the Mn ions to the surface of the ZnSe seeds. The temperature is increased in order to diffuse the Mn dopant into the ZnSe crystal lattice. Multiple injections of Zn precursor solution is added to the reaction vessel in progressively increasing amounts to add a passivation layer, which results in better optical properties. Due to the thermal stability of the ZnSe:Mn QDs growing at this point, the orange fluorescence of the QDs could be monitored with a UV lamp, while the reaction was still taking place at a temperature of 260 °C. In addition, another passivation layer was added, a ZnS outer shell, to give the QDs further optical enhancement and stability.

2.1.1 Basic chemical reactions

1 mmol (95%$ZnC_{36}H_{30}O_4$ + 5%$MnC_{36}H_{30}O_4$) + 1 mmol $SeC(NH_2)_2$ → 1 mmol **$Zn_{0.95}Mn_{0.05}Se$** + 1 mmol $C_{37}H_{34}O_4N_2$ **(core reaction)**

0.90 mmol $ZnC_{36}H_{30}O_4$ + 1.1 mmol $SC(NH_2)_2$ → 0.90 mmol **ZnS** + 0.20 mmol $SC(NH_2)_2$ + 0.90 mmol $C_{37}H_{34}O_4N_2$ **(shell reaction)**

2.1.2 Synthesis materials

The precursors used to make the core ZnSe:Mn QDs were zinc stearate ($ZnSt_2$), purchased from Acros Organics, selenourea ($SeC(NH_2)_2$), purchased from Aldrich, and manganese stearate ($MnSt_2$), synthesized in house using anhydrous manganese(II)chloride ($MnCl_2$), purchased from Acros Organics, and tetramethylammonium hydroxide pentahydrate (TMAH), purchased from Sigma-Aldrich. The precursors used to make the ZnS shell of the QDs were zinc stearate ($ZnSt_2$),

purchased from Acros Organics, and 99% thiourea ($SC(NH_2)_2$), purchased from Acros Organics. The solvents used for the synthesis was octadecene ODE, purchased from Aldrich, and anhydrous ethanol, purchased from Aldrich. The surfactants used were 80% - 90% oleylamine, purchased from Acros Organics, and stearic acid (SA), purchased from Acros Organics.

2.1.3 Synthesis procedure

The Mn-doped ZnSe/ZnS QDs were synthesized under air-free conditions, using a one-pot method. The synthesis presented forthwith was modified from Pradhan *et al* (2007)[28] and Acharya *et al* (2010)[29], in that a ZnS shell was added to the nanoparticles using a thiourea S precursor, and special care was taken to have the synthesis done under air-free conditions. The ZnS shell modification was sourced from Zhu *et al* (2010)[30].

(a)

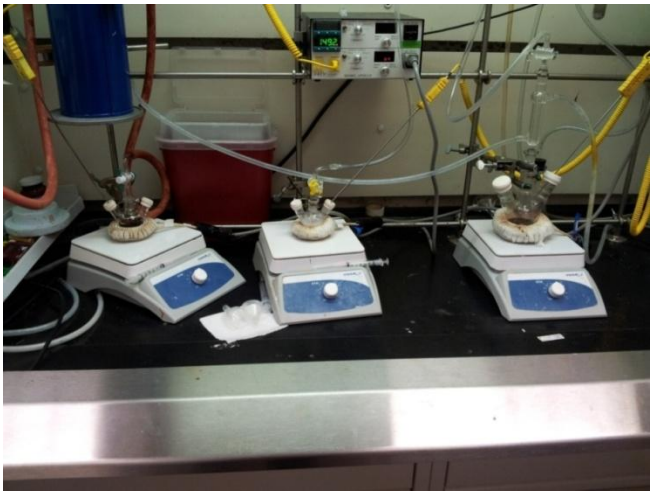

(b)

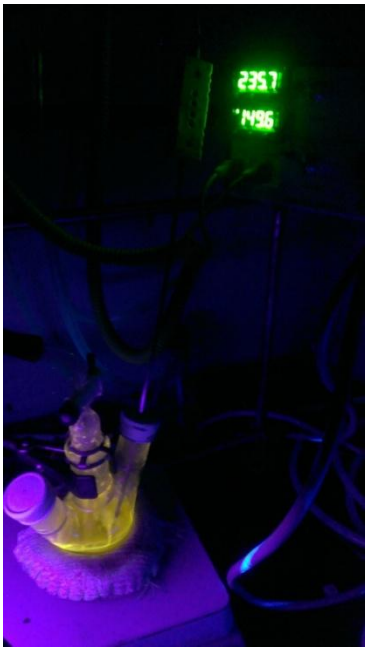

Figure 2.1: (a) *The colloidal synthesis of ZnSe:Mn/ZnS QDs was done in a strictly air-free atmosphere, with precursors prepared under Ar atmosphere and* ***(b)*** *ZnSe:Mn/ZnS QDs synthesized in octadecene illuminated with a blacklight at high tempterature (235.7 °C), indicating their thermal stability. Precursor solutions were prepared in different three-neck flasks under Ar by connecting the reaction vessels to a Schlenkline gas manifold.*

Initially, $MnSt_2$ stock powder was synthesized according to supporting information by Pradhan 2007 *et al*. First 5.690 g of SA was mixed with 37.89 mL of methanol in a reaction flask. The reaction flask was purged with Ar, and the solution was put under stirring and heated to 60 °C until the SA dissolved. Next, the solution was cooled to room temperature.

3.625 g of TMAH was dissolved into 12.63 mL of methanol and added to the reaction flask. 1.259 g of the Mn precursor $MnCl_2$ was dissolved into 12.63 mL of

methanol and added to the primary reaction flask. The resulting mixture was allowed to react at room temperature and under stirring until a white $MnCl_2$ precipitate formed. The precipitate was centrifuged in methanol at 4,000 rpm three times and then re-dispersed into 18 mL of methanol. The solution was dried under vacuum and stored in a 20 mL vial.

For the QD synthesis, 63 mg of $ZnSt_2$ was dissolved into 5 mL of ODE and heated to 260 °C in a reaction flask under Ar. In a separate reaction flask, 123 mg of selenourea (the Se precursor) was mixed with 10 mL of oleylamine 80%-90% and heated to 200 °C, in order to dissolve the selenourea into the oleylamine, in a separate reaction flask under Ar. After the selenourea solution cooled to 130 °C, it was injected into the flask containing the $ZnSt_2$ at 260 °C, after which the temperature was brought to 240 °C. The Mn dopant was prepared by mixing 6.3 mg of $MnSt_2$ into 3 ml of ODE (additional heating was required to fully solubilize the Mn precursor). The Mn precursor was injected into the reaction flask at 240 °C and allowed to react for one hour. For the ZnSe shell, 1.159 g of $ZnSt_2$ and 0.515 g of SA 97% was mixed with 18.4 mL of ODE. The $ZnSt_2$ and SA were dissolved into the ODE by heating the mixture under Ar to 150 °C. The temperature of the reaction was increased to 260 °C (the injection temperature) and 0.96 mL of $ZnSt_2$/SA/ODE was injected and allowed to react for 10 minutes and subsequently an additional 0.96 mL of the same mixture was added again. The reaction flask was cooled to 240 °C for 15 minutes and then heated back to the injection temperature for an injection of 1.33 mL of the of $ZnSt_2$/SA/ODE mixture before setting the temperature to 240 °C. The injections are repeated in this manner at progressively

increasing volumes of 1.69 mL, 2.25 mL, and 2.81 mL at the 260 °C injection temperature, always allowing for a 15 minute anneal step at 240 °C after every injection.

For the ZnS outer shell synthesis, the reaction solution was brought to 70 °C. 86 mg of thiourea was mixed with 3 mL anhydrous ethanol and dissolved with additional heating. The entire thiourea solution was injected into the reaction flask at 70 °C. In order to evaporate the ethanol, the solution was put under vacuum and the temperature was slowly increased, first to 80 °C and then to 120 °C, while always allowing for the solution bubbling to stop before increasing the temperature. Finally the temperature of the reaction mixture was increased to 260 °C and 3.65 mL of the $ZnSt_2$/SA/ODE solution was added. The reaction temperature was then dropped to 240 °C for 30 minutes before being increased to 260 °C for a final injection of 4.75 mL of the $ZnSt_2$/SA/ODE mixture, followed by 30 minutes of annealing at 240 °C.

The synthesized QDs were then washed and centrifuged at 4,000 RPM with acetone for 5 minutes, only once, and finally stored in chloroform.

2.2 Characterization

The ZnSe:Mn/ZnS QDs were structurally characterized with a 2010 JEOL high resolution transmission electron microscope (HRTEM). In conjunction with HRTEM, energy-dispersive X-ray spectroscopy (EDS) measurements were made with an X-ray detector by Oxford Instruments and a high resolution electron energy loss spectrometer. In addition, X-ray diffraction (XRD) was measured with a Rigaku SmartLab setup using a Cu source operating at 40 kV – 44 mA, with a 0.02° step size and a 4°/min scan rate. The scanning range was 10 – 80° 2θ.

Optical characterization was carried out with a Joriba Joban Yvon Fluorolog – 3 spectrofluorometer for photoluminescence measurements, a Cary 5000 UV-Vis-NIR dual beam spectrometer, and dynamic light scattering (DLS) measurements were made with Wyatt Dynapro DLS system. Quantum efficiency measurements were made with a 4 inch integrating sphere.

2.2.1. Transmission electron microscopy

In preparation for TEM imaging, the ZnSe:Mn/ZnS QDs in chloroform were dropped and dried onto a copper grid. In order to induce super-lattice self-assembly, when dropping the QD solution, a solvent immiscible with chloroform, two drops of water in this case, was first dropped onto the grid, following two drops of the QD solution. Utilizing this coordinating solvent method, the QDs self-assemble into a highly ordered lattice, upon drying[31].

The imaged ZnSe:Mn/ZnS QDs from the 2010 JEOL high resolution transmission electron microscope (HRTEM) can be observed in **Figure 2.2a-f**. Ten images were used in conjunction with Digital Micrograph Software to analyze the size of these particular QDs; the average overall diameter turned out to be 5.48 nm, assuming spherical shape.

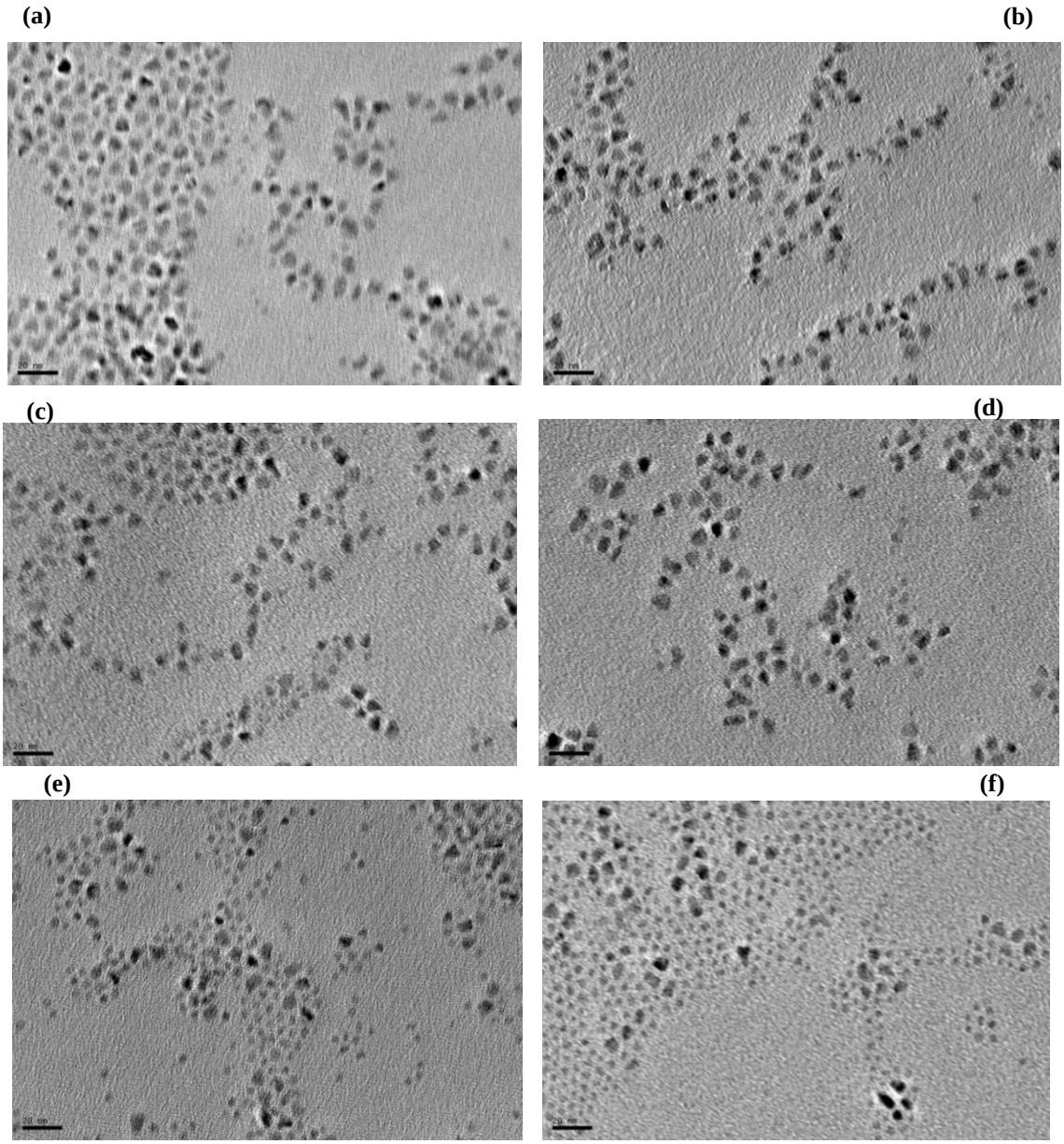

Figure 2.2: (a)-(f) *transmission electron microscopy images of ZnSe:Mn/ZnS QDs. The scale bars are 20 nm.*

2.2.2 Energy-dispersive X-ray spectroscopy

Figure 2.3 is an energy x-ray dispersive spectroscopy EDS spectrum for ZnSe:Mn/ZnS QDs dried onto a TEM grid. Note the presence of all four required elements Zn, Se, S, and Mn. The Cu and C signals are a result of the TEM grid.

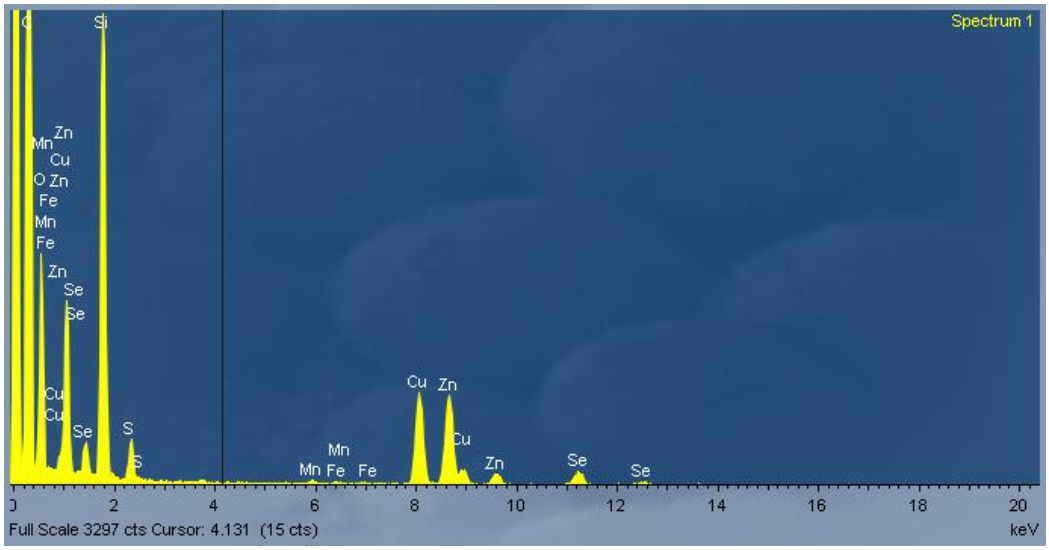

Figure 2.3: *EDS spectrum for ZnSe:Mn/ZnS QDs confirming the presence of Zn, Se, Mn, and S.*

2.2.3 X-ray diffraction

In order to identify the actual phases of the nanomaterial that results from the ZnSe:Mn/ZnS QD synthesis, XRD measurements were taken with a a Rigaku SmartLab XRD setup, using a Cu source operating at 40 kV – 44 mA, with a 0.02° step size and a 4°/min scan rate. In preparation for the XRD measurement, colloidal ZnSe:Mn/ZnS QDs were dropped onto a zero background holder. **Figure 2.4** is the XRD pattern the sample produced. From the XRD pattern three phases were identified from the International

Centre for Diffraction Data (ICDD): zinc selenide (ZnSe), zinc selenium sulfide ($ZnSe_{0.74}S_{0.26}$), and zinc manganese selenide ($Zn_{0.95}Mn_{0.05}Se$).

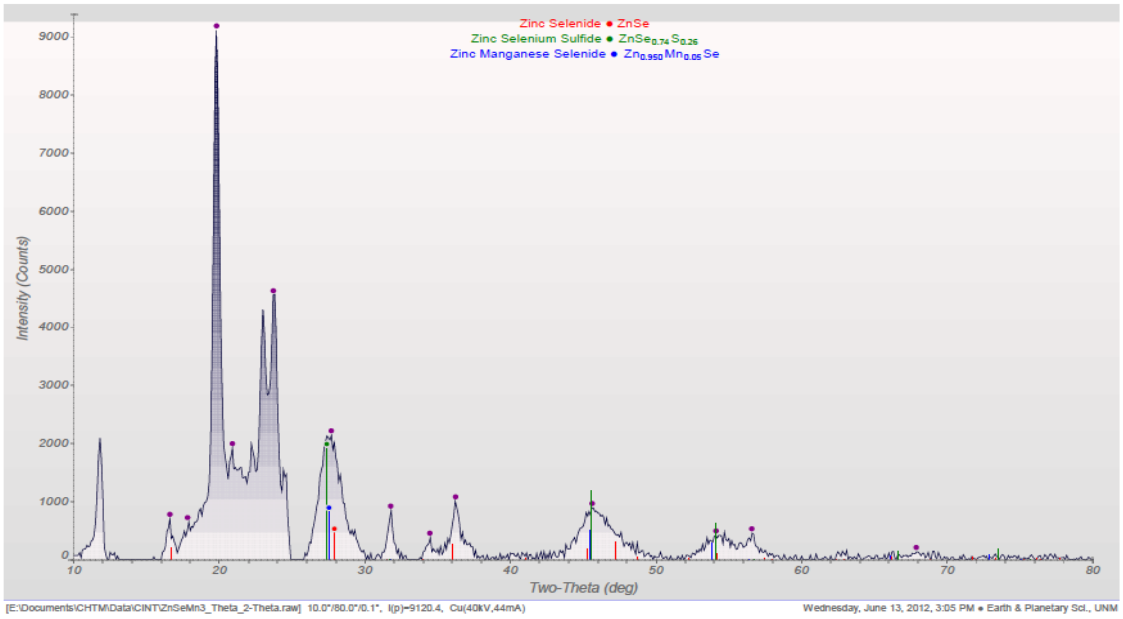

#	Phase ID	Chemical Formula	PDF-#	●	#d-I	RIR	Wt%	FOM	Scale(I)	Shift(x)	Scale(d)	Space Group	a	b	c
1	Zinc Selenide	ZnSe	01-077-8903		60	5.50	0.0	2.4	0.050	-0.220	1.000	tP4/nmm (129)	3.9800	3.9800	5.2300
2	Zinc Selenium Sulfide	$ZnSe_{0.74}S_{0.26}$	04-002-1204	●	17	9.43	0.0	7.0	0.210	-0.200	1.000	cF-43m (216)	5.5990	5.5990	5.5990
3	Zinc Manganese Selenide	$Zn_{0.950}Mn_{0.05}Se$	01-079-0014		17	10.04	0.0	7.7	0.090	0.300	1.000	cF-43m (216)	5.6721	5.6721	5.6721

Figure 2.4: *Powder XRD spectrum for ZnSe:Mn/ZnS QDs.*

2.2.4 Dynamic light scattering

In order to obtain the average-size and size-distribution, based on the hydrodynamic radius, a measurement using DLS was taken. The ZnSe:Mn/ZnS QDs were diluted in chloroform before the measurement. **Figure 2.5** is the resulting size histogram obtained from DLS, indicating an average hydrodynamic radius of 10.72 nm with a size distribution ranging between ~ ≤1 to 35 nm. The average radius obtained from DLS suggests the particle size to be significantly larger than the 5.48 diameter particle size determined by processing the TEM images through the Digital Micrograph

software. This is likely due to the fact that there is an additional organic layer coating the QDs, the stearic acid surfactant, which cannot be imaged with TEM, and therefore only the inorganic component of the QDs show on TEM. Size data as obtained from DLS accounts for both the inorganic (ZnSe:Mn/ZnS) and organic (stearic acid) surfactant components of the QDs. Stearic acid is a long molecule with an 18 carbon chain, which likely accounts for the size difference.

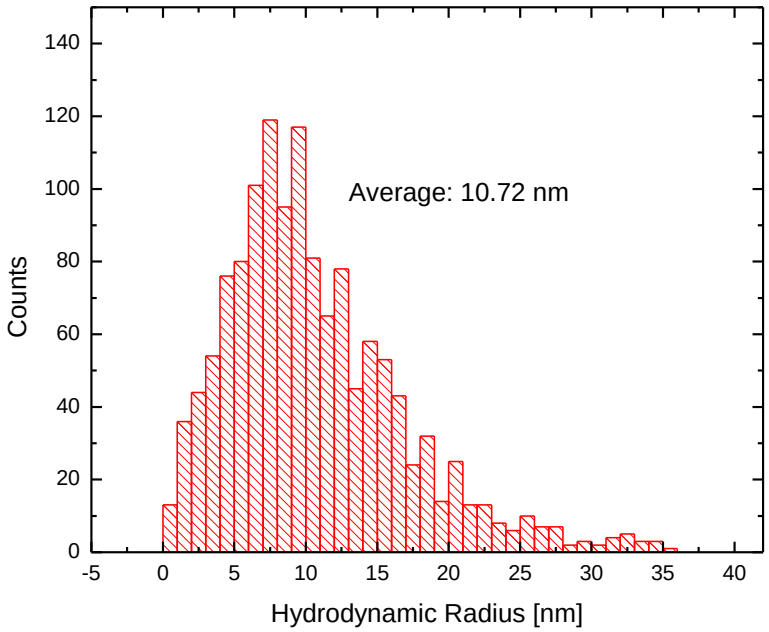

Figure 2.5: *DLS spectrum for ZnSe:Mn/ZnS colloidal QDs in chloroform indicating a reasonably good size distribution with an average hydrodynamic radius of 10.72 nm.*

2.2.5 Zeta Potential

The zeta potential for ZnSe:Mn/ZnS colloidal QDs in chloroform was measured with a Malvern Zetasizer. The zeta potential distribution can be viewed in **Figure 2.6**. The zeta potential is 54.6 mV, which, being between 40 to 60 meV, is indicative of good colloidal stability.

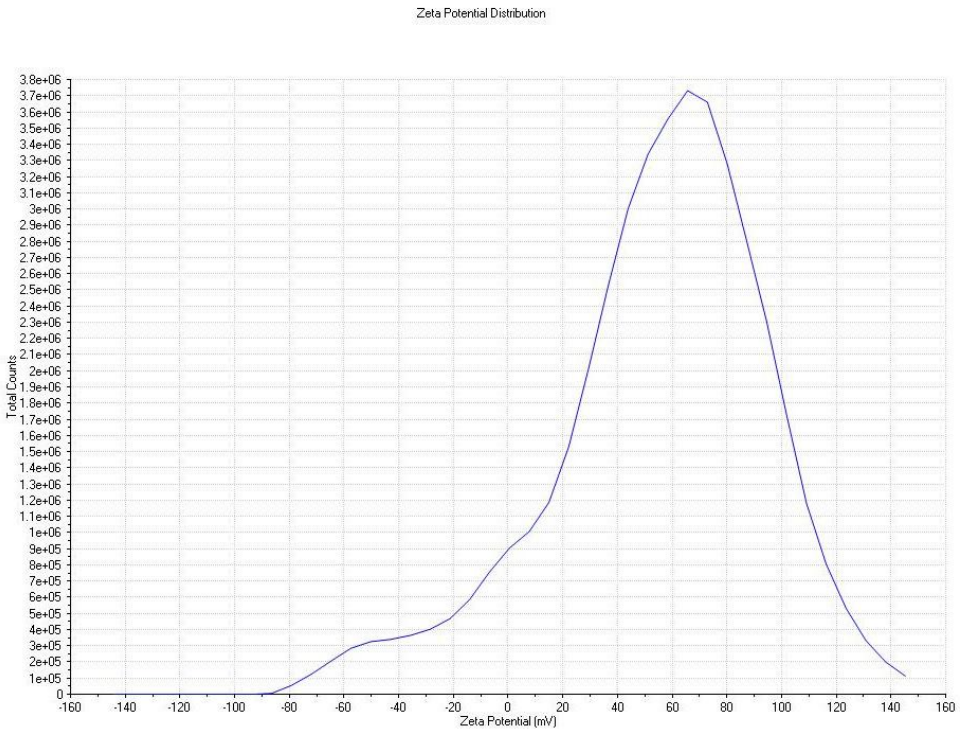

Figure 2.6: *Zeta potential distribution for ZnSe:Mn/ZnS QDs in chloroform showing a peak value of 54.6 mV in the zeta potential distribution curve.*

2.2.6 Absorption

Absorption for ZnSe:Mn/ZnS QDs in chloroform was by measured with a Varian Cary 5000 UV-Vis-NIR spectrophotometer by scanning absorption over 250 nm – 600

nm range, measuring ZnSe:Mn/ZnS QDs in chloroform and pure chloroform. With the dual beam functionality of the spectrophotometer, absorption of pure chloroform was subtracted from the absorption of the colloidal nanocrystal sample, giving an absorption spectrum of the nanocrystals alone (**Figure 2.7**).

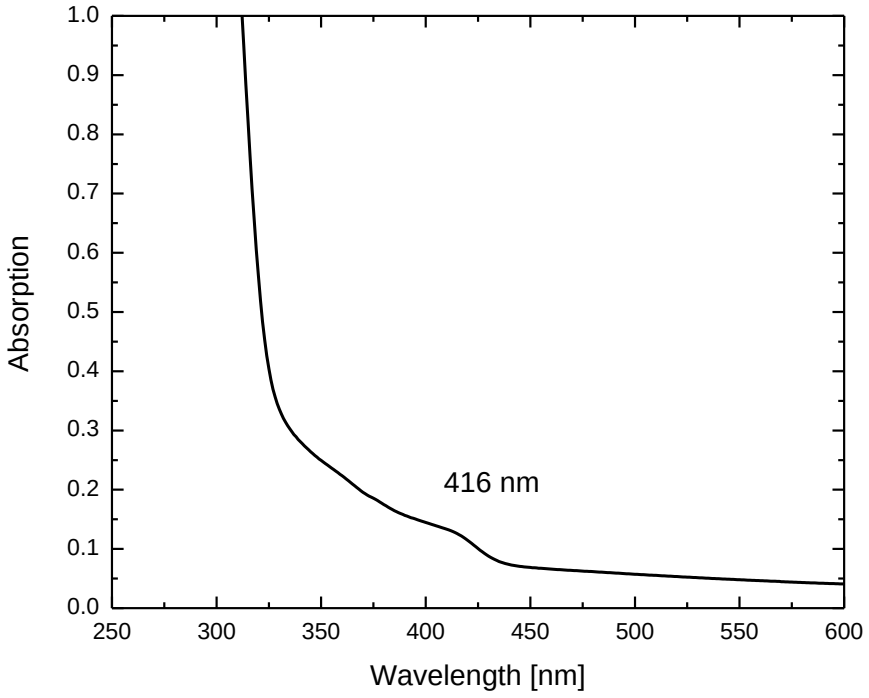

Figure 2.7: *Absorption spectrum for ZnSe:Mn/ZnS QDs in chloroform indicating a small feature around 416 nm wavelength.*

2.2.7 Photoluminescence and quantum efficiency

The photoluminescence excitation (PLE) and photoluminescence (PL) for colloidal $Zn_{0.95}Mn_{0.05}Se$/ZnS QDs in chloroform can be observed from the spectra in

Figure 2.8 (a) and **(b)**, respectively. The sample has a bright orange (597 nm) emission wavelength when excited with near UV (320- 400 nm) wavelength, which is believed to be an atomic energy transition from the manganese dopant. The optimal wavelength as indicated by the PLE spectrum indicates 380 nm optimal excitation wavelength. However, 400 nm wavelength was used to determine the high 86.5% QE, due to the fact that the integrating sphere absorbs UV wavelength. Additionally, as can be seen from **Figure 2.9 (a)** and **(b)**, there is another PL emission feature that can be observed at 487 nm emission wavelength (QE 4.2%) by exciting with a longer 436 nm wavelength. Based on past findings, when making these $Zn_{0.95}Mn_{0.05}Se/ZnS$ QDs hydrophilic with mercaptoacetic acid, via thiol binding to the surface, this 487 nm emission disappears, only leaving the orange 597 nm emission.

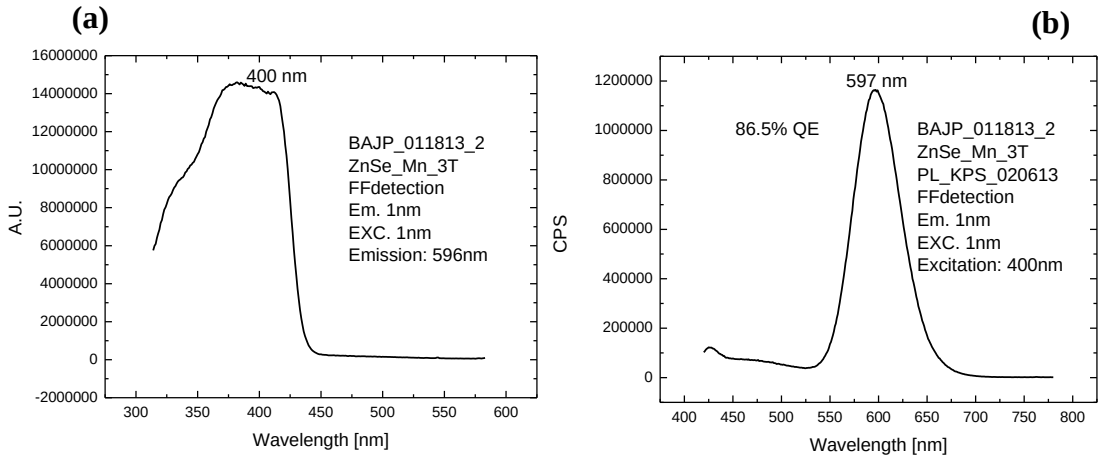

Figure 2.8: *PL* ***(a)*** *excitation and* ***(b)*** *emission spectra for* $Zn_{0.95}Mn_{0.05}Se/ZnS$ *colloidal QDs in chloroform. For the excitation spectrum* ***(a)*** *596 nm parked emission wavelength was used to generate the spectrum. For the emission spectrum* ***(b)*** *400 nm excitation wavelength was used to generate the spectrum. The emission observed in* ***(b)*** *is due to the Mn atomic energy level transitions as a result of the Mn doping in the nanocrystals. The QE for this particular emission peak is 86.5%.*

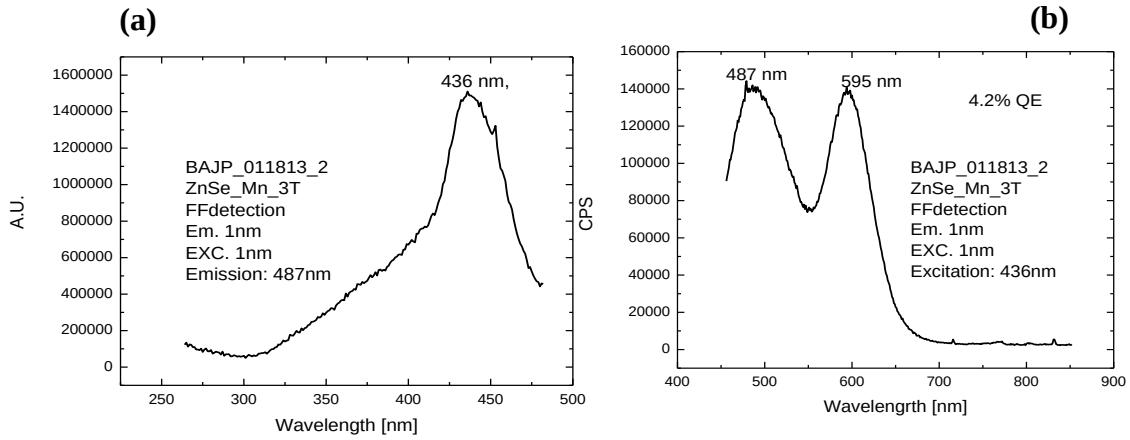

Figure 2.9: *Surface defect PL* ***(a)*** *excitation and* ***(b)*** *emission spectra for* $Zn_{0.95}Mn_{0.05}Se/ZnS$ *colloidal QDs in chloroform. For the excitation spectrum* ***(a)*** *487 nm parked emission wavelength was used to generate the spectrum. For the emission spectrum* ***(b)*** *436 nm excitation wavelength was used to generate the spectrum. The emission observed in* ***(b)*** *at 595 nm wavelength is due to the Mn atomic energy level transitions as a result of the Mn doping in the nanocrystals and the emission observed at 487 nm is believe to be surface defect related and is highly sensitive to surface modification. The QE for the surface defect emission peak is 4.2%.*

2.3 Summary

All in all, the synthesis of highly luminescent, stable ZnSe:Mn/ZnS QDs was successful and has been duplicated several times. The 597 nm Mn emission is relatively stable in comparison to that of the 487 nm surface defect emission, which lowers in QE at a faster rate than the Mn emission. The specific time evolution of the QE stability can be observed in **Figure 2.10**. Note the greater rate at which the QE lowers for the surface defect emission **Figure 2.10b.**

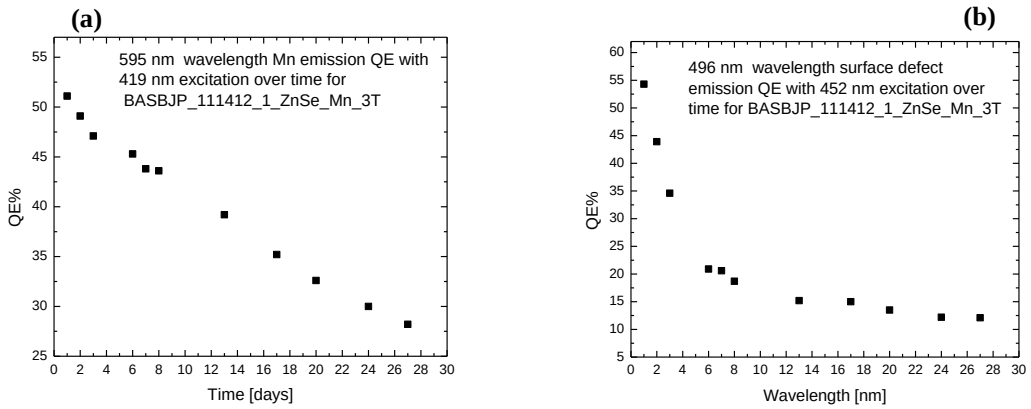

Figure 2.10: *(a) and (b) time evolved QE for Mn and surface defect emission, respectively for ZnSe:Mn/ZnS QDs.*

As a result of the dropping QE, during the next phases of this research (bioconjugation, cytotoxicity, silica linking, and biosensing) the QDs were freshly synthesized about once every two months.

Chapter 3

MMP substrate peptide conjugation to ZnSe:Mn/ZnS quantum dots

3.1 QD peptide conjugation

There are a number of bioconjugation strategies for linking biomolecules to QDs, such as EDC linker molecules, streptavidin / biotin affinity, click chemistry, and thiol-metal affinity. Since the intended QD biosensor would rely on modifications to the biomolecule on the surface of the QD, it would be best to minimize the space between the sensing biomolecule and the luminescent QD surface. Therefore it is intended to use the thiol / metal affinity strategy to link the polypeptides with the small molecule, cysteine. Cysteine contains a thiol molecule, which will bond to metals[32].

3.2 Bioconjugation concept (biosensor assembly)

A polypeptide/QD bioconjugation process was modified from the work of Shi *et al* 2007. A basic solution containing a mix of benzylamine and dimethylformamide with the $Zn_{0.95}Mn_{0.05}Se$/ZnS core/shell QDs and MMP-9 peptide substrate molecules were mixed vigorously with a fixed vortexer. After which, they were washed with PBS and purified with spin dialysis using Microcon 30 kDa centrifuge filters. **Figure 1** illustrates the simplicity of the idea, where a 9-amino-acid residue polypeptide containing the MMP-9 substrate peptide motif as well as a cysteine amino-acid residue at the C-terminus, due to the thiol-metal affinity, covalently bonds to the zinc sulfide surface of the QDs, directly between sulfur and the metallic surface.

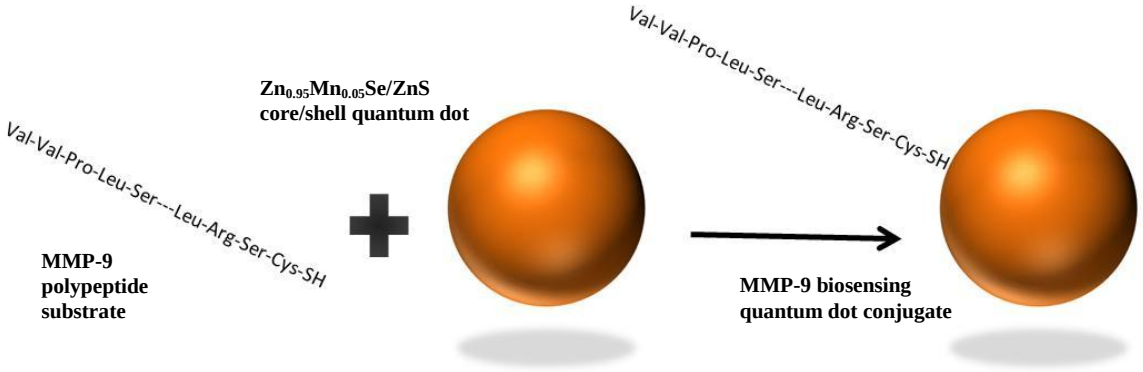

Figure 3.1: *Illustration depicting the bioconjugation process, the assembly of the QD-based biosensor. Due to the thiol-metal affinity, the thiol group in the cysteine amino acid residue on the C-terminus of the polypeptide forms a covalent bond, via nucleophilic substitution reaction, to the surface of the QD.*

3.3 Bioconjugation process

Certain modifications were made from the procedure developed by Shi *et al* 2007, which include replacing pyridine with benzylamine, because pyridine was etching the QDs, causing these particular $Zn_{0.95}Mn_{0.05}Se/ZnS$ QDs to lose a significant portion of their fluorescence intensity. Also, because the benzylamine is already basic, with a measured pH of 11.34, no tetramethyl ammonium hydroxide was added to increase the pH. The reason pH is increased is to negatively charge the thiol groups in order to facilitate the binding of the peptides with the QDs.

3.3.1 Materials

For biofunctionalization, the cys-containing peptides were purchased from GenScript; 99% benzylamine was purchased from Acros Organics; dimethylformamide was purchased from EMD; pH 7.4 phosphate buffered saline solution (PBS) was purchased from Gibco, and artificial cerebral spinal fluid was purchased from Harvard Apparatus.

3.3.2 Procedure

This procedure is a modification of a protocol by [Shi 2007].

1 mL of $Zn_{0.95}Mn_{0.05}Se/ZnS$ QDs in chloroform (as synthesized) was centrifuged with acetone at 4,000 RPM. After pouring off the supernatant, the QDs were re-suspended in 2 ml of 9:1 (v:v) benzylamine/dimethylformamide (DMF) solution. 1 mg of the MMP-9 peptide substrate was dissolved into 0.200 mL of DMF. The peptide/DMF solution was added to the QD/benzylamine/DMF solution, and the resulting mixture was vortexed for 30 minutes. The peptide/QD conjugates were centrifuged and redistributed in 2 mL of DMF. The mixture was centrifuged again and re-dispersed in 2 mL of PBS. The peptide/QD conjugate solution was subjected to 2 cycles of spin dialysis by using 4 Microcon (ultracell YM-30) centrifugal filter devices. Afterwards, the peptide/QD conjugates were dispersed into 2 mL of PBS and stored in a fridge at 4 °C.

3.4 Characterization

Two different batches consisting of the $Zn_{0.95}Mn_{0.05}Se/ZnS$ QDs/peptide conjugates containing the substrate and remnant peptides were measured with a Wyatt dynamic light scattering apparatus. In order to verify the difference in hydrodynamic radius as a result of the different lengths between the remnant and substrate peptides, a size distribution was measured for both samples.

3.4.1 Dynamic light scattering (DLS)

In figure **3.2 (a)** and **(b)** a small decrease in the average hydrodynamic radius can be observed from 3.53 to 3.26 nm.

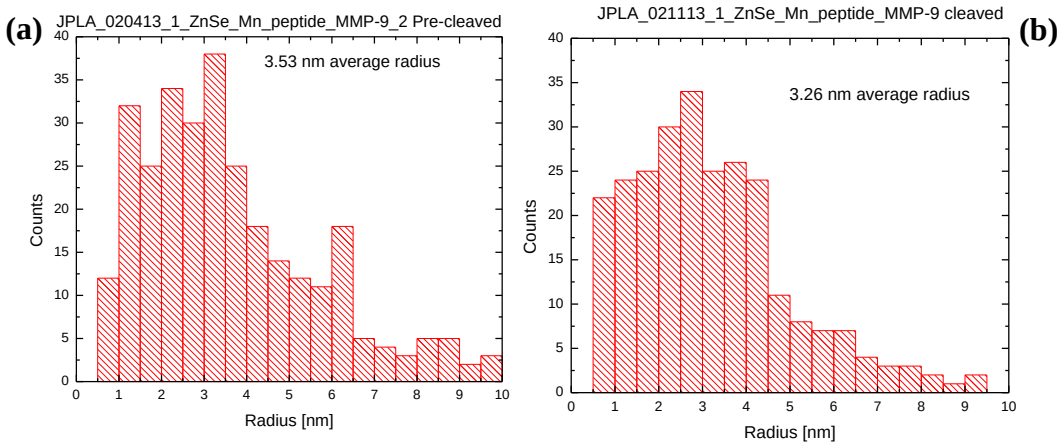

Figure 3.2: *Size distribution histograms as generated by dynamic light scattering (DLS) for $Zn_{0.95}Mn_{0.05}Se/ZnS$ core/shell quantum dots conjugated with **(a)** polypeptides containing 9 amino acid residues and **(b)** polypeptides containing 4 amino acid residues. Though there's not much of a change, the average hydrodynamic radius does decrease for the remnant peptides.*

3.4.2 Zeta potential

Additionally, in order to see if some sort of correlation with surface charge could be made with the increasing QE as a result of the increasing remnant peptide percentage, a series of zeta potential measurements were made with a Malvern Zetasizer (**Figure 3.3**). Solutions were mixed to contain 0%, 25%, 50%, 75%, and 100% remnant peptide/substrate peptide ratios. The Zeta potential increased, overall, from substrate to remnant peptide/QD conjugates, suggesting that the percentage of remnant polypeptide MMP-9 substrates does in fact have an effect on the surface charge of these particular QDs.

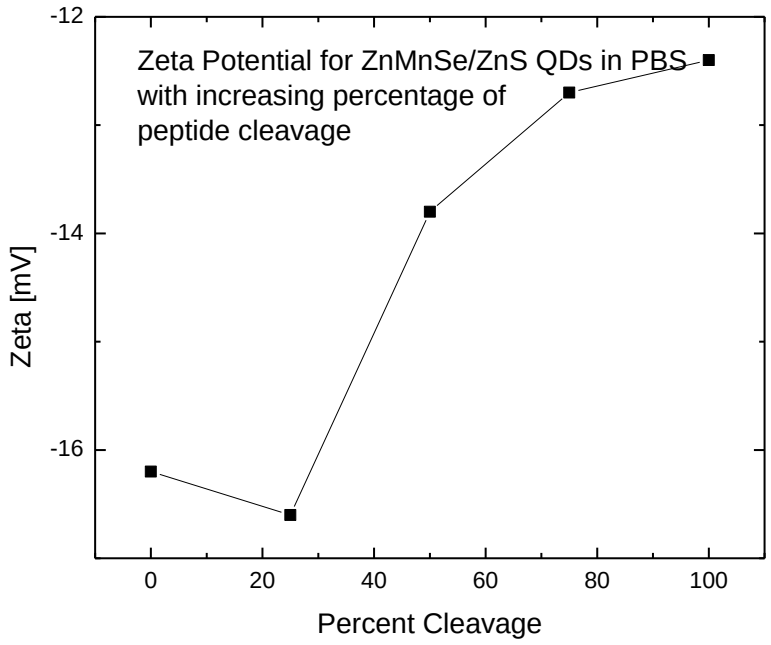

Figure 3.3: *Plot indicating how zeta potential changes with increasing percentage of cleaved peptides.*

3.4.3 Absorption

Absorption was measured using a Varian Cary 5000 UV-Vis-NIR spectrophotometer for substrate and remnant peptide/ $Zn_{0.95}Mn_{0.05}Se/ZnS$ QDs in PBS by scanning between 200 – 800 nm, which can be observed in **Figure 3.4**. Both absorption lines possess a feature at 257 nm, with the substrate peptide/QD feature being slightly lower in absorption than the remnant peptide/QD feature.

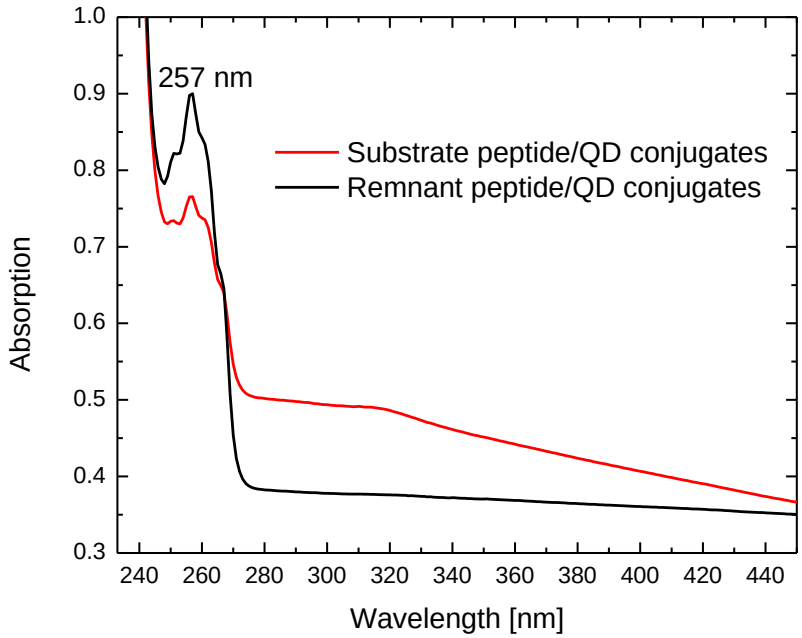

Figure 3.4: *Absorption spectra for substrate and remnant Zn0.95Mn0.05Se/ZnS QDs in PBS. Both lines exhibit a feature at 257 nm.*

3.4.4 Photoluminescence and quantum efficiency

A Horiba Joban Yvon spectrofluorometer was used to characterize the photoluminescence (PL) and photoluminescence excitation (PLE) properties, and the quantum efficiency (QE) of $Zn_{0.95}Mn_{0.05}Se/ZnS$ QDs in chloroform and $Zn_{0.95}Mn_{0.05}Se/ZnS$/peptide QD conjugates.

As described in chapter 2, $Zn_{0.95}Mn_{0.05}Se/ZnS$ QDs has a bright orange (597 nm) emission wavelength when excited with near UV (320- 400 nm) wavelength, which is believed to be an atomic energy transition from the manganese dopant. Additionally, there is another PL emission feature that can be observed at 487 nm emission wavelength (QE 4.2%) by exciting with a longer 436 nm wavelength, which is believed to be surface defect related.

Based on past findings, when making $Zn_{0.95}Mn_{0.05}Se/ZnS$ QDs hydrophilic with mercaptoacetic acid, via thiol binding to the surface, this, surface defect related, 487 nm emission disappears, only leaving the orange 597 nm emission. The past hydrophilization experiments were successful because the previously hydrophobic stearic acid capped $Zn_{0.95}Mn_{0.05}Se/ZnS$ QDs became readily dispersible in water due to the thiol bonding of mercaptoacetic acid to the metallic ZnS surface. Because of this, observing the loss of the 487 nm surface defect emission can be used as a verification to ensure that the peptides have bonded to the QD surfaces via thiol boding from the cysteine residue.

When applying the peptide conjugation procedure, the 487 nm surface defect emission does in fact go away. Most remarkably is that the QE of the orange 593 nm emission drops to 39.1%.

Figure 3.5 (a) and **(b)** are the PLE and PL spectra for colloidal $Zn_{0.95}Mn_{0.05}Se/ZnS$/peptide conjugates in PBS, respectively. The optimal excitation red shifts considerably to 318 nm, as opposed to 380 nm for the non-conjugated QDs studied in Figure 6. When the remnant peptides (the 4 amino acid peptide that results after MMP-9 cleaves it) were conjugated to the colloidal $Zn_{0.95}Mn_{0.05}Se/ZnS$ QDs, the QE ends up being 90.8%. **Figure 3.6 (a)** and **(b)** are the PLE and PL spectra, respectively, for the peptide/QD conjugated using the remnant peptide.

Again 400 nm excitation wavelength was used to excite the samples in the integrating sphere during QE measurement because the walls of the integrating sphere absorb UV. This drastic change between QE, 39.1% to 90.8%, for the substrate and remnant samples is a notable preliminary result for the viability of these particular peptide/QD conjugates as a biosensing system of MMP-9 enzymes.

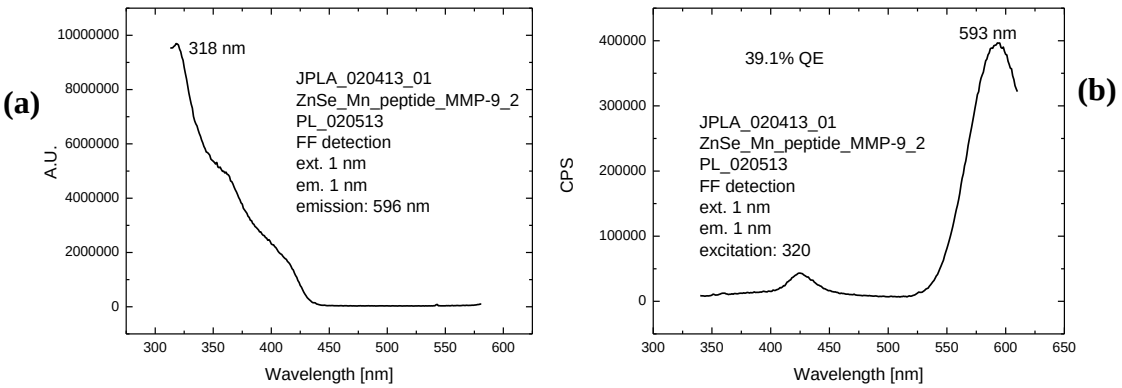

Figure 3.5: (a) *excitation and* ***(b)*** *emission spectra for* $Zn_{0.95}Mn_{0.05}Se/ZnS$*/peptide colloidal QD conjugates in PBS with the substrate 9 amino acid residue polypeptide. For the excitation spectrum* ***(a)*** *596 nm parked emission wavelength was used to generate the spectrum. For the emission spectrum* ***(b)*** *320 nm excitation wavelength was used to generate the spectrum, which has a 595 nm maximum emission wavelength. The emission observed in* ***(b)*** *is due to the Mn atomic energy level transitions as a result of the Mn doping in the nanocrystals. The QE for this particular emission peak is 39.1%, as determined from the integrating sphere with an excitation of 400 nm.*

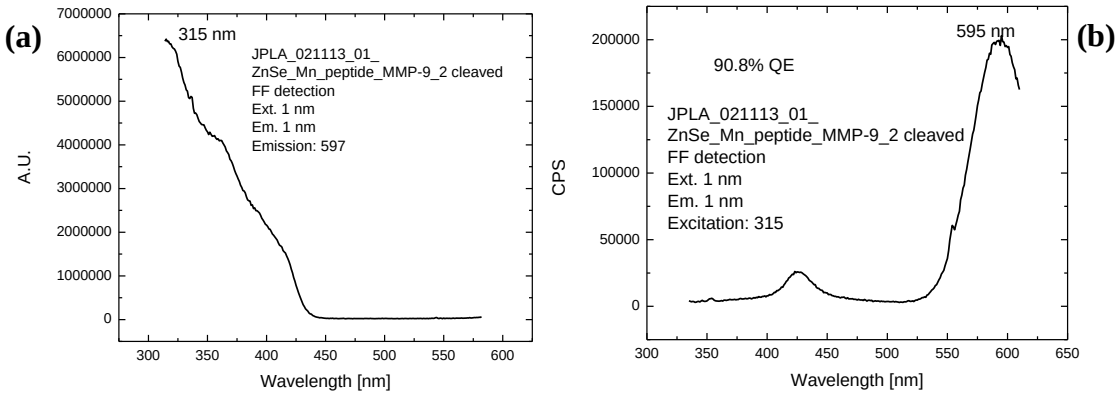

Figure 3.6: (a) *excitation and* ***(b)*** *emission spectra for* $Zn_{0.95}Mn_{0.05}Se/ZnS$*/peptide colloidal QD conjugates in PBS with the substrate 4 amino acid residue polypeptide. For the excitation spectrum* ***(a)*** *597 nm parked emission wavelength was used to generate the spectrum. For the emission spectrum* ***(b)*** *315 nm excitation wavelength was used to generate the spectrum. The emission observed in (b) is due to the Mn atomic energy level transitions as a result of the Mn doping in the nanocrystals. The QE for this particular emission peak is 90.8%, a dramatic increase from the substrate sample seen in* ***Figure 3.3****.*

The reliability of this biosensing idea was further tested by ensuring that the QD / peptide ratio was the same during peptide bioconjugation for both the substrate and remnant polypeptides, by diluting the QDs undergoing conjugation with the substrate peptide to 1 µM and the QDs undergoing conjugation with the remnant peptide to 2 µM in chloroform. This is because 1 mg of remnant peptides is nearly twice as many moles as 1 mg of the substrate peptides.

3.5 Dilution factor determination

The protocol by Shi *et al* 2007 called for a 1 µM concentration of QD sample as a starting point. As the $Zn_{0.95}Mn_{0.05}Se/ZnS$ QDs were heavily concentrated after synthesis a protocol for measuring the particle molarity was developed. In addition concentration was be determined by just how much chloroform solvent dilution was required to reach 1 µM concentration for substrate peptide and 2 µM for remnant peptide. The MW for the substrate peptide ({val}{val}{pro}{leu}{ser}{leu}{arg}{ser}{cys}) is 973.20, and the MW for the remnant peptide ({leu}{arg}{ser}{cys}) is 477.58. 1 mg of substrate peptide is equivalent to 0.001 mmol, and 1 mg of remnant peptide is equivalent to 0.002 mmol.

To determine how much chloroform is needed to dilute the colloidal QD solution a number of measurements and calculations were made.

First 1 mL of the sample was dried and then calcinated at 750 °C, in an oven, in order to determine a QD mass per solution volume concentration.

In order to determine the particle molarity, the reactions of the synthesis has to be analyzed, first. **(Rxn. 1)** is the chemical reaction for the synthesis of the core ($Zn_{0.95}Mn_{0.05}Se$) phase of the QDs.

1 mmol (95%$ZnC_{36}H_{30}O_4$ + 5%$MnC_{36}H_{30}O_4$) + 1 mmol $SeC(NH_2)_2$ → 1 mmol **$Zn_{0.95}Mn_{0.05}Se$** + 1 mmol $C_{37}H_{34}O_4N_2$ **(Rxn. 1)**

1 mmol $Zn_{0.95}Mn_{0.05}Se$ **Phase. 1**

(Rxn. 2) is the chemical reaction for the synthesis of the shell (ZnS) phase of the QDs.

0.90 $ZnC_{36}H_{30}O_4$ + 1.1 $SC(NH_2)_2$ → 0.90 mmol **ZnS** + 0.20 mmol $SC(NH_2)_2$ + 0.90 mmol $C_{37}H_{34}O_4N_2$ **(Rxn. 2)**

0.90 mmol ZnS **Phase. 2**

Knowing both of the reactions for phase 1 and phase 2, the core and the shell, respectively, of the $Zn_{0.95}Mn_{0.05}Se$/ZnS QDs the theoretical molar quantities can be determined, which are 1 mmol for $Zn_{0.99}Mn_{0.01}Se$ (phase 1) and 0.90 mmol for ZnS (phase 2), after which, *Eqn. 3* and *4* can be used to determine the mass quantity of phase 1 and phase 2. By knowing the mass quantities for $Mass_1$ and $Mass_2$, the percent masses, $\%\ Mass_1$ and $\%\ Mass_2$ can be calculated from *Eqn. 1* and *2*.

$$\%\ Mass_1 = \frac{Mass_1}{Mass_1 + Mass_2} \qquad Eqn.1$$

$$\%\ Mass_2 = \frac{Mass_2}{Mass_1 + Mass_2} \qquad Eqn.2$$

$$Mass_1 = 1\ mmol\ Zn_{0.99}Mn_{0.01}Se \times MW_{Zn_{0.95}Mn_{0.05}Se} \quad Eqn.3$$

$$Mass_2 = 0.90\ mmol\ ZnS \times MW_{ZnS} \quad Eqn.4$$

Where $MW_{Zn_{0.99}Mn_{0.01}Se}$ and MW_{ZnS} are the molecular weight of $Zn_{0.95}Mn_{0.05}Se$ and ZnS, respectively.

Eqn. 5 is the total sample mass, which was determined, as stated before, through drying and calcination of 1 mL of as synthesized $Zn_{0.95}Mn_{0.05}Se$/ZnS QD sample in chloroform.

$$Total\ Sample\ Mass = Sample\ Mass_1 + Sample\ Mass_2 \quad Eqn.5$$

The sample masses for the two separate phases are determined from *Eqn. 6* and *7*.

$$Sample\ Mass_1 = \%Mass_1 \times Total\ Sample\ Mass \quad Eqn.6$$

$$Sample\ Mass_2 = \%Mass_2 \times Total\ Sample\ Mass \quad Eqn.7$$

Using the densities and molecular weights of the two different phases, the separate volumes for each sample can be calculated from *Eqn.8* and *9*.

$$Volume_1 = M_{Zn_{0.95}Mn_{0.05}Se} \times MW_{Zn_{0.95}Mn_{0.05}Se} \times \frac{1}{\rho_{Zn_{0.95}Mn_{0.05}Se}} \quad Eqn.8$$

$$Volume_2 = M_{ZnS} \times MW_{ZnS} \times \frac{1}{\rho_{ZnS}} \quad Eqn.9$$

Where $M_{Zn_{0.95}Mn_{0.05}Se}$, M_{ZnS}, $\rho_{Zn_{0.95}Mn_{0.05}Se}$, and ρ_{ZnS} are the molarities and densities of $Zn_{0.95}Mn_{0.05}Se$ and ZnS, respectively.

The total volume of the sample can be determined from *Eqn. 10*, and the volume of a single $Zn_{0.95}Mn_{0.05}Se$/ZnS QD from *Eqn. 11*. Take the total volume of the sample and divide it by the volume of a single $Zn_{0.95}Mn_{0.05}Se$/ZnS QD to determine the total number of QDs in the sample, as in *Eqn. 12*. The QDs were estimated as circles with an average radius of 2.74 nm, as determined by TEM.

$$Volume_{total} = Volume_1 + Volume_2 \quad Eqn.10$$

$$Volume_{QD} = \frac{4}{3} \times \pi \times r^3 \quad Eqn.11$$

$$Total_{QD} = \frac{Volume_{Total}}{Volume_{QD}} \quad Eqn.12$$

Calculate the particle molarity from *Eqn. 13*. In order to determine how much chloroform solvent to dilute the sample with in order to achieve a 1 µM concentration, a spreadsheet was used to develop a plot of Particle Molarity vs. Dilution **(Figure 3.7)**.

$$Particle\ Molarity = \frac{Total_{QD}}{Avogadro\ constant} \quad Eqn.13$$

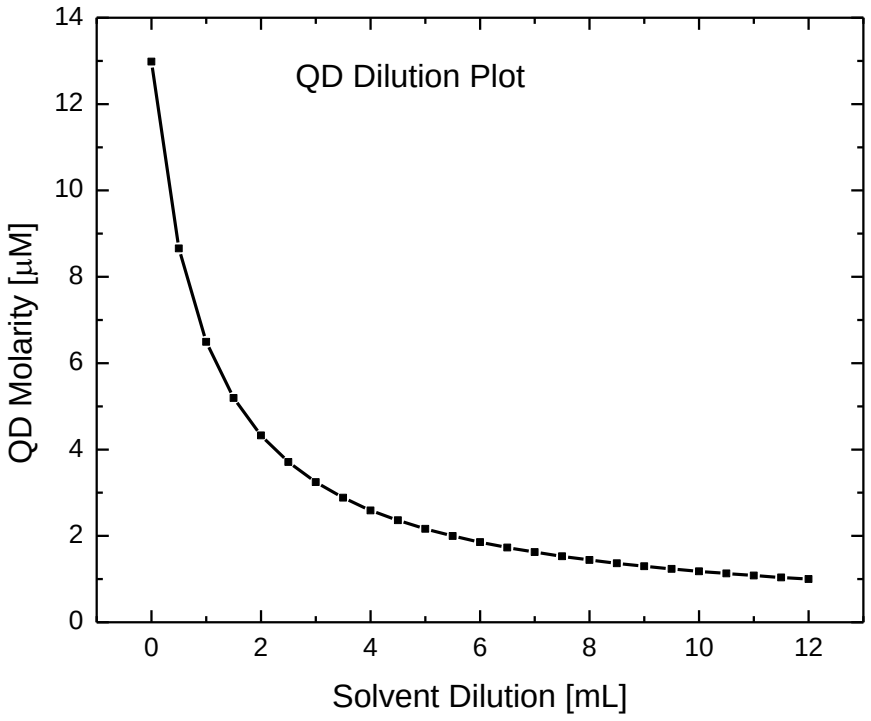

Figure 3.7: *A plot for determining how much chloroform solvent to use to dilute 3.2 mg/mL of* $Zn_{0.95}Mn_{0.05}Se/ZnS$ *QDs in chloroform.*

For substrate peptide bioconjugation, 1 mL of 1 µM $Zn_{0.95}Mn_{0.05}Se/ZnS$ QDs in chloroform was centrifuged with acetone at 4,000 RPM. After pouring off the supernatant the QDs were re-suspended in 2 ml of 9:1 (v:v) benzylamine/dimethylformamide (DMF) solution. 1 mg of the MMP-9 peptide substrate was dissolved into 0.200 mL of DMF. The peptide/DMF solution was added to the QD/benzylamine/DMF solution, and the resulting mixture was vortexed for 30 minutes. The peptide/QD conjugates were centrifuged and redistributed in 2 mL of DMF. The mixture was centrifuged again and re-dispersed in 2 mL of PBS. The peptide/QD conjugate solution was subjected to 2 cycles of spin dialysis by using 4 Microcon (Ultracell YM-30) centrifugal filter devices.

Afterwards, the peptide/QD conjugates were dispersed into 2 mL of PBS, resulting in 0.5 µM particle concentration, and stored in a fridge at 4 °C.

Similarly, for remnant peptide bioconjugation, the same procedure was followed, with the added exception that 1 ml of 2 µM $Zn_{0.95}Mn_{0.05}Se/ZnS$ QDs in chloroform was centrifuged with acetone at 4,000 RPM, at the start, and the final peptide/QD conjugates were dispersed into 4 mL of PBS, giving a final concentration of 0.5 µM particle concentration.

With the QD / peptide ratios the same for both batches and the samples normalized to 0.5 µM after bioconjugation, the QE values still increased between substrate and remnant peptide from 1.7% to 20%. **Figure 3.8** is the PL intensity dependence on the percentage of remnant peptides from 0%, 25%, 50%, 75%, and 100% for $Zn_{0.95}Mn_{0.05}Se/ZnS$/peptide conjugates, all normalized to 0.5 µM. Furthermore, **Figure 3.9** illustrates the QE dependence on the percentage of remnant peptides from 0%, 25%, 50%, 75%, and 100% for $Zn_{0.95}Mn_{0.05}Se/ZnS$/peptide conjugates, all normalized to 0.5 µM, as well. This substantial increase in PL intensity and QE% is an indication of a fluorometric method for quantifying MMP-9 enzyme activity levels, in which fluorescence increases with MMP activity.

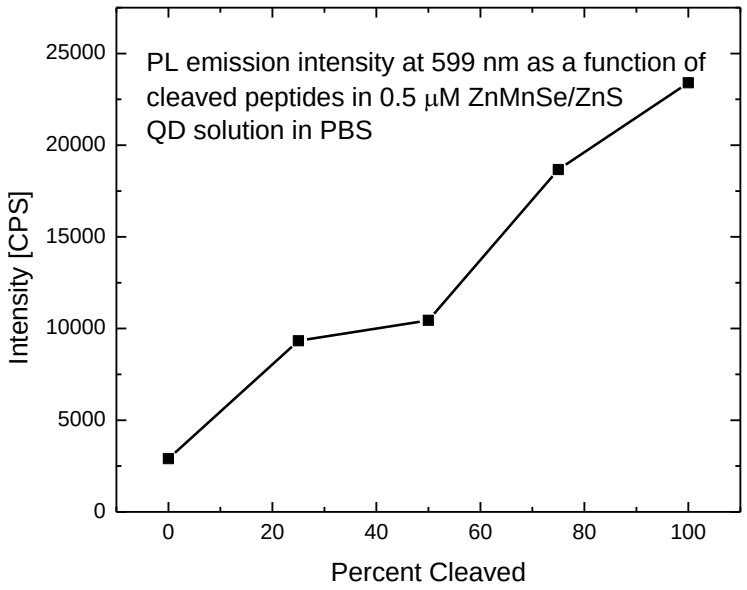

Figure 3.8: *A PL emission intensity vs. percent peptide cleavage plot indicating that with normalized concentrations intensity still increases as a function of cleaved peptide percentage.*

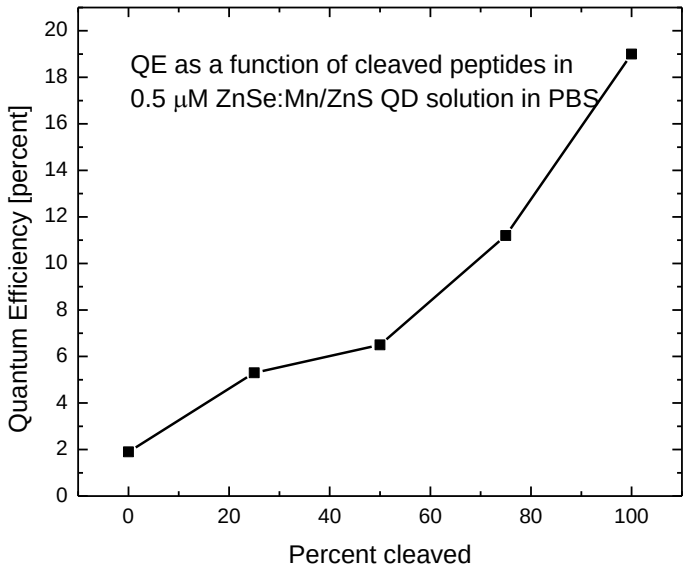

Figure 3.9: *Quantum efficiency vs. percent peptide cleavage plot indicating that with normalized concentrations QE also increases as a function of cleaved peptide percentage.*

3.6 Photoluminescence of peptide conjugated QDs in CSF

As the overall idea with this biosensor development is *in vivo* biosensing in cerebral spinal fluid (CSF), the $Zn_{0.95}Mn_{0.05}Se/ZnS$/peptides QD bioconjugates were dispersed in sterile CSF, and the PLE and PL of the remnant and substrate peptides were characterized, and, fortunately, the optical behavior was similar to the QD bioconjugates in PBS, in that the remnant peptide QD bioconjugates were far less quenched than the substrate. The QE increases from 2.6 % to 9.2% between substrate and remnant peptide, respectively. Note the 5 nm blue shift from the emission between substrate and remnant peptide bioconjugates in **Figure 3.10** and **Figure 3.11**.

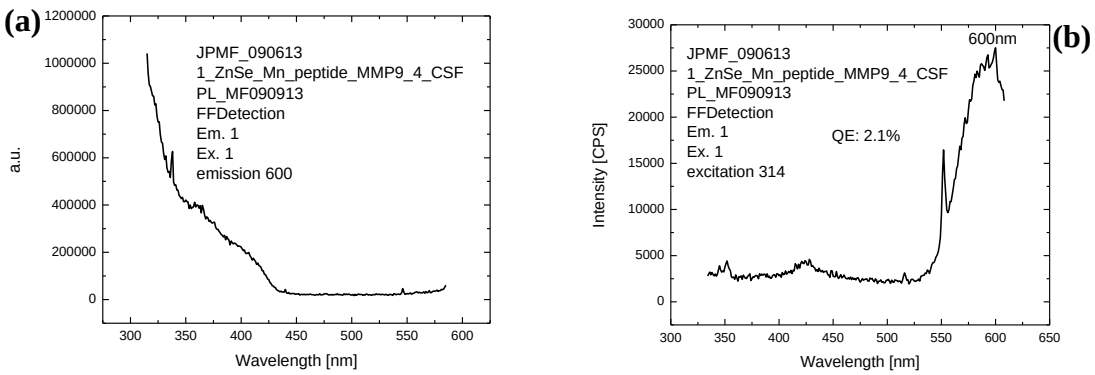

Figure 3.10: *PLE (a) and PL (b) spectra for substrate peptide coated ZnSe:Mn/ZnS core/shell QDs in CSF using 600 nm parked emission for PLE and 314 nm parked excitation wavelength for PL. The QE is 2.1%.*

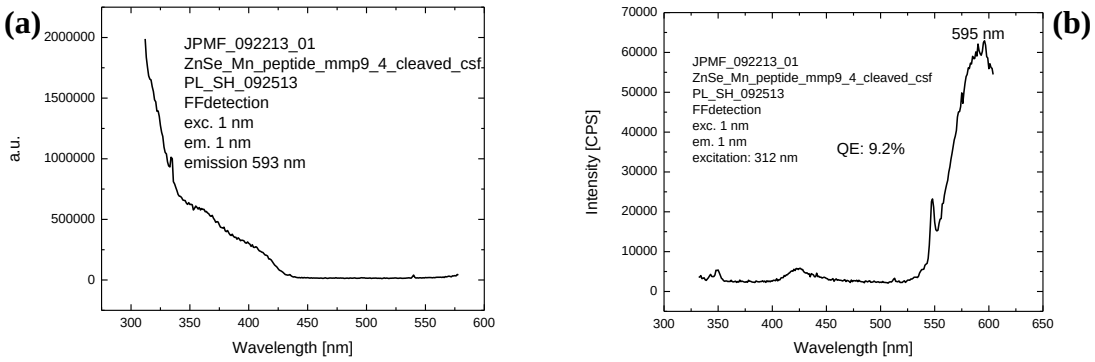

Figure 3.11: *PLE (a) and PL (b) spectra for remant peptide coated ZnSe:Mn/ZnS core/shell QDs in CSF using 593 nm parked emission for PLE and 312 nm parked excitation wavelength for PL. The QE is 9.2 %.*

3.7 Summary

Encouragingly, the 9 amino-acid peptide substrate does have a quenching effect on the fluorescence of the $Zn_{0.95}Mn_{0.05}Se/ZnS$ colloidal QDs when it is bioconjugated at the surface of the ZnS shell. Even more exciting is that the fluorescence is quenched much less when conjugating the 4 amino-acid peptide (what the longer peptide will look like after it is cleaved by MMP-9). Whether this will result in a de-quenching effect when these particular peptide/QD (substrate) conjugates are incubated with active MMP-9 remains to be seen, but if there ends up being a significant brightening of the quenched fluorescence, then it is the first step to realizing the proposed in vivo, quantitative, multiplexing, real time biosensing system for matrix metalloproteinase.

Chapter 4

ZnSe:Mn/ZnS QD-based MMP-9 biosensing experiments

4.1 ZnSe:Mn/ZnS QDs and peptide property dependent effects on QD fluorescence

Clinically relevant concentrations of MMPs depend on the MMP type. For instance, diabetic patients express MMP-2 at levels around 1000 – 1500 ng/mL, MMP-8 at around 5 ng/mL, and MMP-9 at 400 – 800 ng/mL for MMP-9 in serum[33], as was determined using enzyme-linked immunosorbent assay (ELISA). These levels are only slightly elevated from that of the healthy controls. As for the CSF, active MMP-9s are generally expressed at 1.80 ± 0.63 ng/mL for healthy individuals and 7 ± 2.4 ng/mL for seizure patients[34]. In comparison to MMP-9 levels in serum, in would seem that active MMP-9 is expressed at far lower concentrations in CSF. In addition, MMP activity can be detected as early as in 20 minutes, via the use of bioluminescent quencher/QD conjugates[35].

In the case of fluorescent peptide/QD conjugates, as was discussed in Chapter 3, the length of the peptide appeared to affect the QY. Specifically, cys-containing peptide/QD conjugates containing 9 amino-acid (AA) residues have lower QY than cys-containing peptide/QD conjugates containing 4 AA residues. This phenomenon was the first step in lending credence to the idea of ZnSe:Mn/ZnS peptide/QD conjugates as nano-biosensors for MMP activity, quantifying MMP activity based on the change in fluorescence as a result of MMPs cleaving peptides.

However, upon further consideration, it appears that peptide length may not be the sole reason for the change in fluorescence observed between the remnant and substrate peptide/QD conjugates. Additional peptide properties, such as charge and hydrophobicity, most likely account for the change in fluorescence as well.

Using the Peptide Property Calculator from Genscript[36], the vendor which supplied the peptides used in these experiments, several properties of three different peptides were calculated: molecular weight (MW), charge, isoelectric point, acidity, and hydrophobicity.

The three peptides examined were the 9 AA substrate cys-containing peptide, {Val}{Val}{Pro}{Leu}{Ser}*{Leu}{Arg}{Ser}{Cys}*; the 4 AA cys-containing remnant peptide, *{Leu}{Arg}{Ser}{Cys}*; and the14 AA cys-containing peptide, **{Glu}{Asp}{Glu}{Asp}{Glu}**{Val}{Val}{Pro}{Leu}{Ser}*{Leu}{Arg}{Ser}{Cys}*. The 14 AA peptide possesses the same MMP-9 substrate motif as in the 9 AA peptide; however, additional negatively charged aspartic acid {Asp} and glutamic acid {Glu} residues were added to the AA sequence to give the peptide an overall charge of -4, making it acidic, as well as decreasing the molecule's hydrophobicity from that of the substrate 9 AA peptide, making it more stable in aqueous media. The 9 AA peptide has a charge of +1, is basic, and has a higher hydrophobicity than the 14 AA peptide.

In observing the PL behavior between the 14 AA peptide/QD conjugates and the 4 AA peptide/QD conjugates, the QY of the 14 AA is higher than the 4 AA peptide/QD conjugates, which is opposite to the case of the 9 AA and the 4 AA peptide/QD conjugates, as described in Chapter 3. This means that it is not necessarily the length of

the peptide of the conjugates but rather other properties, such as peptide charge and hydrophobicity, which may be responsible for the change in QY, as the charge between the 14 AA peptide (-4) is quite different from the charge of the 9 AA and 4 AA peptide (+1). The hydrophobicity for the three different peptides is different as well.

In this chapter, various biosensing data are presented on the sensitivity of the peptide-coated ZnSe:Mn/ZnS QDs, discussed throughout the dissertation up to this point, to active MMP-9 enzymes. The sensitivity of the peptide/QD conjugates to MMP-9 enzymes is analyzed based on MMP and QD concentration, sensing media; water or CSF medium, as well as the substrate peptide type, 14 AA and 9 AA peptides.

4.2 Commercial assay from Anaspec

The active MMP-9 enzymes used in this research were purchased from Anaspec. To verify the MMP activity, a commercial assay, SensoLyte® 520 MMP - 9 Assay Kit, also from Anaspec, was used. This is a fluorometric assay that utilizes FRET pairing between quenchers (QXL520™) and fluorophores (5-FAM), linked by an MMP peptide substrate; the AA sequence of the substrate, here, is proprietary. Upon cleavage **by** the active MMPs, the FRET pairs are separated and the previously quenched fluorescence is restored. The technique allows for continuous and endpoint measurements at 490 nm excitation and 520 nm emission wavelengths.

4.2.1 Materials

Mouse MMP - 9 (Recombinant, Catalytic Domain) and the SensoLyte® 520 MMP - 9 Assay Kit were purchased from Anaspec. 384 well plates were purchased from Thermo Scientific, and artificial CSF was purchased from Harvard Apparatus.

4.2.2 Assay procedure

The procedure was based on the protocol supplied by Anaspec[37]. MMP-9 enzymes were diluted in assay buffer to concentrations of 2 µg/mL, 0.2 µg/mL, 0.02 µg/mL, and 0.002 µg/mL. The MMP-9 substrate was diluted in assay buffer to a ratio of 1:100. The different MMP-9 dilutions were added to triplicate wells, 20 µL per well. Additionally, triplicate wells were setup to have 20 µL of 2 µg/mL, 0.2 µg/mL, 0.02 µg/mL, 0.002 µg/mL, and 0 µg/mL solution. 20 µL of the assay MMP substrate was added to all wells, creating overall concentrations of 1 µg/mL, 0.1 µg/mL, 0.01 µg/mL, 0.001 µg/mL, and 0 µg/mL MMP9 solutions. The reagents were mixed by gently shaking the orbital plate for 30 seconds.

4.2.3 Assay results

In a Tecan Infinite 200 PRO Microplate Reader, the fluorescence was monitored at 490 nm excitation and 520 nm emission wavelength at 5 minute intervals, using 100% gain. The assay manual instructs that the measurements be taken over the course of 30 to 60 minutes. However, the measurements were done beyond 60 minutes. Still, the measurements could be repeated and continued for an even longer time because the

signal for 1000 ng/mL MMp-9 is still increasing and measurements should continue until the signal saturates. During the first run of measurements, the MMP-9 kinetics was studied at room temperature. The data are shown in **Figure 4.1**. Very little sensitivity can be observed between 0 to 100 ng/mL concentrations. Measurements with 1,000 ng/mL MMP-9 wells show a clear signal, as indicated by the higher slope on the kinetics line in **Figure 4.1**.

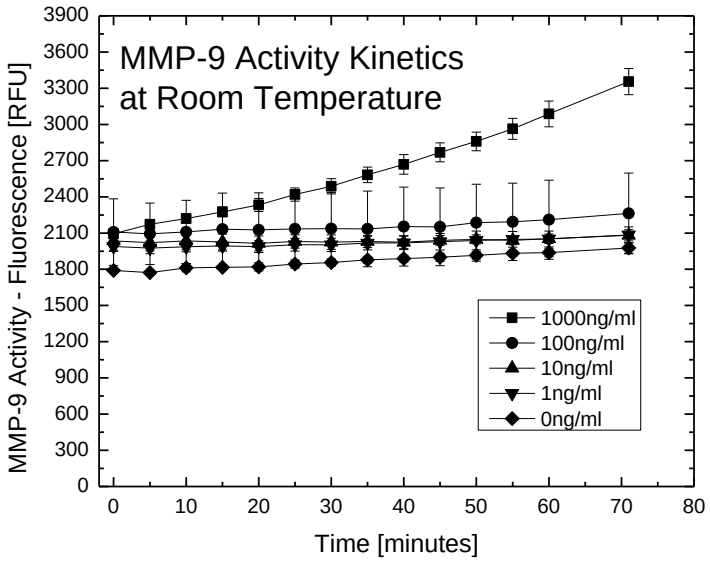

Figure 4.1: *MMP-9 activity kinetics at room temperature as measured with the SensoLyte® 520 MMP - 9 Assay Kit.*

The second set of measurements, again using 490 nm excitation and 520 nm emission wavelength at 5 minute intervals, was done with the internal temperature of the microplate reader set to 37 °C. As shown in **Figure 4.2**, the first 35 minutes, the signals from the 0 to 100 ng/mL samples again show little sensitivity, with the 1,000 ng/mL sample giving the highest signal. Since the results were practically the same as those obtained at room temperature, it was concluded that the internal heater in the microplate

reader was faulty. After 35 minutes, the well plate was transferred to a CO_2 incubator at 37 °C. The proceeding measurements indicated a significant increase in MMP-9 activity, which can be noticed in the **Figure 4.2** plot. After undergoing a half hour of incubation, as is also illustrated in **Figure 4.2**, the sensitivity for MMP-9 at the 100 ng/mL concentration goes up significantly, becoming more discernable on the spectra, unlike the previous measurements without incubation.

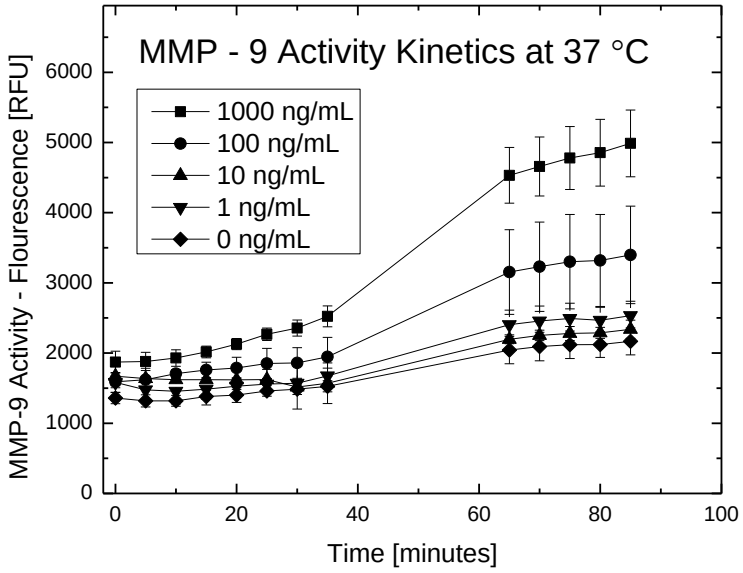

Figure 4.2: *MMP-9 activity kinetics at 37°C as measured with the SensoLyte® 520 MMP - 9 Assay Kit. The microplate reader was set to 37°C for the first 35 minutes, but the rate increase is a result of the samples being in a CO_2 incubator at 37°C for 30 minutes, suggesting that the internal heater in the plate reader was faulty.*

The 0 ng/mL MMP-9 activity curves in both **Figures 4.1** and **4.2** shows a signal that slightly increases with time. Ideally it should be flat, but, as was confirmed with the vendor, there is sometimes a small increase in background. This background did not turn

out to be temperature dependent. Temperature does in fact affect enzyme activity, however, observation of **Figures 4.1** and **4.2** does not show any clear indication of temperature dependency with regards to MMP-9 activity. Testing for MMP-9 activity at 41.5 ºC, in what is considered to be extreme body temperature elevation, does not show any noticeable increase in MMP-9 activity (**Figure 4.3)**.

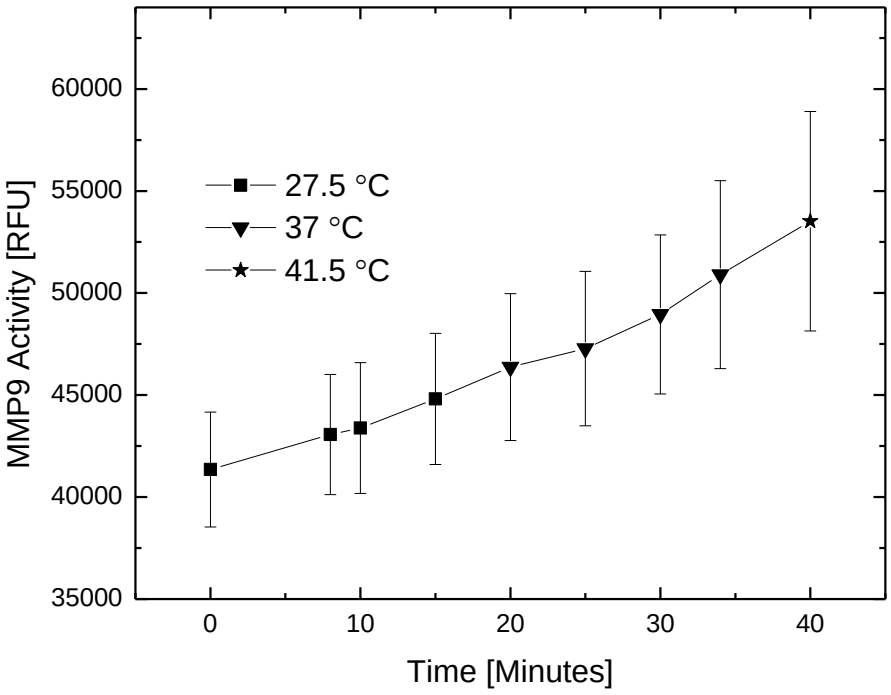

Figure 4.3: *Fluorometric response of MMP assay substrate for 1000 ng/mL MMP9 with increasing temperature from 27.5 ºC to 41.5 ºC.*

4.3 Verifying QD emission in the plate reader

Before testing the sensitivity of the peptide/QD conjugates to MMP-9 enzymes, it was at first important to verify the ability to detect QD fluorescent emission using the

particular Tecan Infinite 200 PRO microplate reader microplate reader, with the optimal excitation (319 nm) and emission (595 nm) wavelengths.

4.3.1 Procedure

In a 384-well plate, five wells were loaded with 20 µL volumes of the peptide/QD conjugates (synthesized according to the protocol outlined in Chapter 3) in CSF, with concentrations of 0.25 µM, 0.13 µM, 0.06 µM, 0.03 µM, and 0 µM.

4.3.2 Results

At first, using 319 nm excitation and 595 nm emission wavelengths, no reading could be observed from the fluorescent conjugates, using 100 % gain. The gain was tested at 10 % intervals from 100 to 10 %, and no signal could be observed. However, upon setting the gain to ‘optimal’, in which the machine optimizes the gain in order to receive the best measurement, the fluorescent readings could finally be observed. The optimal gain setting was 255%, which is the maximum gain. **Figure 4.4** shows the fluorescent signals from the peptide/QD conjugates for varying QD concentration. As expected, the fluorescence intensity decreases with the QD concentration.

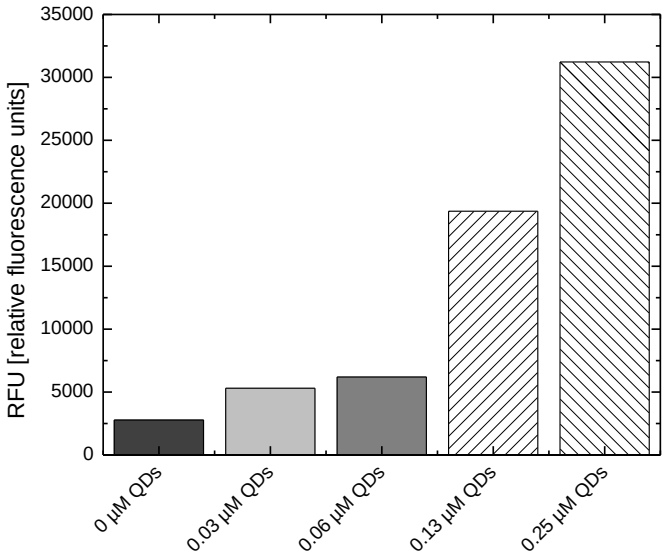

Figure 4.4: *QD fluorescence with respect to concentration as read from the Tecan microplate reader, set on 'optimal' gain.*

4.4 MMP-9 biosensing (positively charged peptide)

Following successful detection of QD emission from the microplate reader, the experiment protocol for MMP-9 QD-based biosensing was developed. Taking the results of cytotoxicity studies (outlined in Chapter 6) into consideration, the first biosensing experiment was set up to have the peptide/QD conjugates at a constant concentration of 0.13 µM, a concentration which showed minimal cytotoxic effect on macrophage cells, with varying MMP-9 solutions of 1000 ng/mL, 100 ng/mL, 10 ng/mL, 1 ng/mL, and 0 ng/mL, the same that was used in the commercial assay. Furthermore, the experiment was done in two different media, water and CSF.

4.4.1 Materials

Active mouse MMP - 9 (Recombinant, Catalytic Domain) enzymes were purchased from Anaspec. 384 well plates were purchased from Thermo Scientific and artificial CSF was purchased from Harvard Apparatus.

4.4.2 Procedure

A 384-well plate was seeded with 10 µL per well of 0.25 µM peptide/QD conjugates in water and in CSF. 2000 ng/mL, 200 ng/mL, 20 ng/mL, and 2 ng/mL concentrations of active MMP-9 enzymes in water and the same concentrations in CSF were prepared. The different MMP-9 dilutions in water were added in 10 µL quantities to triplicate wells containing 10 µL of the peptide/QD conjugates in water, making 0.13 µM peptide/QDs concentrations for every well. Likewise, the MMP dilutions in CSF were added in 10 µL quantities to triplicate wells containing 10 µL of the peptide/QD conjugates in CSF, also making 0.13 µM peptide/QD concentrations for every well. The reagents were mixed by gently shaking the orbital plate for 30 seconds before being placed into a CO_2 incubator at 37 °C.

4.4.3 Results

Fluorescence measurements were made with the Tecan Infinite 200 PRO Microplate Reader. The measurements were taken using 319 nm excitation and 595 nm emission wavelengths with the optimized gain setting. The results shown in **Figure 4.5** and **Figure 4.6** reveal that the 9-AA peptide/QD conjugates showed moderate

fluorescence sensitivity (no statistically significant change in fluorescence intensity as a function of the active MMP-9 concentration) to active MMP-9 enzymes.

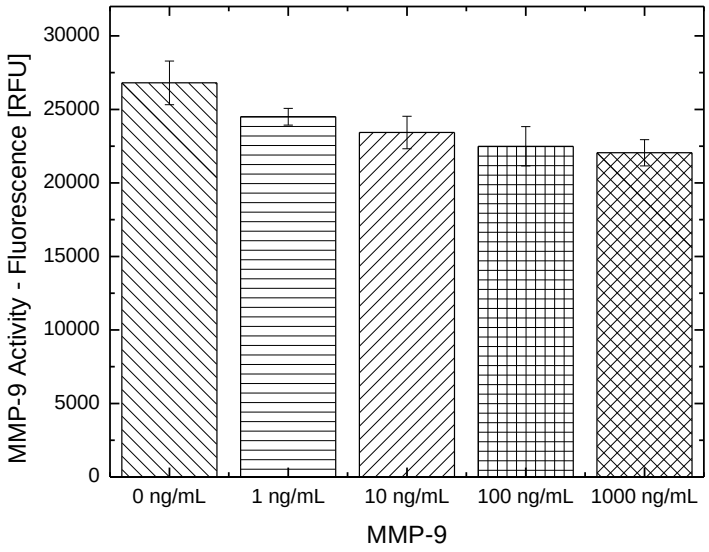

Figure 4.5: *Fluorometric responses to varying concentrations of active MMP-9 enzymes from peptide/QD conjugates in water, using the 9 AA peptides, after 2 hours and 20 minutes of incubation at 37 °C.*

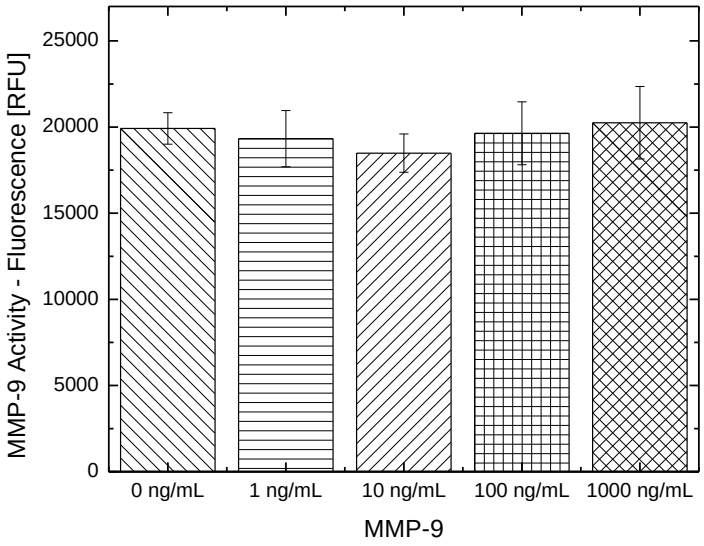

Figure 4.6: *Fluorometric responses to varying concentrations of active MMP-9 enzymes from peptide/QD conjugates in artificial CSF, using the +1 charge 9 AA peptides, after 2 hours and 20 minutes of incubation at 37 °C.*

4.5 Characterization of ZnSe:Mn/ZnS QDs with negatively charged peptides

One possible reason for the lack of fluorescence sensitivity in the QD biosensors to active MMP-9 enzymes is non-compatibility in protein-protein interaction. With MMPs, there is an active Zn^{2+} region. The 9 AA cys-containing peptide, as was determined from the Genscript Peptide Property Calculator, is basic and has a +1 charge and an isoelectric point of 8.55 (the pH at which the surface charge of the molecule is neutral). It is quite possible that the positively charged peptide repels the Zn-ion of the active region of the MMP-9, and perhaps a negatively charged peptide should be considered. The 14 AA cys-containing peptide

(**{Glu}{Asp}{Glu}{Asp}{Glu}**{Val}{Val}{Pro}{Leu}{Ser}*{Leu}{Arg}{Ser}{Cys}*) contains the MMP-9 cleavage motif but has additional negatively charged aspartic acid {Asp} and glutamic acid {Glu} residues, making it acidic and more hydrophilic, giving it a -4 charge, and an isoelectric point of 3.64. The 14 AA peptide also had the peculiar property of having a QY that was higher than the QY of the remnant (4 AA) Peptide/QD conjugates, in contrast to the fluorescence from the 9 AA Peptide/QDs being more quenched than the 4 AA Peptide/QDs, as was discussed in Chapter 3.

4.5.1 Optical characterization

In order to verify the discovery that the 14 AA peptide/QDs are brighter than the 4 AA peptide/QDs, the bioconjugation protocol, as detailed in Chapter 3, was repeated, twice, with the 14 AA peptides and the 4 AA peptides being conjugated to the QDs separately and at the same time.

Keeping the peptide to QD ratio equal for both substrate and remnant peptides, 1 mg ($6.3X10^{-4}$ mmol) of the 14 AA peptides (MW=1590.72) was conjugated to 1 mL of 1 µM ZnSe:Mn/ZnS QDs in 1:9 (v:v) benzylamine/DMF, and 0.3 mg ($6.3X10^{-4}$ mmol) of 4 AA peptides (MW=477.58) were conjugated to 1 µM ZnSe:Mn/ZnS QDs in 1:9 (v:v) benzylamine/DMF.

Immediately after bioconjugation, both substrate and remnant peptide/QDs were subjected to 30 minutes of vortexing simultaneously. The reaction tubes were observed under a black light, and indeed brighter fluorescence was observed for the 14 AA

peptide/QDs conjugates, and significantly less fluorescence was seen for the 4 AA peptide/QDs conjugates.

Figure 4.7 (a) is an image of the reaction tubes immediately after 30 minutes of vortexing and (b) after 3 cycles of washing and 2 cycles of spin dialysis.

(a)

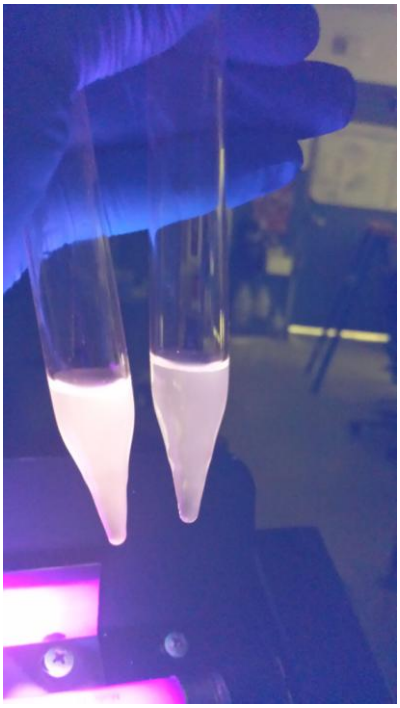

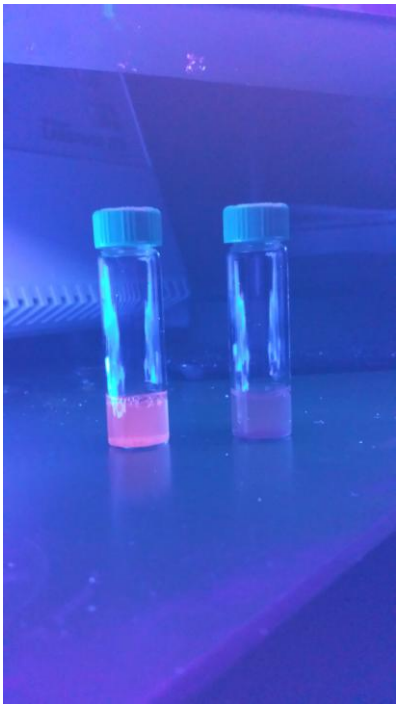

(b)

Figure 4.7: *Results of simultaneous peptide/QD conjugation for (a) conjugates after being vortexed simultaneously and (b) after washing and dialysis. In both figures the sample on the left contains the QDs conjugated to the -4 charge 14 AA substrate peptides, and the sample on the right contains QDs conjugated to the +1 charge 4 AA remnant peptides. Note the obvious visual difference in fluorescence intensity.*

4.6 MMP-9 biosensing with negatively charged peptide

With the new interesting results regarding the fluorescence intensity difference between the 14 AA and 4 AA, substrate and remnant respectively, peptide/QD conjugates, the sensitivity of the negatively charged peptide/QD bioconjugates was investigated. In addition, positive controls, remnant peptide/QD conjugates, were included in the experiment. Also, the QD concentration was increased from 0.13 µM to 0.25 µM.

4.6.1 Materials

Active mouse MMP - 9 (Recombinant, Catalytic Domain) enzymes and assay buffer solution (a component of the SensoLyte® 520 MMP - 9 Assay Kit) were purchased from Anaspec. 384 well plates were purchased from Thermoscientific and artificial CSF was purchased from Harvard Apparatus.

4.6.2 Procedure

A 384 well plate was seeded with 10 µL per well of 0.50 µM peptide/QD conjugates in CSF. 10000 ng/mL, 1000 ng/mL, 100 ng/mL, 10 ng/mL, and 1 ng/mL concentrations of active MMP-9 enzymes in CSF were prepared. The different MMP-9 dilutions in CSF were added in 10 µL quantities to triplicate wells containing 10 µL of the peptide/QD conjugates in CSF, making 0.25 µM peptide/QDs concentrations for every well. The reagents were mixed by gently shaking the orbital plate for 30 seconds before being placed in a CO_2 incubator at 37 °C.

4.6.3 Results

Fluorescence measurements were made with the Tecan Infinite 200 PRO Microplate Reader. The measurements were taken using 319 nm excitation and 595 nm emission wavelengths with the optimized gain setting. **Figure 4.8** reveals that the 14 AA negatively charged peptide/QD conjugates show poor fluorescence sensitivity (very small reduction in fluorescence intensity for active MMP-9 concentrations of 100 ng/mL and above) to active MMP-9 enzymes. As expected, the positive control showed a much lower signal, which implies that the 14 AA substrate peptides did not get cleaved.

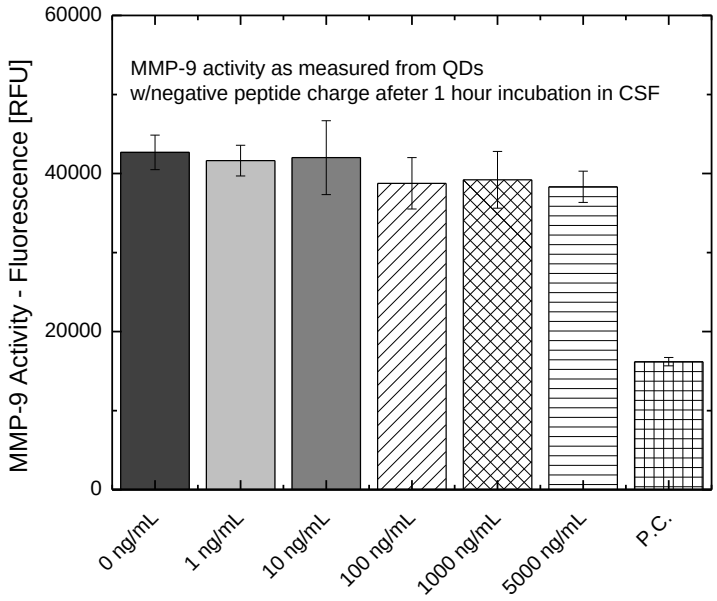

Figure 4.8: *Fluorometric responses to varying concentrations of active MMP-9 enzymes from peptide/QD conjugates in CSF, using the 14 AA peptides, after 1 hour of incubation at 37°C.*

Additionally, the procedure described in section 4.6.2 was repeated with the peptide/QD conjugates dispersed into the assay buffer solution that came with the MMP-

9 assay package from Anaspec, as the assay buffer is supposed to provide the most ideal conditions for the highest MMP-9 activity. However, the peptide/QD conjugates in the assay buffer still lacked fluorescence sensitivity to MMP-9s, as can be seen from **Figure 4.9**.

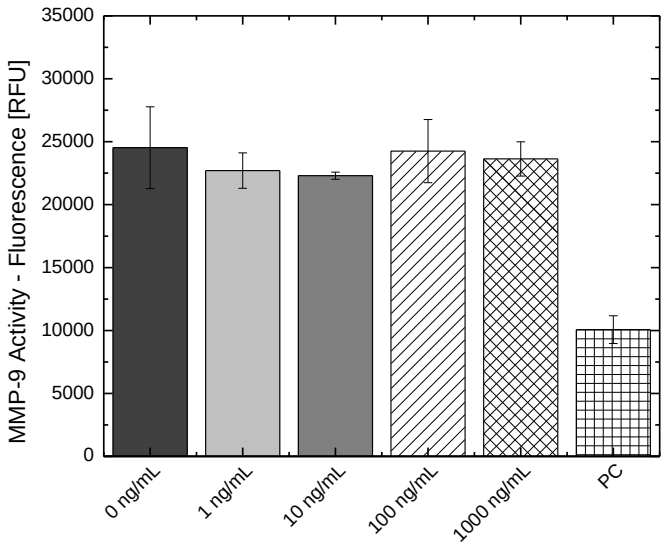

Figure 4.9: *Fluorometric responses to varying concentrations of active MMP-9 enzymes from peptide/QD conjugates in assay buffer, using the 14 AA peptides, after 1 hour of incubation at 37°C.*

4.7 MMP-9 biosensing with varying QD concentration

In light of the multiple biosensing trials being unable to produce any kind of convincing MMP-9 detection, a different experiment was carried out, in which the peptide/QD concentrations were varied. The idea behind this was to find a lower concentration of biosensors that will be more comparable to the concentration of MMP-9s, as it is possible that the high concentration of the peptide/QD conjugates

overwhelmed the concentration of MMPs, preventing any noticeable change in fluorescence.

4.7.1 Materials

Active mouse MMP - 9 (Recombinant, Catalytic Domain) enzymes were purchased from Anaspec. 384 well plates were purchased from Thermo Scientific.

4.7.2 Procedure

Multiple dilutions of the 14 AA peptide/QD conjugates were prepared at concentrations of 0.50 µM, 0.40 µM, 0.30 µM, 0.20 µM, 0.10 µM, and 0.05 µM in water. Additionally, positive controls, 4 AA peptide/QD conjugates, were diluted to 0.25 µM, 0.20 µM, 0.15 µM, 0.10 µM, 0.05 µM, and 0.03 µM concentrations. MMP-9 enzymes were diluted to 2,000 ng/mL in water. 10 µL of each 14 AA peptide/QD conjugate concentration was mixed with 10 µL of 2,000 ng/mL MMP-9 enzymes in individual wells in a 384-well plate, making concentrations of 0.25 µM, 0.20 µM, 0.15 µM, 0.10 µM, 0.05 µM, and 0.03 µM. Negative controls (14 AA peptide/QD conjugates without MMP-9s) and positive controls (4 AA peptide/QD conjugates) were added to adjacent wells at 0.25 µM, 0.20 µM, 0.15 µM, 0.10 µM, 0.05 µM, and 0.03 µM concentrations. The reagents were mixed by gently shaking the orbital plate for 30 seconds before being placed in a CO_2 incubator at 37 °C for 1 hour and 39 minutes and again for an accumulated time of 20 hours and 37 minutes.

4.7.3 Results

Fluorescence measurements were made with the Tecan Infinite 200 PRO Microplate Reader. The measurements were taken using 319 nm excitation and 595 nm emission wavelengths with the optimized gain setting.

While the sensitivity was not high, the peptide/QD biosensors begin to show a little fluorescence sensitivity to MMP-9 activity at 0.15 µM peptide/QD concentration after 1 hour and 39 minute incubation time, and at 0.15 and 0.20 µM peptide/QD concentrations after 20 hour and 37 minute incubation time. These results can be seen in **Figure 4.10** and **Figure 4.11**.

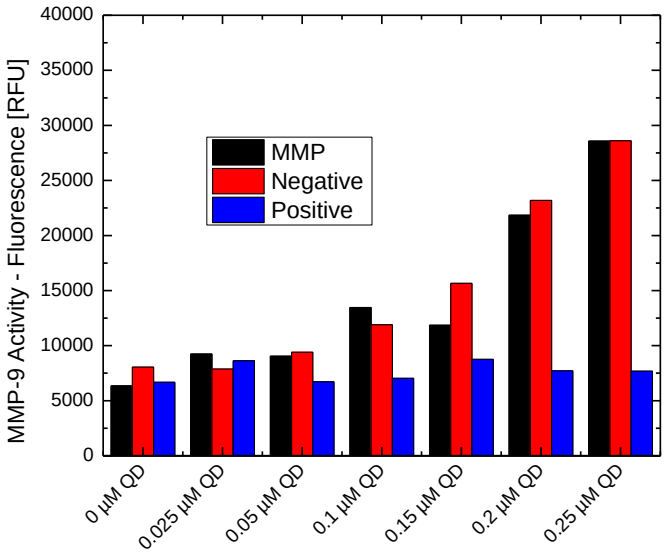

Figure 4.10: *Fluorescence-based biosensing of MMP-9, after 1 hour and 39 minutes of incubation at 37 °C, with varying peptide/QD conjugate concentrations. 0.15 µM concentration shows the most sensitivity to MMP-9.*

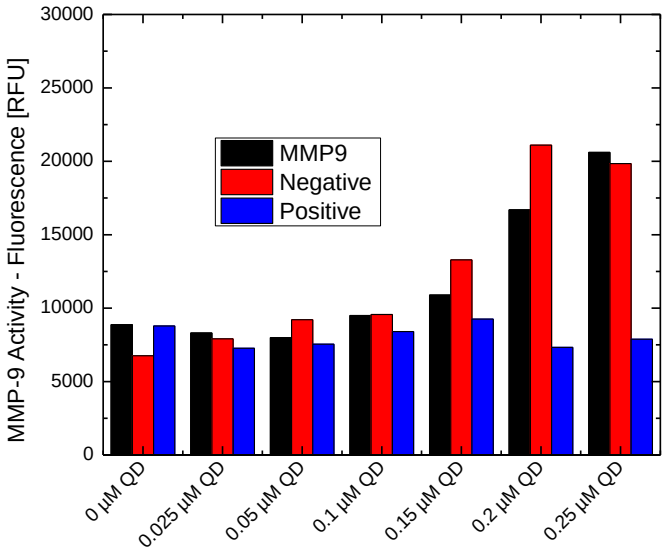

Figure 4.11: *Fluorescence based biosensing of MMP-9, after 20 hour and 37 minutes of incubation at 37 °C, with varying peptide/QD conjugate concentrations. 0.20 µM and 0.15 µM concentrations shows the most sensitivity to MMP-9. Note the decrease in overall QD fluorescence from that of* ***Figure 4.10****.*

4.8 MMP-9 biosensing with varying peptide concentration

It is speculated that the density of peptides on the surface of the QDs was perhaps too high, resulting in a steric hindrance that would be harming the sensitivity of the MMP-9 biosensor. As a result, experiments were conducted in which peptides, both remnant and substrate, were conjugated to the surfaces of QDs at 33% and 66% of their usual concentrations. The PL behavior of the 14 AA peptide/QD conjugates for 33% and 66% peptide concentration indicates consistent behavior with that of previous 100% peptide concentration, as can be observed in **Figures 4.12**, **4.13, 4.14, 4.15**, **4.16**, and

4.17, with the exception that the degree of quenching was less for 66% and even less for 33% samples.

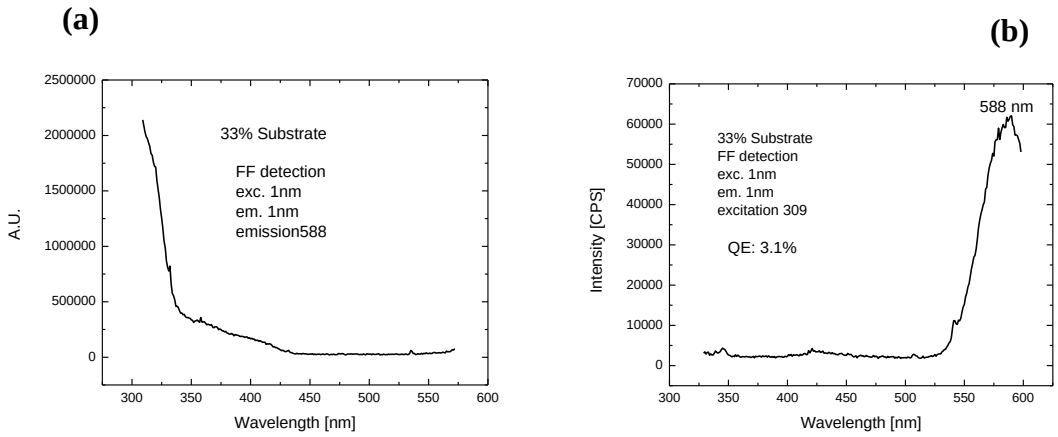

Figure 4.12: ***(a)*** *Excitation and* ***(b)*** *emission spectra for colloidal peptide/QD conjugates in CSF with 33% substrate polypeptide, using 588 nm and 309 nm for parked emission and excitation wavelengths respectively.*

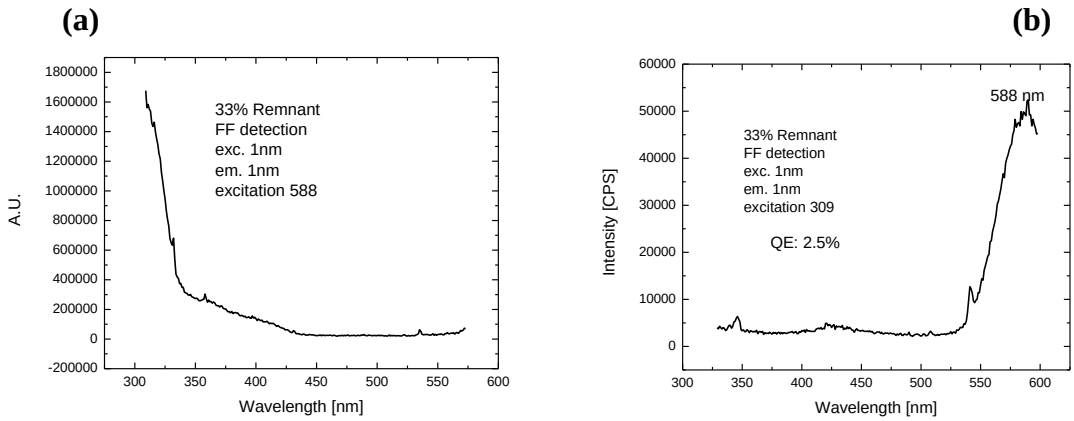

Figure 4.13: ***(a)*** *Excitation and* ***(b)*** *emission spectra for colloidal peptide/QD conjugates in CSF with 33% remnant polypeptide, using 588 nm and 309 nm for parked emission and excitation wavelengths respectively.*

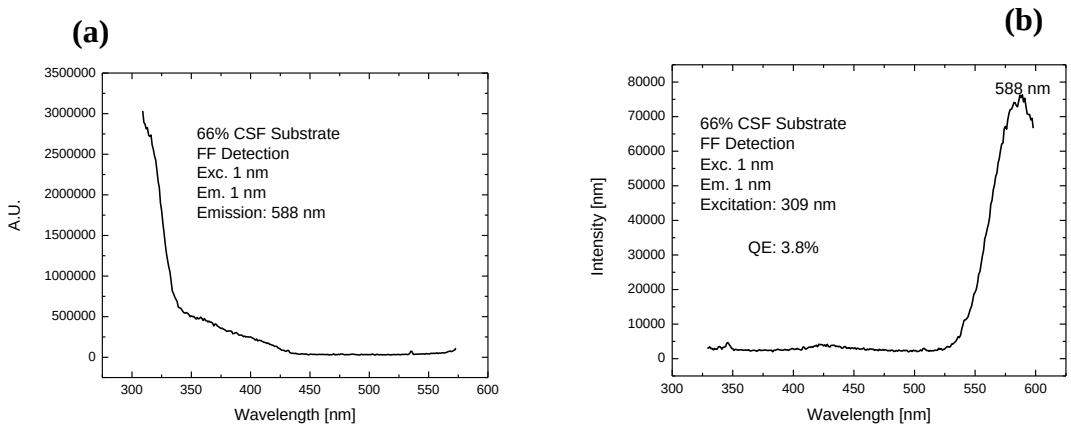

Figure 4.14: ***(a)*** *Excitation and* ***(b)*** *emission spectra for colloidal peptide/QD conjugates in CSF with 66% 14 AA substrate polypeptide, using 588 nm and 309 nm for parked emission and excitation wavelengths, respectively.*

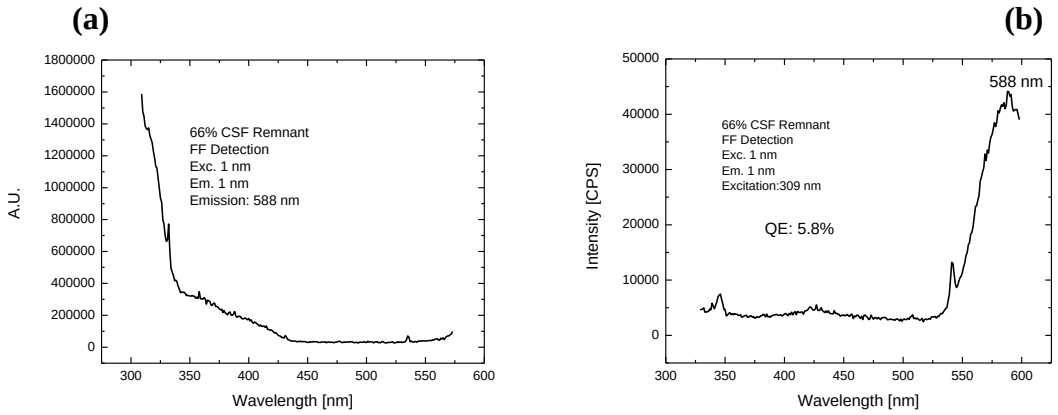

Figure 4.15: ***(a)*** *Excitation and* ***(b)*** *emission spectra for colloidal peptide/QD conjugates in CSF with 66% remnant polypeptide, using 588 nm and 309 nm for parked emission and excitation wavelengths, respectively.*

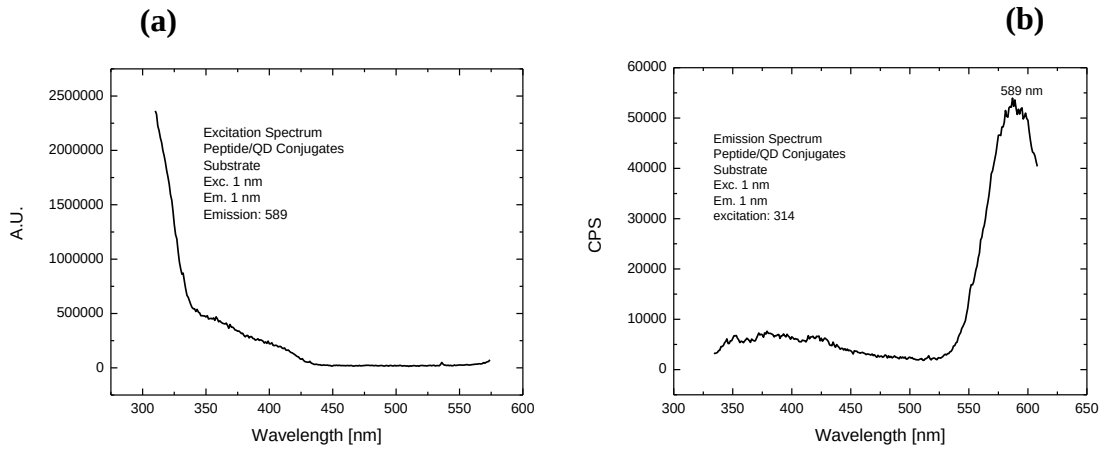

Figure 4.16: (a) *Excitation and* ***(b)*** *emission spectra for colloidal peptide/QD conjugates in CSF with 100% 14-AA substrate polypeptide, using 589 nm and 314 nm for parked emission and excitation wavelengths, respectively.*

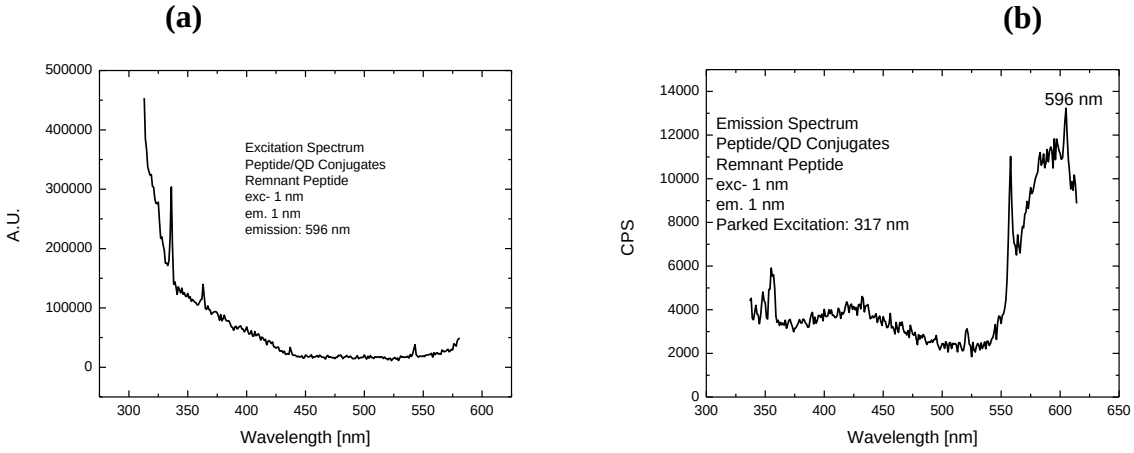

Figure 4.17: (a) *Excitation and* ***(b)*** *emission spectra for colloidal peptide/QD conjugates in CSF with 100% remnant polypeptide, using 596 nm and 317 nm for parked emission and excitation wavelengths, respectively.*

4.8.1 Materials

Active mouse MMP - 9 (Recombinant, Catalytic Domain) enzymes were purchased from Anaspec. 384 well plates were purchased from Thermo Scientific.

4.8.2 Procedure

Remnant and substrate 14 AA substrate peptide/QD conjugates were synthesized according to the bioconjugation procedure detailed in Chapter 3, with the exception that the peptides were conjugated to the QDs at 33% and 66% of their usual concentration, with the intention that the conjugated peptides at the surface of the QDs would have a lower surface density.

A 384 well plate was setup with triplicate wells for 0.25 µM QDs with 33% and 66% of original peptide coating for both 14-AA substrate and remnant peptides. The QD biosensors were incubated with MMP-9 at 1 µg/mL concentration in CSF for 1 hour.

4.8.3 Results

Fluorescence measurements were made with the Tecan Infinite 200 PRO Microplate Reader. The measurements were taken using 309 nm excitation and 588 nm emission wavelengths with the optimized gain setting.

The results are shown in **Figure 4.18**. For the first time, the 66% peptide/QD conjugates show a statistically significant ($p=0.04$) response to active MMP-9. However,

the response is an increase in fluorescence rather than a decrease, as the positive controls would lead one to believe.

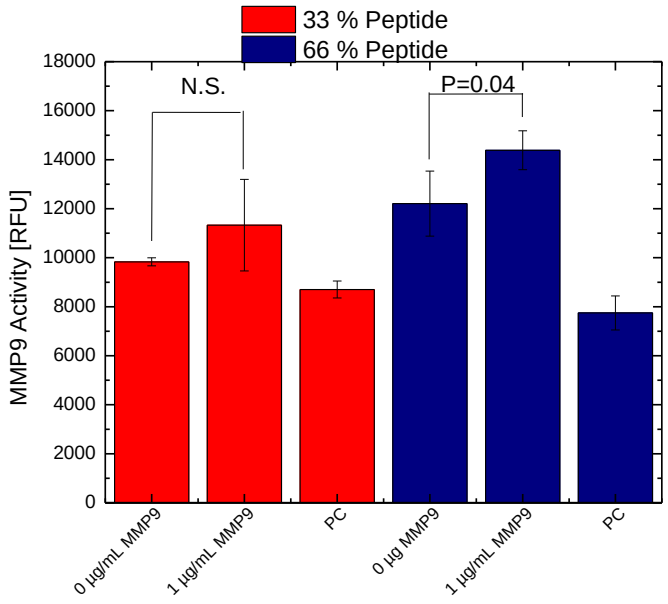

Figure 4.18: *Fluorometric responses to 1 µg/mL of active MMP-9 in CSF for 66% 14-AA peptide/QD conjugates and 33% 14-AA peptide/QD conjugates.*

4.9 MMP-9 biosensing with dilute peptide concentrations

Indeed, as the results from **Figure 4.18** suggest, steric hindrance may have been a primary cause for the lack of an MMP-9 sensing signal. 66% peptide/QD conjugates were beginning to show an increased signal; therefore, further experimentation was explored in which peptides, both remnant and substrate were conjugated to the surfaces of QDs at

10%, 1%, and 0.1% of their usual concentrations. The QD concentration for this experiment was 0.25 µM.

Figures 4.19, **4.20**, **4.21**, **4.22**, **4.23**, and **4.24** are the PLE and PL for 10%, 1%, and 0.1% peptide/QD conjugates, which do not indicate much of a change in PL intensity between substrate and remnant peptides, as peptide densities on the surface of the QDs have become very low at this point.

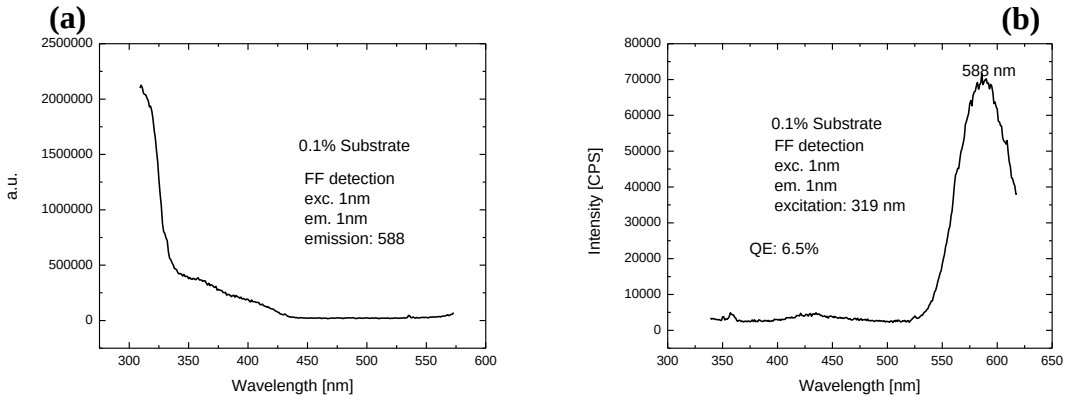

***Figure 4.19: (a)** Excitation and **(b)** emission spectra for colloidal peptide/QD conjugates in CSF with 0.1% 14-AA substrate polypeptide, using 588 nm and 319 nm for parked emission and excitation wavelengths, respectively.*

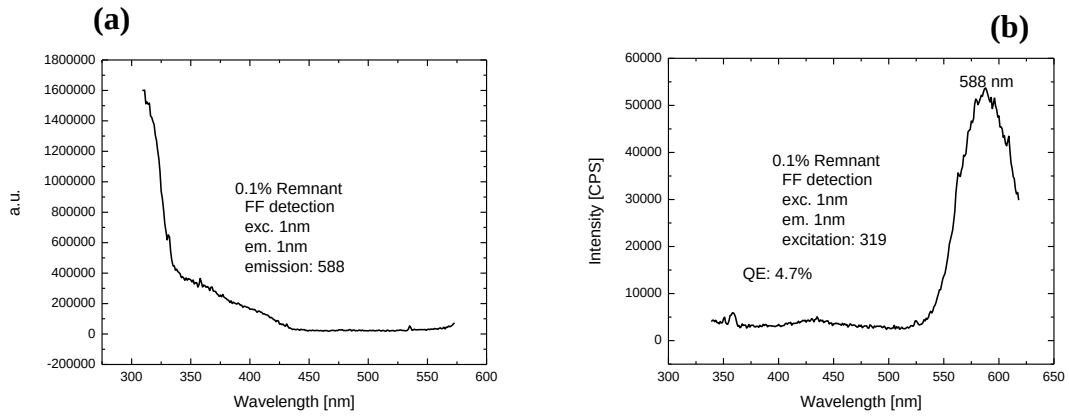

Figure 4.20: ***(a)*** *Excitation and* ***(b)*** *emission spectra for colloidal peptide/QD conjugates in CSF with 0.1% 14-AA remnant polypeptide, using 588 nm and 319 nm for parked emission and excitation wavelengths, respectively.*

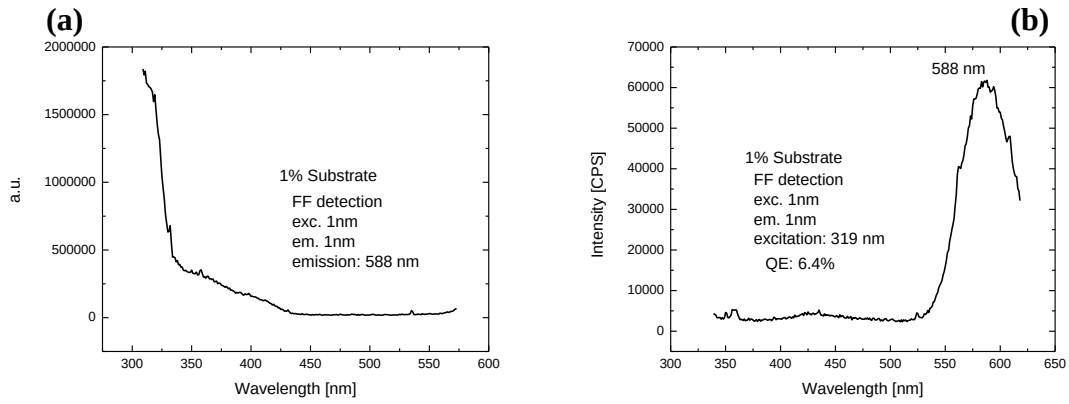

Figure 4.21: ***(a)*** *Excitation and* ***(b)*** *emission spectra for colloidal peptide/QD conjugates in CSF with 1% 14-AA substrate polypeptide, using 588 nm and 319 nm for parked emission and excitation wavelengths, respectively.*

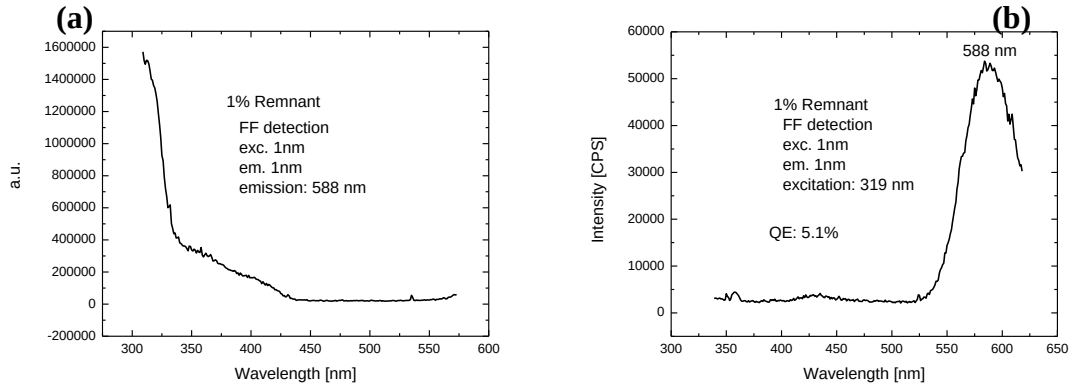

Figure 4.22: ***(a)*** *Excitation and* ***(b)*** *emission spectra for colloidal peptide/QD conjugates in CSF with 1% remnant polypeptide, using 588 nm and 319 nm for parked emission and excitation wavelengths, respectively.*

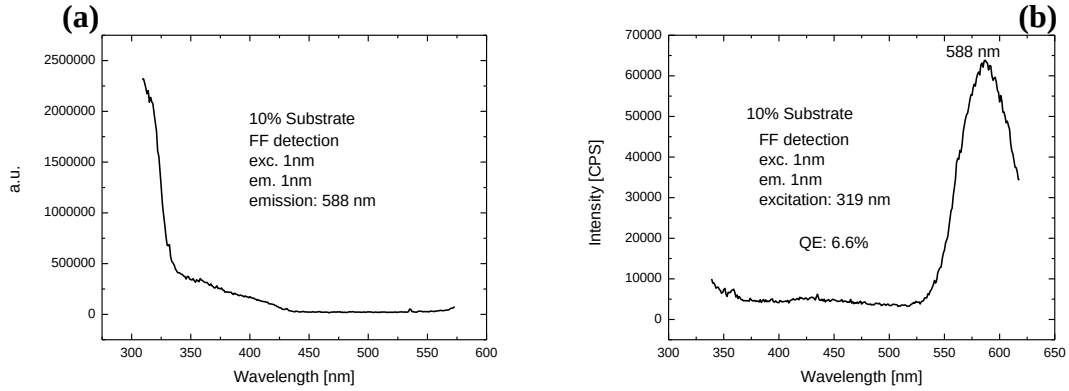

Figure 4.23: ***(a)*** *Excitation and* ***(b)*** *emission spectra for colloidal peptide/QD conjugates in CSF with 10% 14-AA substrate polypeptide, using 588 nm and 319 nm for parked emission and excitation wavelengths, respectively.*

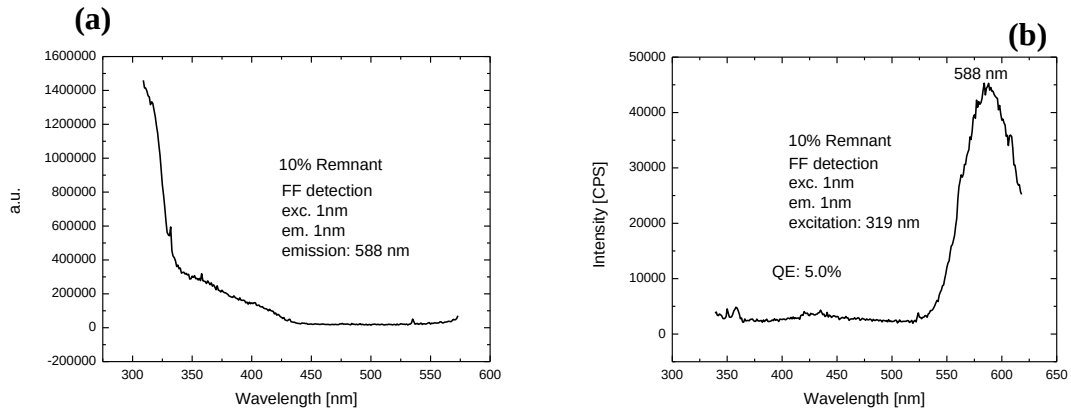

Figure 4.24: (a) *Excitation and* ***(b)*** *emission spectra for colloidal peptide/QD conjugates in CSF with 10% remnant polypeptide, using 588 nm and 319 nm for parked emission and excitation wavelengths, respectively.*

4.9.1 Materials

Active mouse MMP - 9 (Recombinant, Catalytic Domain) enzymes were purchased from Anaspec. 384 well plates were purchased from Thermo Scientific.

4.9.2 Procedure

Remnant and substrate peptide/QD conjugates were synthesized according to the bioconjugation procedure detailed in Chapter 3, with the exception that the peptides were conjugated to the QDs at 0.1%, 1%, and 10% of their usual concentration.

A 384-well plate was setup with triplicate wells for 0.25 µM QDs with 0.1%, 1%, and 10% of original peptide concentration for both 14-AA substrate and remnant

peptides. The QD biosensors were incubated with MMP-9 at 5µg/mL concentration in CSF for 4 hours.

4.9.3 Results

Fluorescence measurements were made with the Tecan Infinite 200 PRO microplate reader. The measurements were taken using 319 nm excitation and 588 nm emission wavelengths, with the optimized (255%) gain setting.

The results are shown in **Figure 4.25**. For 1% and 10% peptide/QD conjugates it does not appear to be a discernable signal between 0 and 5 µg/mL active MMP-9 concentration. However, similar to the results for the 66% peptide/QD conjugates in **Figure 4.18**, it would seem that the signal increases due to the presence of MMP-9s for 0.1% peptide/QD conjugates.

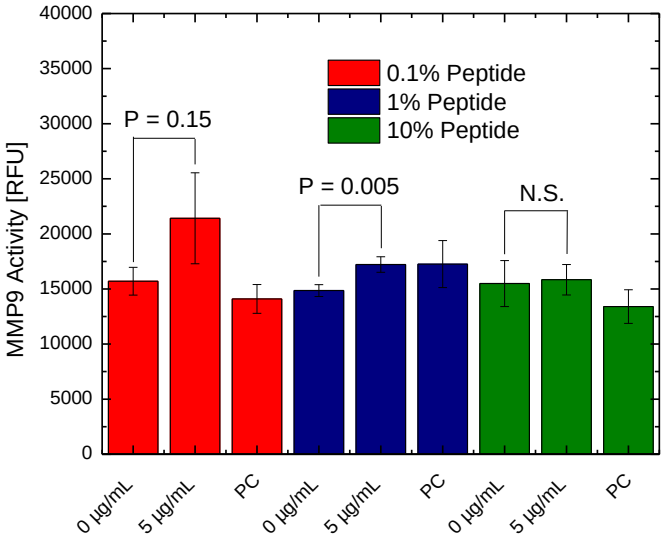

Figure 4.25: *Fluorometric responses to 5 µg/mL of active MMP-9 in CSF for 0.1% ,1%, and 10% peptide/QD conjugates, after 4 hours of incubation.*

4.10 Summary

The 14 AA peptide/QD conjugate biosensors show slight sensitivity to 1000 µg/mL MMP-9s in water at 0.15 µM concentration for 1 hour and 39 minute incubation time, while the biosensors show sensitivity at 0.20 µM and 0.15 µM concentrations after incubating overnight. It is likely that lower concentrations of the biosensors would show sensitivity to 1000 µg/mL MMP-9s, but, after observing **Figure 4.10** and **Figure 4.11**, the biosensors become too dilute for their fluorescent signals to rise above noise level.

In addition, the peptides were diluted, decreasing peptide surface density on the QDs, in order to account for the possibility of steric hindrance. Out of the several dilutions tested, 66% and 0.1% (of normal peptide concentration) show a slightly increased fluorescence signal, in contrast to the positive control remnant peptide/QD conjugates, which usually display lower concentration. Nonetheless, the 14-AA substrate peptide/QD conjugates show some sensitivity to active MMP-9 at 66% and 0.1% peptide concentrations.

Chapter 5

Linking ZnSe:Mn/ZnS quantum dots to silica

5.1 Silica surface modification

In order to covalently bond the synthesized Mn-doped ZnSe/ZnS QDs to a SiO_2 surface for the intended application of optical fiber based MMP biosensing, a silane coupling agent (SCA), 3-mercaptopropyltrimethoxysilane (MPTMS), was used to create a thiol monolayer over SiO_2 microscope slides. Due to the thiol-metal affinity, it was observed that QDs could be covalently bonded to the thiol groups at the surface of the SiO_2.

SCAs generally contain an organofunctional group, a linker, a Si atom, and hydrolyzable groups, generally three alkoxy groups bonded to the Si atom, **Figure 5.1**.

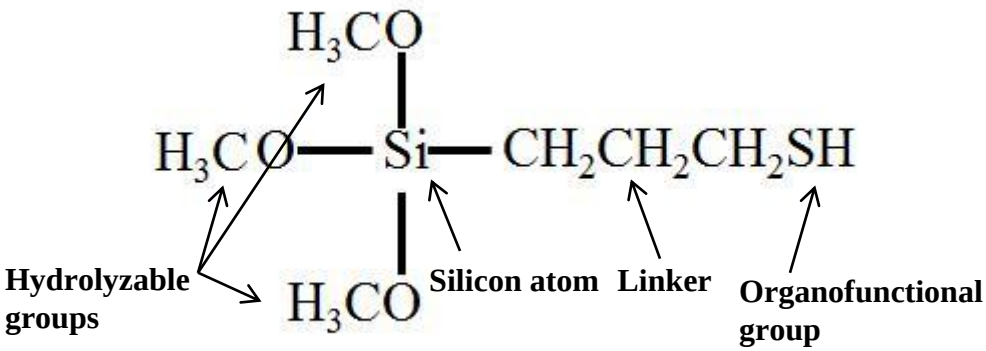

Figure 5.1: *The silane coupling reagent MPTMS and the characteristic components of a silane coupling agent.*

After hydrolysis of the hydrolyzable groups in a SCA, a reactive silanol is formed that can react with hydroxyl (OH) groups to form stable oxane bonds; and so a monolayer

of MPTMS can be formed over OH-modified silica, thus resulting in silane covalently bonded to silica with the thiol molecules at the surface[38].

Figure 5.2 (a) – (d) is a schematic diagram illustrating the chemistry of functionalizing silica with an SCA. Initially hydrolyzable regions of the SCA undergo hydrolysis in the presence of water, forming OH groups, **Figure 5.2(a)**. Following hydrolysis, the compound becomes reactive and the silanol molecules condense together, **Figure 5.2(b)**. In the presence of OH modified silica, the OH groups of the polymerized SCA form hydrogen bonds with the OH groups on the silica, resulting in a SCA monolayer over the silica surface, **Figure 5.2(c)**. Finally, after applying heat and dehydrating the compound, stable covalent bonds form in place of the hydrogen bonds, **Figure 5.2(d)**.

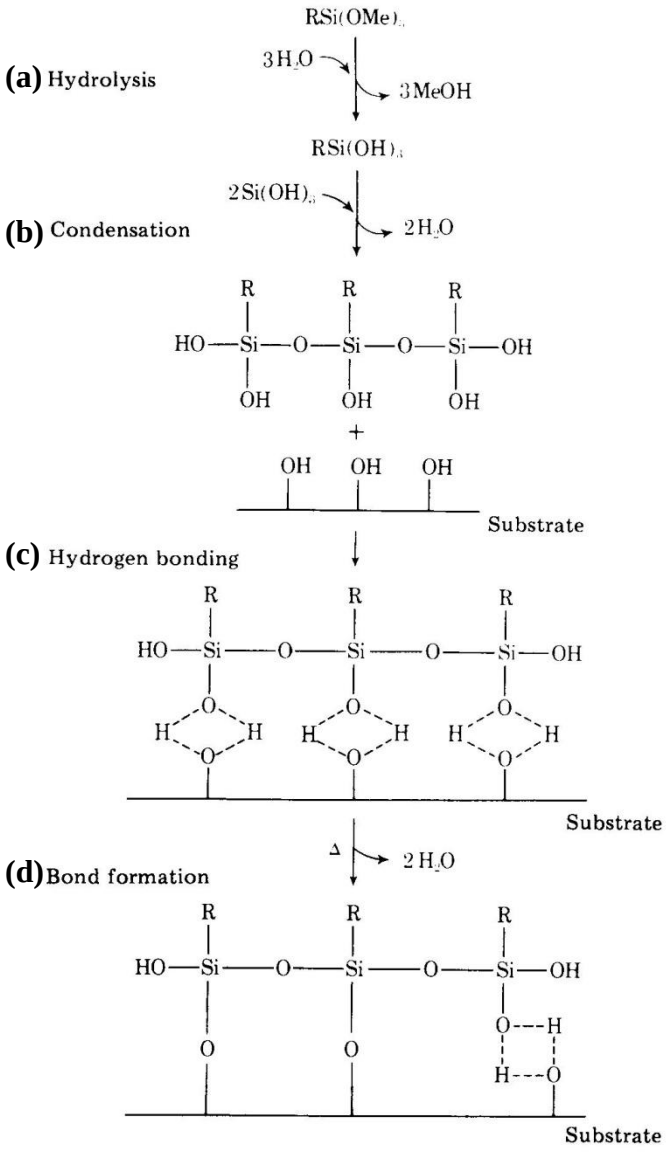

Figure 5.2: *Illustration of the different processes that take place during SCA modification of silica:* ***(a)*** *hydrolysis,* ***(b)*** *condensation,* ***(c)*** *hydrogen bonding, and* ***(d)*** *bond formation*[39].

SCAs can have different functional groups, and in MPTMS SH is the functional group. A monolayer of MPTMS, attached to silica at the hydrolyzable region, will have the SH functional group at the outer most surface. Due to the aforementioned metal

affinity from the thiol molecules, MPTMS can work as a linker for covalently bonding ZnSe:Mn/ZnS QDs to silica, **figure 5.3**.

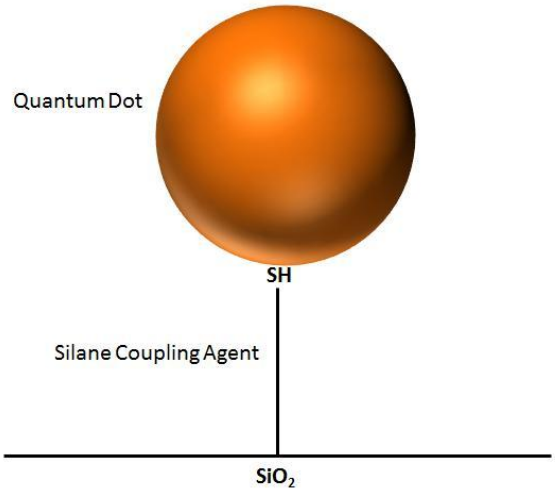

Figure 5.3: *Illustration of a tethered QD covalently linked to the SH group in MPTMS modified silica.*

5.2 Silica modification processes

In this work, two different procedures were developed to attach the QDs to silica. The first process (Procedure 1) involves functionalizing the silica with MPTMS first before dropping the QDs over the functionalized silica. The second process involves coating the QDs with MPTMS first and then dropping the coated QDs onto silica. The second procedure (Procedure 2) works better, as the fluorescence from the QDS on silica could still be detected, whereas in the first procedure the QDs only show a weak absorption signal and no fluorescence at all.

5.2.1 Materials

Silica glass microscope slides with frosted ends were purchased from Corning. Hydrogen Peroxide was purchased from EMD. 99% 3-mercaptopropyltrimethoxysilane (MPTMS) was purchased from Gelest. 95%-97% sulfuric acid, 99.8% benzene, chloroform, and 99.9% methanol was purchased from Sigma Aldrich. 70% nitric acid was purchased from General Chemical.

5.2.2 Procedure 1

The procedure to modify silica with OH and MPTMS was modified from Hu *et al* 2001[40]. The procedure to covalently bond ZnSe:Mn/ZnS QDs to MPTMS modified silica was developed in house.

For OH modification, the non-frosted portion of the glass slide was submerged into 1 N HNO_3 solution in a glass staining jar for 24 hours. In order to increase OH concentration, the slide was taken out of the nitric acid, rinsed with DI water, and submerged in 1:3 H_2O_2 in H_2SO_4 (piranha solution) for 30 minutes at 70 °C. Following piranha treatment, the glass slide was rinsed with DI water, dried with an N_2 blower, and further dried for 30 minutes in an oven at 100 °C.

Inside an Ar-filled glovebox, the OH-modifies glass slide was submerged in a solution mixture of 0.25g of MPTMS in 20 mL of benzene for 30 minutes. The MPTMS modified slide was rinsed with benzene, chloroform, methanol, and DI water before being dried with an N_2 blower. The MPTMS modified plate was dehydrated in an oven for 30 minutes at 100 °C.

The MPTMS plate was placed in a petri dish over a cloth soaked in either chloroform or toluene (depending on the solvent the QDs are in). The QDs were dropped over the silica plate until the surface of the plate was covered with the colloidal QD solution. The setup can be seen in **figure 5.4**. Subsequently, the petri dish containing the silica plate was covered on placed on a Barnstead/Lab-Line Lab-Rotator (orbital shaker) at a gentle shaking speed (not enough to cause the solution to fall off the plate, but to roll over it gently) for 2 hours.

Figure 5.4: *Setup of colloidal QD solution on glass slide in petri dish over solvent soaked cloth. The soaking of the cloth in solvent prevents evaporation of the colloidal solution when the petri dish is covered with a lid.*

The plate was rinsed thoroughly with chloroform or toluene (depending on the solution the QDs are in).

5.3 Optical characterization (Procedure 1)

Unfortunately with procedure 1, no QD fluorescence could be detected while making measurements in a HoribaJobanYvon Fluorolog-spectrofluorometer. Without fluorescence, UV-Vis absorption from a Varian Cary spectrophotometer was used to verify that the QDs stayed attached as a result of thiol binding after washing the slide with toluene. The absorption properties of glass slides were measured for the QD-modified slide, a blank slide (not treated with piranha or OH-modified), and a control slide, and the QD-modified slide minus the blank slide, subtracting the absorption contribution from the silica substrate. **Figure 5.5** shows the absorption spectrum for Mn-doped ZnSe/ZnS QDs in toluene, where an absorption feature can be observed at 423 nm. The absorption measurements taken from a blank slide and the QD-modified slide can be seen in **figure 5.6**. The absorption feature at 423 nm can be observed for the QD-modified slide but not for the blank slide. Furthermore, in **figure 5.6**, the 423 nm absorption feature can be observed more clearly in the absorption spectra for the QD-modified slide with the absorption line of the blank slide subtracted out.

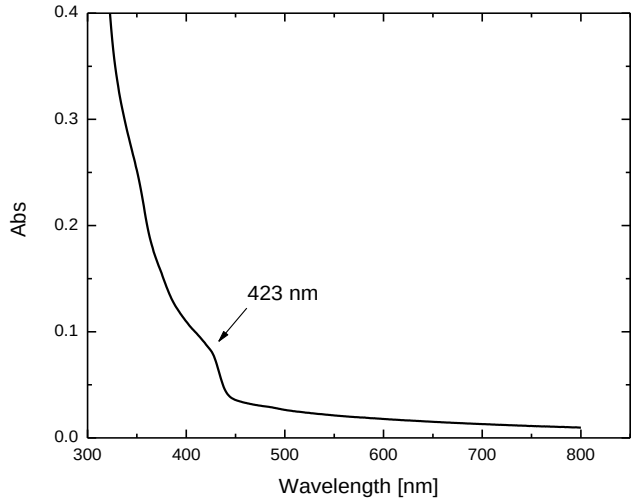

Figure 5.5: *UV-Vis absorption measurement for ZnSe:Mn/ZnS QDs in toluene with an absorption feature at ~423 nm.*

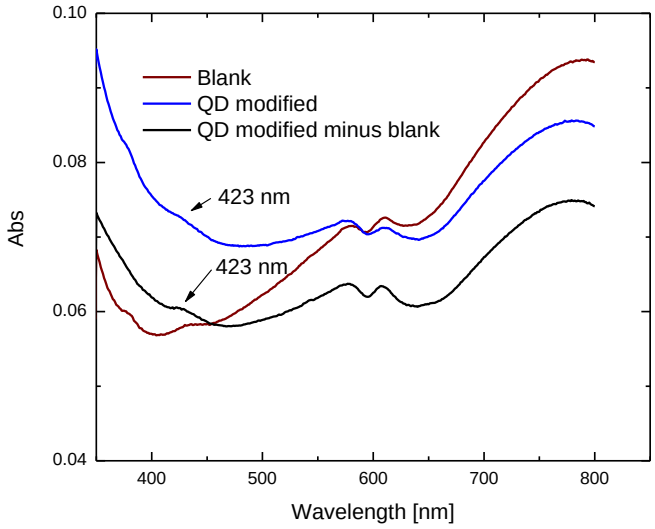

Figure 5.6: *UV-Vis absorption measurements for the QD-modified (blue), the blank (brown), and QD-modified minus the blank slide (black).*

5.4 QD pre-modification

With the failure to produce fluorescently active QDs covalently bonded to the surface of silica, a new method of initially coating the QDs with MPTMS was implemented (Procedure 2). **Figure 5.7** is an illustration of an MPTMS coated ZnSe:Mn/ZnS QD. Since the QDs were coated with MPTMS first, the silica was made only to be OH-modified without MPTMS modification. After orbital shaking the QDs onto the silica and thoroughly washing the slides with chloroform, the QDs on the silica maintained their fluorescence. In order to have increased silica surface area, the frosted portion of the silica slide was treated and modified with QDs.

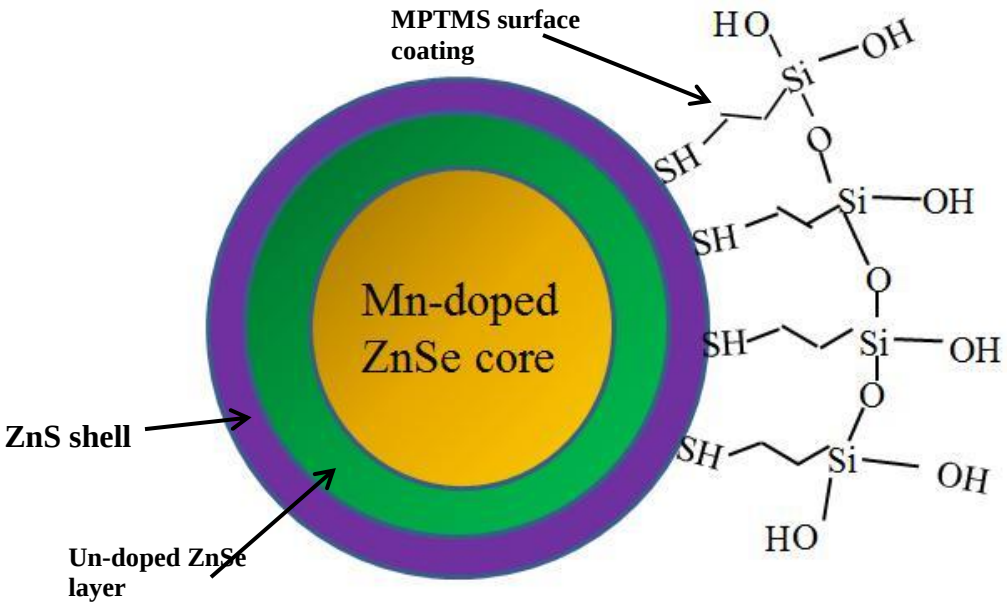

Figure 5.7: *Illustration of the MPTMS coated ZnSe:Mn/ZnS QD nanocomposite. The QD is coated partially with MPTMS so it can bond to silica and still have conjugation sites available for cys-peptides.*

5.4.1 Procedure 2

The frosted portion of the silica slide was OH-modified the same way as in procedure 1. The procedure to coat ZnSe:Mn/ZnS QDs with MPTMS was adapted from Garcia-Cerda *et al* 2010[41].

In an N_2 filled glovebox, MPTMS was mixed with 2 mL of ZnSe:Mn/ZnS QDs in chloroform at a 1:1 mass ratio (in this case 11.45 mg MPTMS/11.45 mg QDs). The mixture was placed into a 25 mL three-neck flasks, capped with two rubber septa on the outer necks and a condenser and nitrogen adaptor on the center neck. The three-neck flask reaction apparatus was removed from the glovebox and put under N_2 by connecting it to the Schlenkline gas-manifold. With water flowing through the condenser, the solution was heated to a reflux temperature (54.6 °C) and stirred for 6 hours. After the reaction, the solution was cooled to room temperature and purified through centrifugation with acetone. The MPTMS modified QDs were dispersed in 2 mL of chloroform and stored in a vial.

The MPTMS coated QDs were shaken onto the OH-modified silica similar to that described in procedure 1. The slide was placed on a chloroform soaked cloth in a petri dish. The colloidal QDs were dropped onto the slide in chloroform until the entire frosted portion of the slide surface was covered with solution. The petri dish was covered and the solution was gently shaken with the orbital shaker, just enough to smoothly flow the solution over the slide without spilling over, for two hours. Afterwards, the QD-modified silica slide was dried at low heating temperature and then baked in an oven at 120 °C for 30 minutes to dehydrate the MPTMS linker and form covalent bonds between the linker and the silica.

5.5 Optical characterization (Procedure 2)

While Procedure 1 produced QD-modified slides without visible fluorescence, Procedure 2 produces QD-modified slides with visible QD fluorescence. **Figure 5.8 (a) – (c)** are images of the QDs on silica after orbital shaking. **Figure 5.8 (a)** is an image of the QD modified slide immediately after baking it in the oven. Figure 5.8 (b) is an image of the slide after thoroughly washing the slide in chloroform, and figure 5.8 (c) is the slide with a small section cut off for PL and QE characterization.

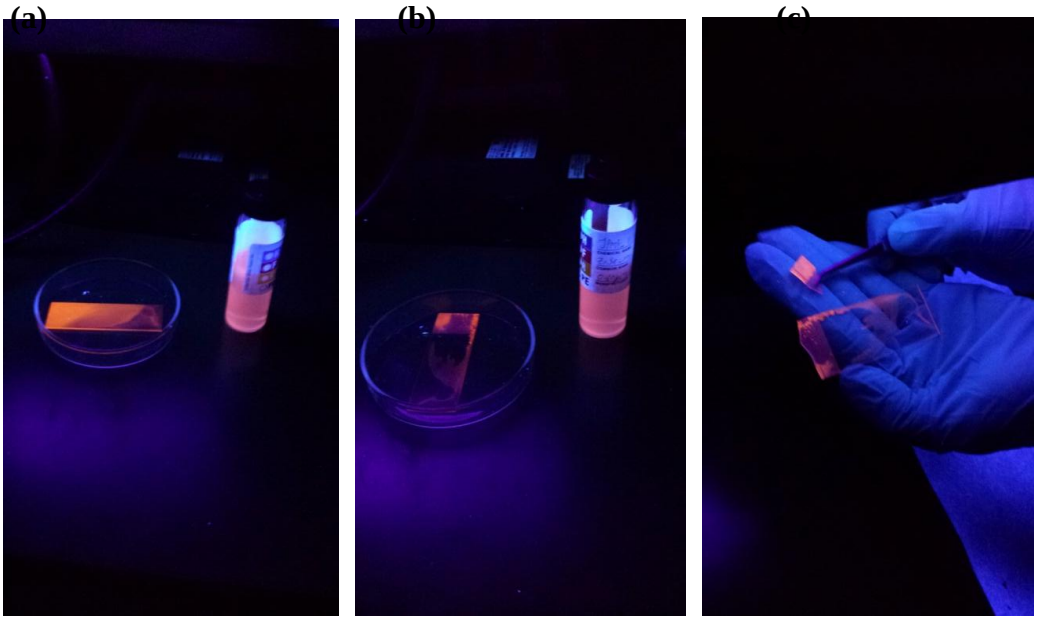

Figure 5.8: (a) *the ZnSe:/Mn/ZnS QD modified silica after baking at 120 °C in the oven for 30 minutes,* ***(b)*** *the QD modified silica after being thoroughly washed with chloroform, and* ***(c)*** *a small section of the glass slide cut out for characterization. The characteristic orange 598 nm Mn emission can be clearly seen in the images.*

5.5.1 Photoluminescence

The QD modified silica was characterized for PLE, PL, and QE with a HoribaJobanYvon Fluorolog-3 spectrofluorometer. **Figure 5.9 (a)** and **(b)** are the PLE and PL, respectively, for ZnSe:Mn/ZnS QDs on silica, as prepared by Procedure 2. The parked emission wavelength for the PLE measurement was 598 nm, and the parked excitation wavelength for the PL measurement was 380 nm. The PLE spectrum in Figure 5.9 (a) shows an increase in intensity at wavelengths below 380 nm, but at lower wavelengths the glass would begin to show a fluorescence peak. The QE for the emission seen in Figure 5.9 (b) turned out to be 8%. The spectral slit widths for the PL measurements were 1 nm for both excitation and emission.

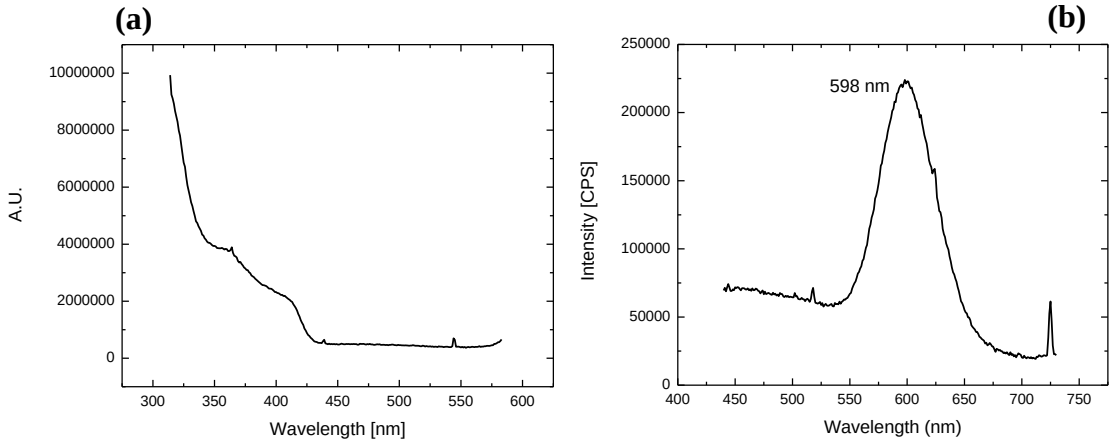

***Figure 5.9: (a)** PLE and **(b)** PL spectrum for ZnSe:Mn/ZnS QD modified silica with 598 nm parked emission for PLE and 380 nm parked excitation for PL.*

5.6 Absorption spectra for QD supernatant

It is important that the QDs are only partially coated in MPTMS so that there are still bioconjugation sites available for the peptides. In order to verify partial coating the

presence of MPTMS in the supernatant from the centrifugation step was analyzed via near-IR absorption from a Varian Cary spectrophotometer. First the near-IR absorption spectrum was measured for pure MPTMS in order to note any absorption features that MPTMS might have. Taking note of the MPTMS absorption features, the absorption spectrum of the reaction supernatant was measured and no MPTMS features are identified. The idea is that if MPTMS is still detected in the supernatant then it is likely that the QD surfaces are saturated with MPTMS. Since no MPTMS absorption features show up on the measured spectrum, it is likely that the QDs are not saturated with MPTMS and open surface area is open for peptide bioconjugation for the biosensing application of these QDs. Additionally, the near-IR absorption spectrum for the partially MPTMS coated QDs was measured, and incidentally no MPTMS features show up either. **Figure 5.10** is a near-IR absorption plot of MPTMS, the MPTMS coated QDs, and the reaction supernatant. However, as was illustrated in **Figure 5.2**, through the modification process, MPTMS undergoes hydrolysis, condensation, and dehydration before being applied to a surface, the QD surface in this case, and might suggest a different near-IR absorption spectrum.

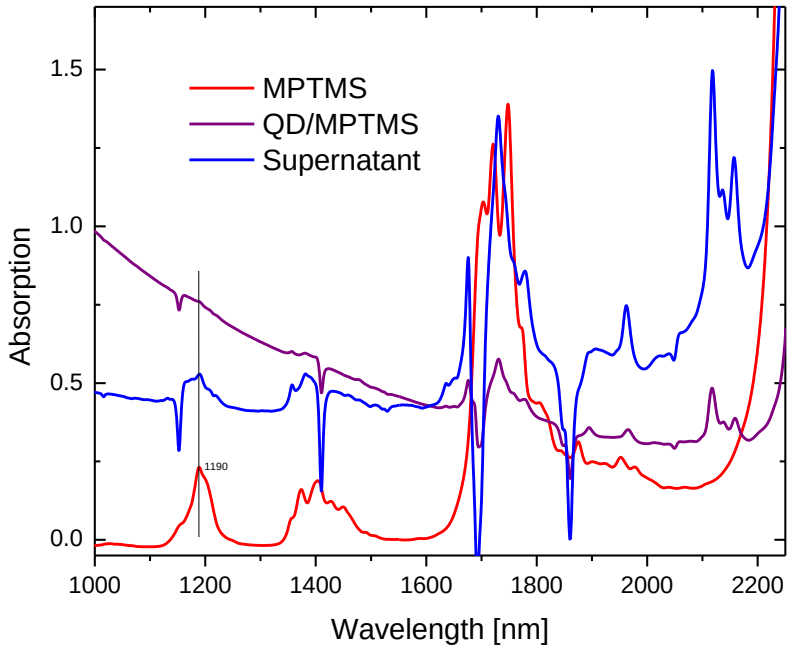

Figure 5.10: *Near-IR absorption spectrum for MPTMS (red), MPTMS coated ZnSe:Mn/ZnS QDs (purple), and supernatant (blue).*

5.7 Summary

It would seem that with the methods applied, coated the QDs with MPTMS first (Procedure 2) is significantly more affective at attaching these QDs to silica, and maintaining their fluorescence, than coating the silica with MPTMS first (Procedure 1). The fluorescently active QDs covalently bonded to silica are not as bright as the colloidal QDs, yet the brightness thus achieved has been satisfactory. A lack of MPTMS absorption features from the supernatant suggests partial MPTMS coating on the QDs. As for attaching the QDs to the tips of silica optical fibers, a different lab procedure using the same chemistry presented herein can be applied.

Chapter 6

Macrophage cytotoxicity studies with peptide coated Mn-doped ZnSe/ZnS quantum dots

6.1 *in vivo* QD potential and inherent cytotoxicity

A particular interesting prospect has been the use of QDs for *in vivo* applications, such as imaging, biomarkers, and drug and disease treatment development. The high stability, large stokes shifts, and high absorptivity coefficients of QDs make them more suitable for complex *in vivo* conditions[42, 43]**.** As such, QDs are ideal candidates for advancements in the biomedical field[44] with a high potential that has generated a lot of worldwide attraction in the field of research, and as a result, numerous methods have been developed to try and utilize QDs to their fullest extent. QDs are widely known for their contribution to biosensing and tracking, cellular imaging, tissue staining, and other *in vivo* and *in vitro* research and diagnostic purposes[45].

However, it is paramount for the benefits of engineered nanoscale products to outweigh their toxicity, which poses potential risks to human health. Numerous studies provide evidence that QD toxicity is a complex issue that depends not only on diversity of their individual physicochemical properties, core and shell materials, size, charge, dose (concentration), functional groups of the cap, but also on their mechanical, photolytic and oxidative stability in different environments[46]. For instance, the toxicity associated with conventional semiconductor II-IV series, zinc sulfide (ZnS), zinc-selenide (ZnSe), cadmium selenide (CdSe), and cadmium telluride (CdTe) QD cores in leaching of primary core components of the QDs: cadmium (Cd), tellurium (Te), and selenium (Se)

into surroundings upon oxidation or photolysis and damage of the shell. Heavy metal Cd ions are infamously known to be toxic to animal and human cells[47, 48, 49].

Therefore, for a comprehensive evaluation of toxicity of each QD type tailored for a specific application separate testing should be performed for any particular cell type, organism and route of administration.

Research shows that toxicity varies based upon the amount of QD dosage. In the case of maltodextran-coated CdS QDs, the borderline between toxic and non-toxic is shown to be less than 3.28 nM, but not any greater than 4.92 nM[50]. Based off of their inherent toxicity, scientists have attempted to change the components of the QDs to make them more biocompatible. A potential solution is to avoid the use of heavy metals, such as lead, mercury, and cadmium and instead use transition metals[3]. Replacing the Cd component with Zn in ZnSe doped with Mn ions, or CdTe capped with SiO_2 has been proven to be fairly efficient in reducing QD toxicity[4]. Other options include QDs capped with L-glutathione (GSH) and thioglycolic acid (TGA) that have allowed the QDs to be more tolerable *in vivo*[51].

Zn has much lower toxicity than Cd. However, some materials, which may not be toxic in their bulk form, might in fact be toxic at the nano scale. Since the QD-based MMP biosensor will ultimately be placed inside the spinal column of the human body, it becomes necessary to assess potential QD toxicity. In order to characterize the cytotoxic potential of peptide coated Mn-doped ZnSe/ZnS core/shell QDs on human cells, the ApoTox-Glo Triplex assay (Promega) was used. Macrophage cells were chosen for evaluation of QD cytotoxicity based on several reasons. First, resident macrophages (MF) of the brain and spinal cord, or microglia, come into direct contact with foreign

molecules, including QDs (and phagocytose them), therefore acting as the first and main form of active immune defence in the CNS. And second, MF are capable of releasing MMPs, which are responsible for cleaving the peptides conjugated to the QDs, and as a result mimicking the real life situation of peptide/QD exposure to the insides of the spinal column.

6.2 The ApoTox-Glo® Triplex assay

The chosen assay can provide information regarding cytotoxicity, viability, and apoptosis effects that the material under test has on the cells. The degree of cytotoxicity, viability, and apoptosis was measured using substrates, which when cleaved by appropriate enzymes induce quantifiable light signal that can be measured with a plate reader. The assay's reagents include solutions of substrates that release fluorescent molecules when cleaved by protease enzymes for live and dead cells. The substrate, glycyl-phenylalanyl-aminofluorocoumarin (GF-AFC), enters live cells and is cleaved by protease enzymes to release the florescent AFC. The intensity of AFC fluorescence is the indicator of cell viability. Another substrate, bis-alanylalanyl-phenylalanyl-rhodamine 110 (bis-AAF-R11O), does not enter live cells and is cleaved by dead cell proteases, releasing a fluorescent substance known as R110. The intensity of the R11O fluorescence is the indicator of cell cytotoxicity. To measure apoptosis, the Caspase-Glo 3/7 reagent consisting of a caspase substrate in solution will result in a luminescent signal upon cleavage, a signal proportional to the degree of apoptosis taking place during treatment.

The QDs under test are of interest for *in vivo* biosensing applications and therefore must display very little cytotoxicity, if any. In this chapter, the low cytotoxic

properties of peptide coated Mn-doped ZnSe/ZnS non Cd containing QDs at low concentrations, particularly < 25 μM (1.2 mg/mL), are reported.

6.3 Procedures

6.3.1 Materials

Murine macrophage RAW 264.7 cells were purchased from ATCC, DMEM cell media was purchased from Life Technologies. The ApoTox-Glo® Triplex assay kit was purchased from Promega. Digitonin, ionomycin, and staurosporine were purchased from Sigma-Aldrich. 384 well plates were purchased from Thermo Scientific.

6.3.2 Cell Preparation

The cell cultures were prepared using 4 different 384 well-plates seeded with mouse macrophage cells at a concentration of 5,000 cells per well in DMEM cell media containing 10% fetal bovine serum and 1% penicillin/streptomycin. Each of the four wells corresponded to 6, 12, 24, and 48 hour incubation treatments, with triplicate wells set up for the 6 hour treatment and hextuplicate wells for the 12, 24, and 48 hour treatments.

6.3.3 ZnSe:Mn/ZnS QD synthesis

The QDs were synthesized as detailed in chapter 2.

6.3.4 QD bioconjugation

Cysteine containing peptides were conjugated to the ZnSe:Mn/ZnS QDs as detailed in chapter 3.

6.3.5 Cytotoxicity, viability, and luminescence assay

The ApoTox-Glo® Triplex assay kit was purchased from Promega. For the testing, the QD bioconjugates were incubated with the cells at 0.2500, 0.1250, 0.06250, and 0.03125 µM concentrations for each treatment. Each individual well consisted of 20 µL total volume of solution with 10 µL of cells in cell media and 10 µL of QDs in water. Background measurements were taken and subsequently subtracted from every average reading. As a control, measurements involving untreated cells were included. Positive controls include treatments from 2 compounds known to be toxic, digitonin and ionomycin (markers for cytotoxicity and necrosis, respectively), as well as staurosporine, a compound known to induce apoptosis. The concentrations for the positive controls were 15 µg/mL for digitonin (15 minute incubation time) used for the 6 hour treatment, 30 µg/mL for digitonin (25 minute incubation time) used for the 12, 24, and 48 hour treatments, 100 µM for ionomycin (6 hour incubation time) used for all four treatment times, and 10 µM for staurosporine (6 hour incubation time) used for all treatment times.

Measurements were taken with a Tecan Infinite 200 PRO Microplate Reader, measuring fluorescence from the bottom of the well plate.

Cytotoxicity/viability reagents were added to the wells immediately after the incubation period, and following a brief mixing in an orbital shaker for 30 seconds, the

plate was incubated for 30 minutes before plate measurements were taken. Viability measurements were taken using 400 nm excitation wavelength and 505 nm emission wavelength for all 4 treatment times (6, 12, 24, and 48 hours). Cytotoxicity measurements were taken using 485 nm wavelength excitation and 520 nm emission wavelength. The caspase reagent was added last to every well and was briefly mixed with an orbital shaker for 30 seconds and then incubated for 30 minutes, before measurements were taken with the plate reader.

6.4 Results

6 Hour Incubation Time: **Figure 6.1** shows that the viability of the cells were affected by all three positive controls, most particularly 60% lower viability from Ionomycin ($p=0.0002 << 0.01$) and 51% lower viability by staurosporine ($p=0.0002 << 0.01$), and to a smaller extent by 16% from digitonin ($p=0.069$). However, none of the QD concentrations showed any appreciable difference or statistical significance when comparing the QD treated cells with the untreated cells, indicating that there is no viability effect on the cells from the QDs at six hours.

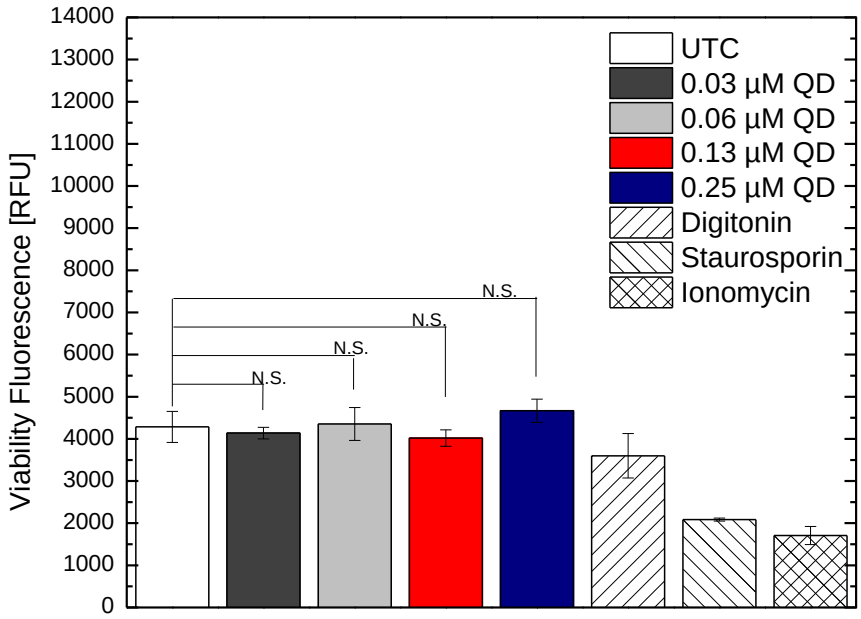

Figure 6.1: *Macrophage cell viability bar graph depicting the cytotoxic effect of Mn-doped ZnSe/ZnS peptide coated QD from a six-hour treatment on macrophage cells. Results are in expressed in mean ± s.d., n=3. UTC – untreated cells, N.S. – not significant, RFU – relative fluorescence units.*

Likewise, in **Figure 6.2**, there is no real difference between the cytotoxicity from the QDs in relation to the untreated cells even taking into account relatively large standard deviations on some fraction of the data. Though in this case, higher intensity indicates a higher cell death, and a significantly higher intensity could be observed in the positive controls, a 119% increase in cell cytotoxicity for digitonin ($p=0.059$), a 429% increase for staurosporine ($p=0.0009 << 0.01$), and a 452% increase for ionomycin ($p=0.002 < 0.01$). Despite the fact that digitonin was intended to indicate cytotoxicity, both staurosporine and ionomycin received higher intensity levels, all three were

significantly more toxic than any of the QD concentrations or the untreated control. No QD concentrations from the 6 hour cytotoxicity test showed any statistically significant increases in cell cytotoxicity.

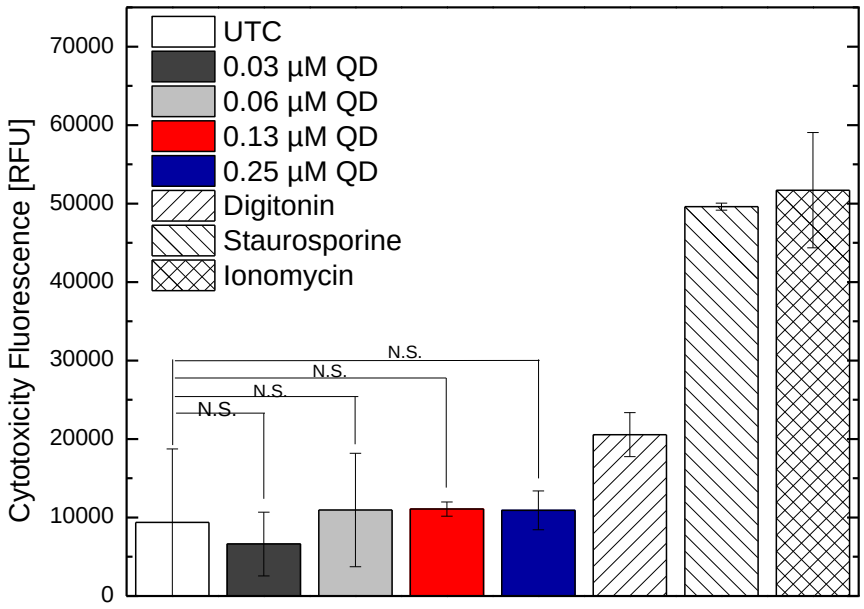

Figure 6.2: *Macrophage cell cytotoxicity bar graph depicting the cytotoxic effect after a six hours treatment of Mn-doped ZnSe/ZnS peptide coated QDs on macrophage cells in cell media. Results are in expressed in mean ± s.d., n=3. UTC – untreated cells, N.S. – not significant, RFU – relative fluorescence units.*

Figure 6.3 shows the luminescence results from 6 hour incubation in which induced apoptosis was quantified. The cells treated with staurosporine, the positive control for induced apoptosis, show a 607% higher signal ($p=0.00002 <<< 0.01$) than that of the untreated cells. A small sign of induced apoptosis can be seen from the

luminescent signal from the cells treated with 0.25 µM QDs, with a 96% increase in luminescence (p=0.00009 <<<0.01) from that of the untreated cells.

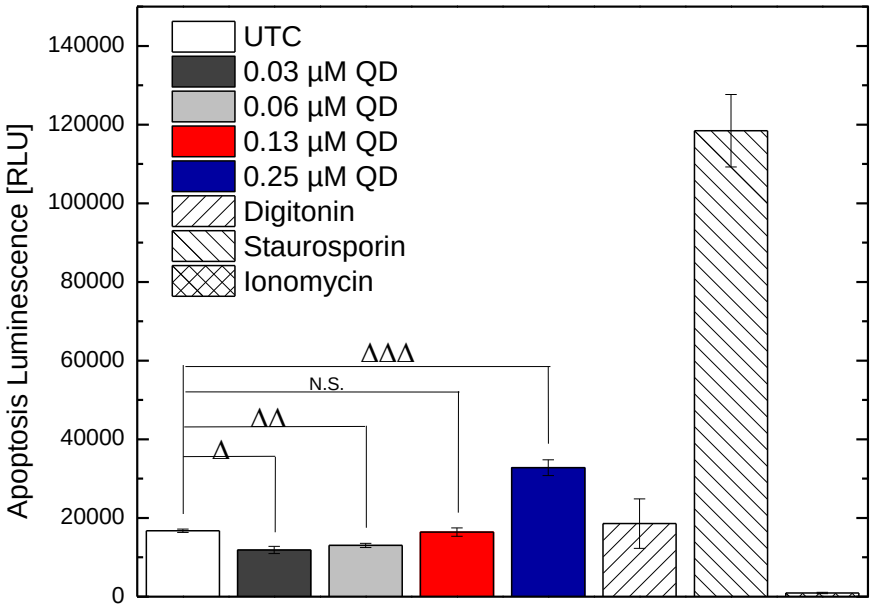

Figure 6.3: *Macrophage cell induced apoptosis bar graph depicting induced apoptosis after a six-hour treatment of Mn-doped ZnSe/ZnS peptide coated QDs on macrophage cells in cell media. Results are in expressed in mean ± s.d., n=3. Δ p=0.0005 (<0.01), ΔΔ p=0.0004 (<0.01), and ΔΔΔ p=0.00009(<<0.01). UTC – untreated cells, N.S. – not significant, RLU – relative luminescence units.*

12 Hour Incubation Time: It can be seen from **Figure 6.4** that cell viability starts to become an issue at the 12 hour incubation time, which scales inversely with concentration. The fluorometric response with regards to cell viability, when compared with the untreated cells, decreases by 50% (p=0.0000007 <<< 0.01) for 0.25 µM QDs, 19% (p=0.001 < 0.01) for 0.13 µM QDs, 13% (p=0.005 < 0.01) for 0.06 µM QDs, and

8% (p=0.009 < 0.01) for 0.03 µM QDs. All three positive controls decrease significantly in comparison to the untreated by 62% (p=0.000000003 <<<0.01) for digitonin, 48% (p=0.000000006 <<< 0.01) for staurosporine, and 65% (p=0.0000000003 <<< 0.01)) for ionomycin. Of interesting note is how comparable the 0.025 µM QDs signal is to that of the positive controls.

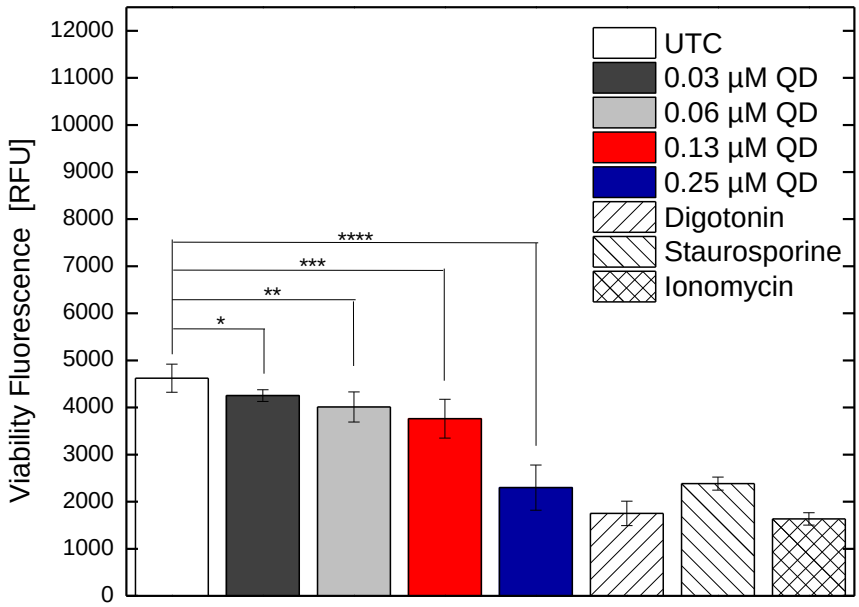

Figure 6.4: *Macrophage cell viability bar graph depicting the cytotoxic effect of Mn-doped ZnSe/ZnS peptide coated QD from a twelve-hour treatment on macrophage cells. Results are in expressed in mean ± s.d., n=6. * p=0.009 (<0.01), ** p=0.005 (<0.01), *** p=0.001 (<0.01), **** p=0.0000007 (<<<0.01). UTC – untreated cells, N.S. – not significant, RFU – relative fluorescence units.*

Figure 6.5 shows cytotoxicity results for 12 hour treatments. The three positive controls display a significantly higher fluorescent response in comparison to the untreated, particularly a 1319% increase ($p=0.00000003 <<< 0.01$)) with digitonin and a 1370% increase ($p=0.000000003 <<< 0.01$) with ionomycin, and a smaller but still statistically significant 360% increase ($p=0.0000013 <<< 0.01$) with staurosporine. Conflicting with the viability data from **Figure 6.4**, it would seem that the signals from three of the four QD concentrations show no statistically significant variability for cytotoxicity, with 0.13 µM QD having a 70% increase ($p=0.009 < 0.01$) over the untreated, which is drastically lower than the positive control signals.

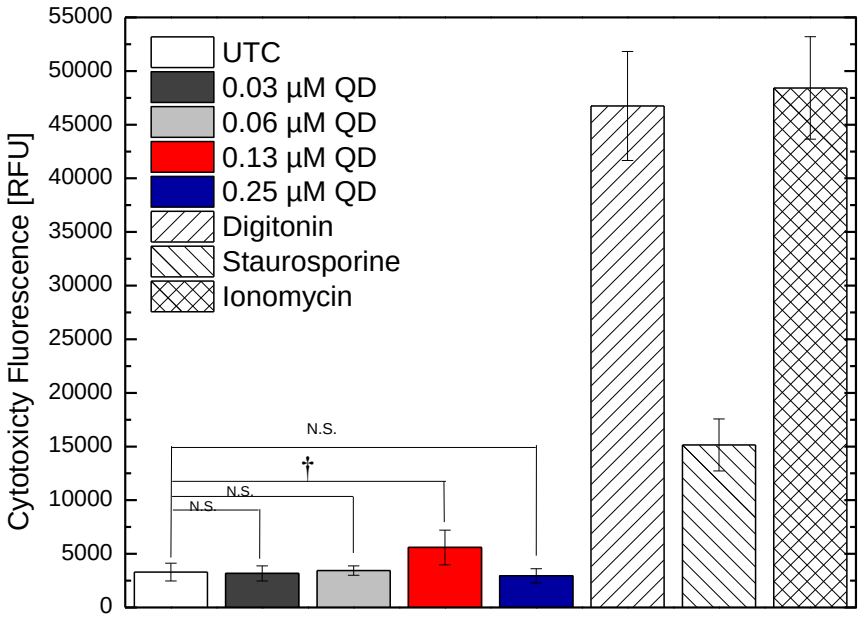

Figure 6.5: *Macrophage cell viability bar graph depicting the cytotoxic effect of Mn-doped ZnSe/ZnS peptide coated QD from a twelve-hour treatment on macrophage cells. Results are in expressed in mean ± s.d., n=6. † p= 0.009 (<0.01). UTC – untreated cells, N.S. – not significant, RFU – relative fluorescence units.*

With **Figure 6.6**, a small degree of induced apoptosis is seen from the 0.25 µM QDs with a 96% signal increase from that of the untreated cells, while none of the other three concentrations show any statistically significant variation in luminescence. The 96% increase is minor when compared to the 1149% signal increase (p=0.00000000009 <<< 0.01) from the staurosporine control.

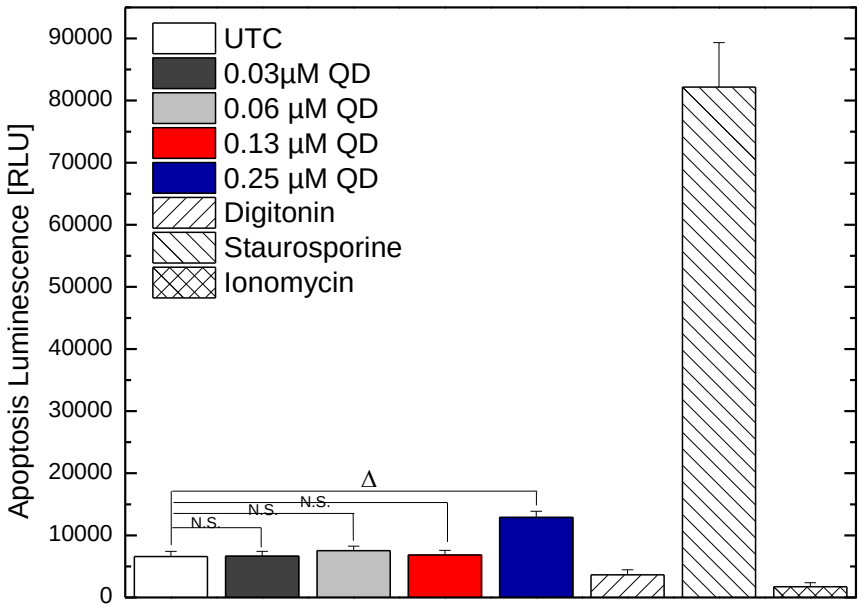

Figure 6.6: *Macrophage cell induced apoptosis bar graph depicting induced apoptosis after a twelve-hour treatment of Mn-doped ZnSe/ZnS peptide coated QDs on macrophage cells in cell media. Results are in expressed in mean ± s.d., n=6. Δ p=0.00000002 (<<<0.01). UTC – untreated cells, N.S. – not significant, RLU – relative luminescence units.*

24 Hour Incubation Time: As seen from the 24 hour viability data in **Figure 6.7**, the fluorometric response of digitonin was 30% that of the untreated cells (p=0.0013 < 0.01). Staurosporine shows a 60% (p=0.000000008 <<< 0.01) decrease in viability from that of the control. Likewise, the ionomycin shows a 52% decrease in viability (p=0.0000000003 <<< 0.01). The 50% decrease in viability of the highest QD concentration shown in the 12 hour trial is seen here as well (p=0.00000005 <<< 0.01) with viability as a whole continuing to scale inversely for 0.03 μM with 94% of the

untreated, 0.06 µM with 85% of untreated and 0.13 µM with 77% of the untreated, ($p=0.1$, $p=0.002 < 0.01$ and $p=0.0002 << 0.01$, respectively). This indicates a decrease in viability of the QDs during a 24 hour treatment for the 0.25 µM concentration, almost equal with that of the positive controls.

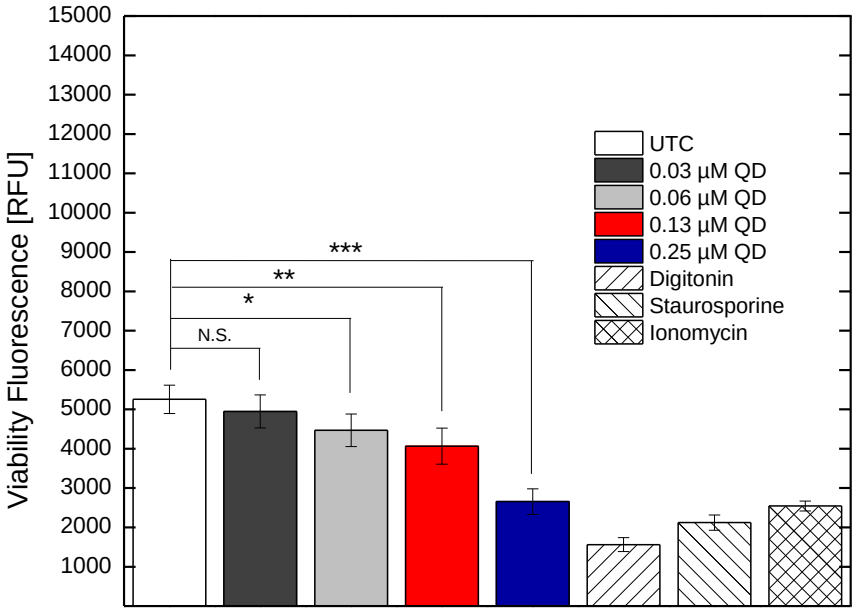

Figure 6.7: *Macrophage cell viability bar graph depicting the cytotoxic effect of Mn-doped ZnSe/ZnS peptide coated QD from a twenty-four hour treatment on macrophage cells. Results are in expressed in mean ± s.d., n=6. * p=0.002 (<0.01), ** p=0.0002 (<<0.01), *** p=0.00000005 (<<<0.01). UTC – untreated cells, N.S. – not significant, RFU – relative fluorescence units.*

In **Figure 6.8**, ionomycin showed particularly strong cytotoxic effects with an increase in fluorometric intensity of 1,739% over the untreated cells ($p=0.0000000000005 <<< 0.01$) with staurosporine increasing over the untreated control by 795% ($p=0.00000003 <<< 0.01$) and digitonin by 846% ($p=0.0000002 <<< 0.01$). 0.25 µM QDs show an increase of 315% over the untreated control, and though, it is statistically significant ($p=0.000003 <<< 0.01$) this is significantly less than the positive controls. All other QD concentrations, however, show no statistical deviation from the fluorometric intensity of the untreated cells.

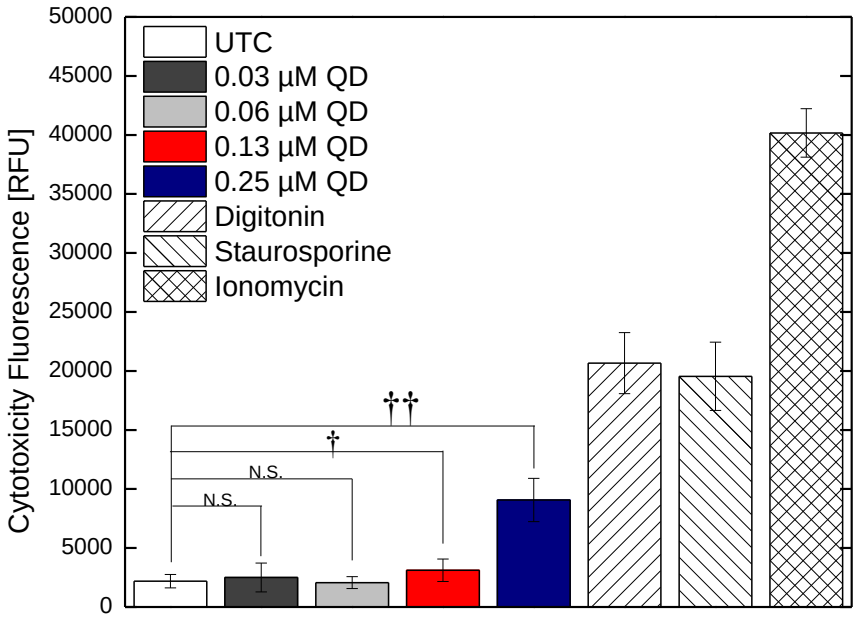

Figure 6.8: *Macrophage cell viability bar graph depicting the cytotoxic effect of Mn-doped ZnSe/ZnS peptide coated QD from a twenty-four twelve-hour treatment on macrophage cells. Results are in expressed in mean ± s.d., n=6. † p=0.03 (<0.05), †† p=0.000003 (<<<0.01). UTC – untreated cells, N.S. – not significant, RFU – relative fluorescence units.*

In testing luminescence at 24 hours in **Figure 6.9**, the intended control, staurosporine, shows greater levels of apoptosis than any other substance tested, with an increase of 306% ($p=0.0000002 <<< 0.01$) over the untreated control, though the other two positive controls are nearly as fluorometrically intense, with digitonin increasing apoptosis by 192% ($p=0.0002 << 0.01$) and ionomycin increasing apoptosis by 76% ($p=0.0002 << 0.01$). However, the 0.25 µM QDs showed an elevation of 219% ($p=0.000002 <<< 0.01$). None of the other QD concentrations show a large increase in apoptosis (though the 0.03 µM shows a significant decrease, it is within the margin of error).

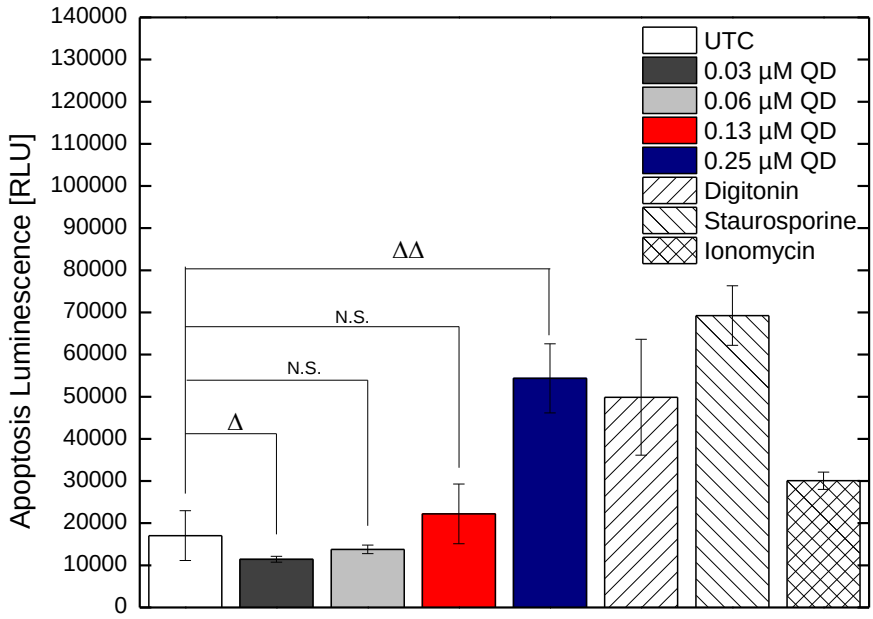

Figure 6.9: *Macrophage cell induced apoptosis bar graph depicting induced apoptosis after a twenty-four hour treatment of Mn-doped ZnSe/ZnS peptide coated QDs on macrophage cells in cell media. Results are in expressed in mean ± s.d., n=6. Δ p=0.02 (<0.05) and ΔΔ p=0.000002 (<<<0.01). UTC – untreated cells, N.S. – not significant, RLU – relative luminescence units.*

48 hour Viability: **Figure 6.10** displays a 72% drop in viability with digitonin ($p=0.002 < 0.01$) over the untreated, with similar decreases seen in the other positive controls (staurosporine showing 52% less viability ($p=0.002 < 0.01$) and ionomycin showing 49% less viability ($p=0.0009 << 0.01$). Continuing the trend started at twelve hours, the cell viability with 0.25 µM QDs is on par with the positive controls, with a decrease in viability by 62% ($p=0.0002 << 0.01$). Consistent with both 12 hour and 24 hour incubation periods, an inverse between viability and QD concentration is observed.

0.03 µM concentration shows a statistically insignificant decrease of 3%, increasing to a 41% drop at 0.13 µM ($p=0.002 < 0.01$).

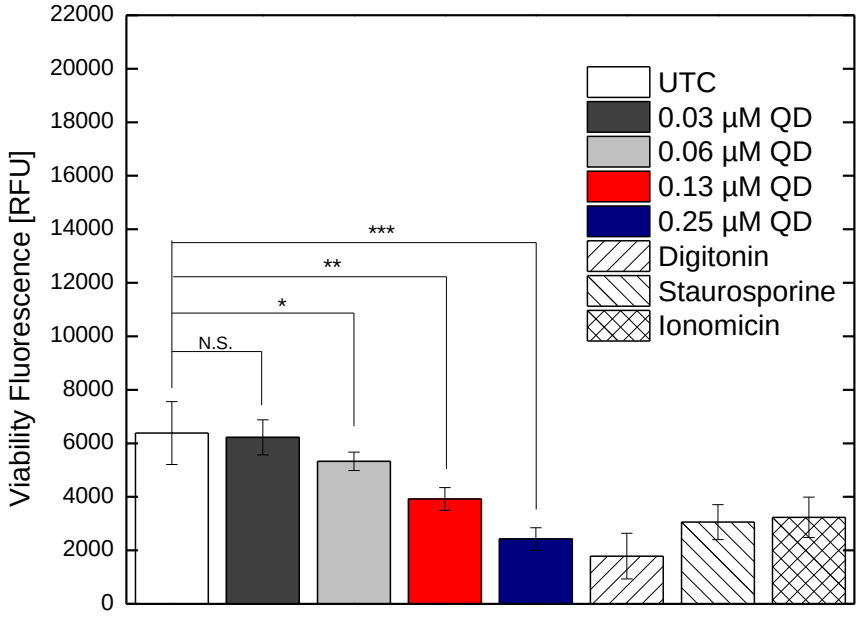

Figure 6.10: *Macrophage cell viability bar graph depicting the cytotoxic effect after a forty-eight hours treatment of Mn-doped ZnSe/ZnS peptide coated QDs on macrophage cells in cell media. Results are in expressed in mean ± s.d., n=6. * p=0.049 (<0.05), ** p=0.002 (<0.01), *** p=0.0002 (<<0.01). UTC – untreated cells, N.S. – not significant, RFU – relative fluorescence units.*

None of the QD concentrations showed any statistically significant cytotoxic effects after 48 hours of incubations (**Figure 6.11**), though the positive controls show significant increases in fluorometric intensity, with digitonin rising by 248% ($p=0.047 < 0.05$). On the other hand, staurosporine increased cytotoxicity by 419% ($p=0.0004 << 0.01$) and ionomycin elevated the effects by 473% ($p=0.0003 << 0.01$).

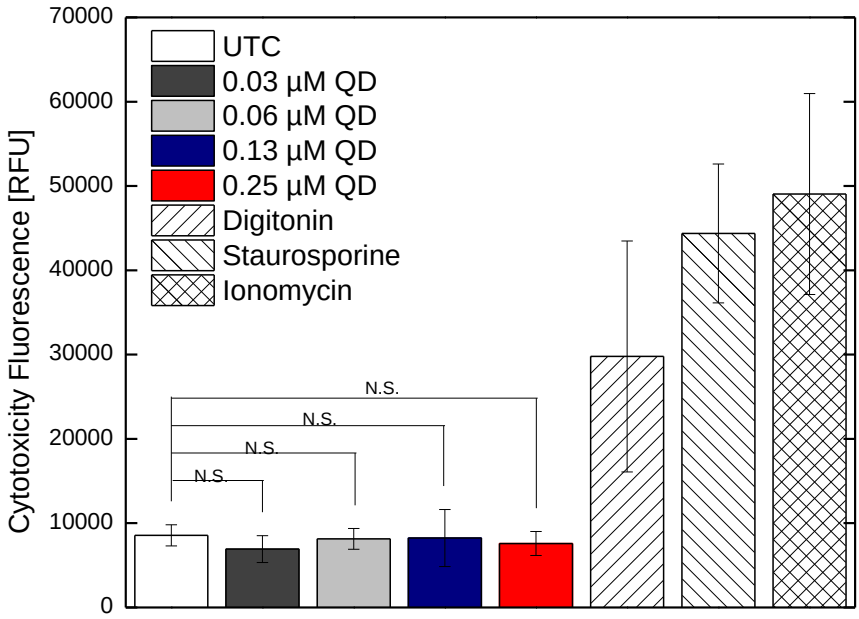

Figure 6.11: *Macrophage cell cytotoxicity bar graph depicting the cytotoxic effect of Mn-doped ZnSe/ZnS peptide coated QD from a forty-eight hour treatment on macrophage cells. Results are in expressed in mean ± s.d., n=6. UTC – untreated cells, N.S. – not significant, RFU – relative fluorescence units.*

8 hours, luminescence readings (**Figure 6.12**) displayed apoptosis elevated by 304% by staurosporine ($p=0.00002 <<< 0.01$), with the other two positive controls significantly lower. Digitonin increased apoptosis by 81% ($p=0.0006 << 0.01$), and ionomycin did the same by just 17% ($p=0.04 < 0.05$). The lowest QD concentration was the only one statistically insignificant. Apoptosis was increased by 17% for 0.06 µM, 45% for 0.13 µM, and 60% for 0.25 µM ($p=0.045 < 0.05$, $p=0.004 < 0.01$ and $p= 0.002 < 0.01$, respectively).

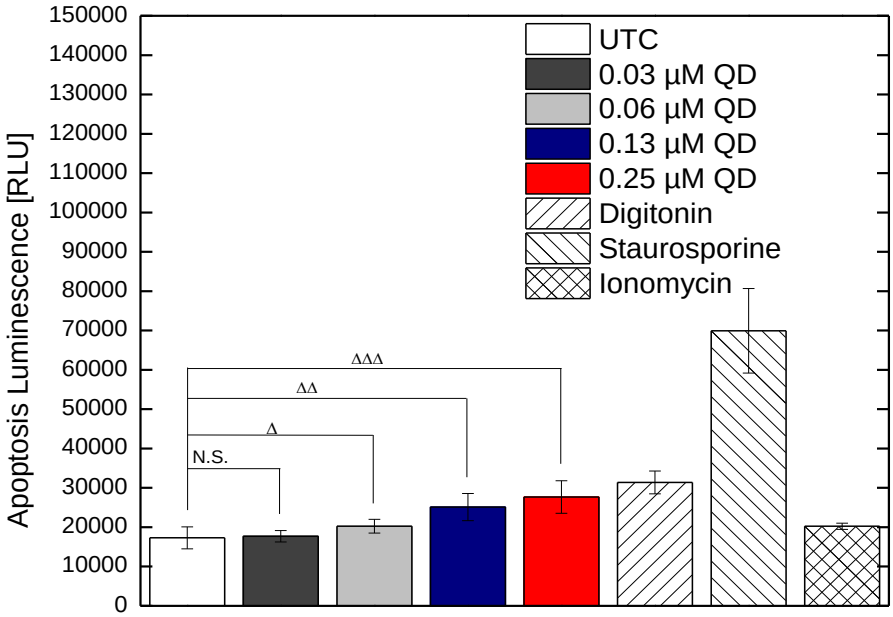

Figure 6.12: *Macrophage cell induced apoptosis bar graph depicting induced apoptosis after a forty-eight six-hour treatment of Mn-doped ZnSe/ZnS peptide coated QDs on macrophage cells in cell media.* Results are in expressed in mean ± s.d., n=6. Δ p=0.045 (<0.05), ΔΔ p=0.004 (<0.01), and ΔΔΔ p=0.002 (<0.01). UTC – untreated cells, N.S. – not significant, RLU – relative luminescence units.

6.5 Summary

The data obtained from the ApoTox-Glo® Triplex assay yielded a complete profile for the effects of cell viability, cytotoxicity, and apoptosis from the peptide coated ZnSe:Mn/ZnS QDs at four different concentrations for four different incubation times. Noteworthy is the higher sensitivity to cell viability that becomes apparent at 12 hours (**Figure 6.4**) and remains fairly consistent for 24 (**Figure 6.7**) and 48 hours (**Figure 6.10**). Most interesting is the fact that despite the drops in viability, the QDs show very

little cytotoxic effect, particularly for 6, 12, and 48 hour incubation times, with an exception for a statistically significant 315% increase in cytotoxicity for the most concentrated 0.25 μM QD solution for 24 hours (**Figure 6.8**).

The main conclusion from the tests is that, despite their low cytotoxicity, these particular QDs still seem to be having an unhealthy effect on the cells at higher concentrations. Lowered viability without any increase in the cytotoxicity biomarker is indicative of an antiproliferation effect on the cells. In the case of primary necrosis, where all the cells die early, cytotoxicity may not be measurable in later testing times[52]. If the cells where to significantly die earlier than the testing time then enzyme markers for cytotoxicity can degrade early on, and cytotoxicity ends up being underestimated[53]. However, in the case of the macrophage cells being treated with the QDs, there is a measurable caspase activation from induced apoptosis at all four incubation times, as seen from the luminescence measurements in figures 3, 6, 9, and 12, with a statistically significant measurable increase in luminescence for the most concentrated 0.25 μM QD for all 4 incubation times, so primary necrosis can be ruled out.

Overall, it would seem that there is very little cytotoxic effect on the macrophage cells from the presence of the peptide coated ZnSe/ZnS:Mn QDs. However, it was fortunate that the ApoTox-Glo® Triplex assay allows for more thorough testing on other effects from the cells. The results outside of the cytotoxicity measurements show that these QDs show a good deal of decreased viability and induced apoptosis, a result which would have gone unnoticed had only cytotoxicity been tested.

We determined the safe concentration limits for these QD to be below 0.125 μM, and the adverse effects associated with the viability decrease, cytotoxicity and apoptosis

to scale with dosage/exposure concentration. We consider our QD to be good candidates for *in vivo* experiments, but further studies exploring the mechanisms of the increased caspase .activation and cytotoxicity at higher QD concentrations are needed

Chapter 7

Conclusions and future work

Photoluminescent colloidal ZnSe:Mn/ZnS QDs have been synthesized and optically and structurally characterized with repeatable results. The colloidal QDs exhibit two different luminescence peaks at 597 nm and 487 nm wavelengths, by using 400 nm and 436 nm excitation wavelengths, respectively. The 597 nm emission signal is attributed to interatomic energy transitions in the Mn-dopant, and the 487 nm emission is attributed to surface defects. As synthesized, and at high concentrations in chloroform, the 597 nm emission has a high intensity with an 86.5% QE.

Conjugating cys-containing peptides to the QDs, which range between 4 and 14 AA residues, results in the lowering of QE. In addition, the excitation for the Mn-transition blue shifts significantly to ~315 nm and the emission slightly blue shifts by a few nm to ~595 nm. The surface defect emission disappears entirely after conjugating peptides to the QDs. The drop in QE is attributed to a quenching effect that the peptides have on the QDs. The amount of quenching varied with respect to the peptide composition in the case of three different peptides: the remnant 4 AA residue Peptide *{Leu}{Arg}{Ser}{Cys},* the substrate 9 AA residue peptide {Val}{Val}{Pro}{Leu}{Ser}*{Leu}{Arg}{Ser}{Cys},* and a substrate 14 AA peptide **{Glu}{Asp}{Glu}{Asp}{Glu}**{Val}{Val}{Pro}{Leu}{Ser}*{Leu}{Arg}{Ser}{Cys}*. The 4 AA and 9 AA peptides are basic with a charge of +1, and the 14 AA peptide is acidic with a -4 charge. The QY of the peptide/QD conjugates with 4 AA have higher QY than the 9 AA, and the 14 AA has a higher QY than the 4 AA peptide (9 AA < 4 AA < 14

AA). The Zeta potentials for all three types of QD/peptide conjugates have negative values, which does not support the idea that the QD/peptide conjugates with 9 AA and 4 AA peptides have a different surface charge than the conjugates with the 14 AA peptides. In addition, the peptide/QD conjugates showed minimal sensitivity to active mouse MMP-9s, particular at lower peptide densities. The peptide concentration during bioconjugation was reduced to 0.1%, 1%, 10%, 33%, and 66% of the standard peptide concentrations, essentially lowering the peptide to QD ratio during bioconjugation. 0.1% and 66% dilutions showed minimal sensitivity to active MMP-9.

Furthermore, the ZnSe:Mn/ZnS QDs were successfully tethered to the surface of glass slides, by partially coating them with MPTMS coupling agent and orbital shaking the colloidal solution over OH-modified silica. The QDs maintain their fluorescence and have an 8% QE when characterized on silica. The successful linking of the Cd-free luminescent QDs to the surface of silica is a step towards the development of an *in vivo* optical fiber biosensing system with QDs covalently bonded to the silica tip of the fiber.

Thorough cytotoxicity studies revealed the Cd-free colloidal peptide coated ZnSe:Mn/ZnS QDs to still display cytotoxic properties when incubated with macrophage cells at different time points and different QD concentrations. The concentrations which showed no cytotoxic effects with regards to cytotoxicity, viability, and induced-apoptosis were below 0.125 μM.

For future work, the sensitivity of the MMP-9 biosensors, developed and experimented with in this dissertation, should be increased. Suggestions to increase sensitivity would be to increase the QD to peptide ratio during bioconjugation, conjugate

energy acceptors/donors to the external ends of the peptides at the surface of QDs, run the experiments at possibly higher peptide/QD conjugate concentrations, run the biosensing experiments in buffer solutions designed for optimization of MMP-9 activity, as opposed to CSF and water, and colloidal stability of the QDs biosensors in solution should be enhanced, as the current biosensors would fall out of solution overnight for CSF and buffer.

As the chemistry for linking these particular QDs to silica has been developed, it still remains to link the QDs to silica and subsequently conjugate peptides to the linked QDs, another step towards the completion of the *in vivo* biosensor.

In order to verify that the MMP-9s are indeed cleaving the peptides attached to the QDs, gel electrophoresis experiments should be implemented. If the peptides are being cleaved, the peptide/QD conjugates should decrease in overall size, which would be discernable with gel electrophoresis.

In addition, cytotoxicity experiments should be repeated for different MMP substrates conjugated to ZnSe:Mn/ZnS QDs, as we've only looked at one peptide substrate. As was discussed in chapter 6, cytotoxicity of nanomaterials can be influenced by surface molecules, surface charge, stability, and particle size. Different peptide substrates have unique amino acid residue sequences and would therefore have their own unique peptide properties such as hydrophobicity, charge, acidity, etc.

References

[1] Verma RP and Hansch C: **Matrix metalloproteinases (MMPs): Chemical–biological functions and (Q)SARs**. *Bioorganic & Medicinal Chemistry* 2007, **15**(6):2223-2268.

[2] Kandasamy AD, Chow AK, Ali MAM, and Schulz R: **Matrix metalloproteinase-2 and myocardial oxidative stress injury: beyond the matrix**. *Cardiovascular Research* 2010 **85**(3):413-423.

[3] Dev R, Srivastava PK, Iyer JP, Dastidar SG, and Ray A: **Therapeutic potential of matrix metalloproteinase inhibitors in neuropathic pain**. *Expert Opin. Investig. Drugs* 2010, **19** (4):455-468.

[4] Dworkin RH, O'Connor AB, Backonja M, Farrar JT, Finnerup NB, Jensen TS, Kalso EA, Loeser JD, Miakowski C, Nurmikko TJ, Portenoy RK, Rice ASC, Stacey BR, Treede R-D, Turk DC, Wallace MS: **Pharmacologic management of neuropathic pain: Evidence-based recommendations**. *Pain* 2007 **132**(3):237-251.

[5] Jenson TS, Madsen CS, and Finnerup NB: **Pharmacology and treatment of neuropathic pains**. *Current Opinion in Neurology* 2009 **22**(5):467-474.

[6] Kawasaki Y, Xu Z, Wang X, Park JY, Zhuang Z, Tan P, Gao Y, Roy K, Corfas G, Lo EH, and Ji R. **Distinct roles of matrix metalloproteinases in the early- and late-phase development of neuropathic pain**. *Nature Medicine* 2008 **14**(3):331-336.

[7] Zigouris A, Batistatou A, Alexiou GA, Pachatouridis D, Mihos E, Drosos D, Fotakopoulos G, Doukas M, Voulgaris S, and Kyritsis AP: **Correlation of matrix metalloproteinase-1 and -3 with patient age and grade of lumbar disc herniation**. *J. Neurosurg. Spine* 2011 **14**:268-272.

[8] Beghi E, Logroscino G, Chio A, Hardiman O, Mitchell D, Swingler R, and Traynor B: **The epidemiology of ALS and the role of population-based registries**. *Biochemica et Biophysica Acta* 2006 **1762**(11-12):1150-1157.

[9] National Institute of Neurological Disorders and Stroke: **Amyotrophic Lateral Sclerosis Fact Sheet**, 2010: http://www.ninds.nih.gov/disorders/amyotrophiclateralsclerosis/detail_amyotrophiclateralsclerosis.htm.

[10] Wagner K: **The need for biomarkers in amyotrophic lateral sclerosis development**. *Neurology* 2009 **72**:11-12.

[11] Niebroj-Dobosz I, Janik P, Sokolowska B, and Kwiecinski H: **Matrix metalloproteinases and their tissue inhibitors in serum and cerebrospinal fluid of patients with amyotrophic lateral sclerosis**. *European Journal of Neurology* 2010 **17**(2):226-231.

[12] Liuzzi GM, Mastroianni CM, Santacroce MP, Fanelli M, D'agostino C, Vullo V, and Riccio P: **Increased activity of matrix metalloproteinases in the cerebrospinal fluid of patients with HIV-associated neurological diseases**. *Journal of Neurovirology* 2000 **6**(2):156-163.

[13] Leppert D, Ford J, Stabler G, Grygar C, Lienert C, Huber S, Miller H, Hauser S, Kappos L: **Matrix metalloproteinase-9 is selectively elevated in CSF during relapses and stable phases of multiple sclerosis**. *Brain* 1998 **121**(12):2327-2334.

[14] Adair J, Charlie J, Dencoff J, Kaye J, Quinn J, Camicioli R, Stetler-Stevenson W, Rosenberg G: **Measurement of gelatinase B in the cerebrospinal fluid of patients with vascular dementia and Alzheimer disease**. *Stroke* 2004: **35**(6):e159-e162.

[15] Stevens LJ and Page-McCaw A**: A secreted MMP is required for reepithelialization during wound healing**. *Mol. Biol. Cell*, 2012 **23**(6):1068-1079.

[16] Schultz GS, Ladwig G, and Wysocki A: **Extracellular matrix: review of its roles in acute and chronic wounds**. *World Wide Wounds* Aug 2005: http://www.worldwidewounds.com/2005/august/Schultz/Extrace-Matric-Acute-Chronic-Wounds.html

[17] Niu L, Li Y, Li X, Gao X, Su X: **Study the cytotoxicity of different kinds of water-soluble nanoparticles in human osteoblast-like MG-63 cells.** *Materials Research Bulletin* 2012, **47**(11):3654-3659.

[18] Su Y, He Y, Lu H, Sai L, Li Q, Li W, Wang L, Shen P, Huang Q, Fan C: **The cytotoxicity of cadmium based, aqueous phase – Synthesized, quantum dots and its modulation by surface coating.** *Biomaterials* 2009, **30**(1):19-25.

[19] Kim GB, Kim YP: **Analysis of Protease Activity Using Quantum Dots and Resonance Energy Transfer.** *Theranostics* 2012, **2**(2):127-138.

[20] Vashist SK, Tewari R, Bajpai RP, Bharadwaj LM, and Raiteri R: **Review of quantum dot technologies for cancer detection and treatment**. *J. Nanotechnology online*, 2006: http://www.azonano.com/Details.asp?ArticleID=1726.

[21] Gao X and Nie S: **Molecular profiling of single cells and tissue specimens with quantum dots.** *Trends in Biotechnology* 2003 **21**(9):371-373.

[22] Alivisatos AP, Gu W, and Larabell C: **Quantum dots as cellular probes**. *Annual. Rev. Biomed. Eng.* 2005 **7**:55-76.

[23] Greenlee KJ and Werb Z: **Matrix Metallopreoteinases in Lung: Multiple, Multifarious, and Multifaceted**. *Physiol Rev* 2007 **87**(1):69-98.

[24] Zheng J: **Immunihistochemistry and immunocytochemistry.** *Methods in Molecular Biology; Phospholipid signaling protocols* 1998 **105**:307-314.

[25] Melville P, Benites N, Ruz-Perez M, and Yokoya E: **Proteinase and phospholipase activities and development at different temperatures of yeasts of yeasts isolated from bovine milk**. *J. Dairy Res.* 2011 **78**(4):385-390.

[26] Turk B, Huang L, Piro E, and Cantley L: **Determination of protease cleavage site motifs using mixture-based oriented peptide libraries.** *Nat. Biotechnol.* 2001 **19**(7):661-667.

[27] Pradhan N, Goorskey D, Thessing J, and Peng X: **An Alternative of CdSe Nanocrystal Emitters: Pure and Tunable Impurity Emissions in ZnSe Nanocrystals.** *J. Am. Chem. Soc.* 2005, **127**(50):17586–17587.

[28] Pradhan N and Peng X: **Efficient and Color-Tunable Mn-Doped ZnSe Nanocrystal Emitters: Control of Optical Performance via Greener Synthetic Chemistry.** *J. Am. Chem. Soc*. 2007, **129**(11):3339-3347.

[29] Acharya S, Sarma DD, Jana NR, Pradhan N: **An alternate route to high-quality ZnSe and Mn-doped ZnSe nanocrystals.** *J. Phys. Chem. Lett*. 2010, **1**(2):485-488.

[30] Zhu H, Prakash A, Benoit DN, Jones CJ, and Colvin VL: **Low temperature synthesis of ZnS and CdZnS shells on CdSe quantum dots.** *Nanotechnology*. 2010, **21**(25):255604.

[31] Murray CB, Sun S, Gaschler W, Doyle H, Betley TA, and Kagan CR: **Colloidal synthesis of nanocrystals and nanocrystal superlattices.** *IBM J. Res. & Dev.* 2001, **45**(1):47-56.

[32] Shi L, Rosenzweig N, and Rosenzweig Z: **Luminescent quantum dots fluorescence resonance energy transfer-based probes for enzymatic activity and enzyme inhibitors.** *Analytical Chemistry*. **79**(1):208-214, 2007.

[33] Marx N, Froehlich J, Siam L, Ittner J, Wierse G, Schmidt A, Scharnagl H, Hombach V, and Koenig W: **Antidiabetic PPARγ-activator rosiglitazone reduces MMP-9 serum levels in type 2 diabetic patients with coronary artery disease**. *Journal of the American Heart Association* 2003, **23**, 283-288.

[34] Li YJ, Wang ZH, Zhang B, Zhe X, Wang MJ, Shi ST, Bai J, Lin T, Guo CJ, Zhang SJ, Kong XL, Zuo X, and Zhao H: **Disruption of the blood-brain barrier after generalized tonic-clonic seizures correlates with cerebrospinal fluid MMP-9 levels**. *Journal of Neuroinflammation* 2013, **10**(80), .

[35] Xia Z, Xing Y, So MK, Koh AL, Sinclair R, and Rao J: **Multiplex detection of protease activity with quantum dot nanosensors prepared by intein-mediated specific bioconjugation**. *Anal. Chem*., 2008, **80** (22), 8649-8655.

[36] Genscript: Peptide property calculator: https://www.genscript.com/ssl-bin/site2/peptide_calculation.cgi

[37] Anaspec: **SensoLyte® 520 MMP – 9 Assay Kit datasheet**.
[38] Gelest: **Silane Coupling Agents: Connecting Across Boundaries**. 2006 catologue:2-3, 11 Feb. 2014. Web: http://www.gelest.com/goods/pdf/couplingagents.pdf
[39] Arkles B: **Tailoring surfaces with silanes.** *Chemtech.* **7:**766-778, 1977.

[40] Hu M, Noda S, Okubo T, Yamaguchi Y, Komiyama H: **Structure and morphology of self-assembled 3-mercaptopropyltrimethoxysilane layers on silicon oxide.** *Applied Surface Science* **181:**307-316, 2001.

[41] Garcia-Cerda LA, Romo-Mendoza LE, Quevedo-Lopez MA: **Synthesis and characterization of NiO nanoparticles and their PMMA nanocomposites obtained by in situ bulk polymerization.** *J. Phys. Chem. Lett.***1**:485-488, 2010.

[42] Gao X, Nie S: **Molecular profiling of single cells and tissue specimens with quantum dots.** *Trends in Biotechnology* 2003, **21**(9):371-373.

[43] Vashist SK, Tewari R, Baipai RP, Bharadwai LM, Raiteri R: **Review of quantum dot technologies for cancer detection and treatment**. [http://www.azonano.com/Details.asp?ArticleID=1726]

[44] Liu J, Wei X, Qu Y, Cao J, Chen C, Jiang H: **Aqueous synthesis and bio-imaging application of highly luminescent and low cytotoxicity Mn^{2+} -doped ZnSe nanocrystals.** *Materials Research Bulletin* 2011, **65**:2139-2141.

[45] Niu L, Li Y, Li X, Gao X, Su X: **Study the cytotoxicity of different kinds of water-soluble nanoparticles in human osteoblast-like MG-63 cells.** *Materials Research Bulletin* 2012, **47**:3654-3659.

[46] Hardman R: **A toxicologic review of quantum dots: Toxicity depends on physicochemical and environmental factors.** *Environmental Health Perspectives* 2006, **114:**165-172.

[47] Bernhoft RA: **Cadmium Toxicity and Treatment.** *Scientific World Journal* 2013.

[48] Lewinski N, Colvin V, Drezek R: **Cytotoxicity of nanoparticles.** *Small* 2008, **4:**26-49.

[49] Derfus AM, Chan WCW, Bhatia SN: **Probing the cytotoxicity of semiconductor quantum dots.** *Nano Letters* 2004, **4:**11-18.

[50] Rodríguez-Fragoso P, Reyes-Esparza J, León-Buitimea A, Rodríguez-Fragoso L: **Synthesis, characterization and toxicological evaluation of maltodextrin capped cadmium sulfide nanoparticles in human cell lines and chicken embryos.** *J Nanobiotechnol* 2012, **10**:47.

[51] Ermilov E, Kuzyniak W, Adegoke O, Sekhosana K, Hoffmann B, Nyokong T, Pries AR, Hopfner M: **Cytotoxicity screening of a series of semiconductor quantum dots for the potential biomedical use.** *The FASEB Journal* 2013, **27**:575.11.

[52] **Promega Corporation [**https://www.promega.com/resources/protocols/technical-manuals/101/apotox-glo-triplex-assay-protocol/

[53] Niles AL: **Update on in vitro cytotoxicity assays for drug development.** *Expert Opin. Drug Discov.* 2008, **3**(6):655-669.